Topics in Physics Beyond the Standard Model with Strong Interactions

by

Catalina Gómez Sánchez

A thesis submitted in conformity with the requirements
for the degree of Doctor of Philosophy
Graduate Department of Physics
University of Toronto

Abstract

Topics in Physics Beyond the Standard Model with Strong Interactions

Catalina Gómez Sánchez
Doctor of Philosophy
Graduate Department of Physics
University of Toronto
2015

In this thesis we study a few complementary topics related to some of the open questions in the Standard Model (SM). We first consider the scalar spectrum of gauge theories with walking dynamics. The question of whether or not a light pseudo-Nambu-Goldstone boson associated with the spontaneous breaking of approximate dilatation symmetry appears in these theories has been long withstanding. We derive an effective action for the scalars, including new terms not previously considered in the literature, and obtain solutions for the lightest scalar's momentum-dependent form factor that determines the value of its pole mass. Our results for the lowest-lying state suggest that this scalar is never expected to be light, but it can have some properties that closely resemble the SM Higgs boson.

We then propose a new leptonic charge-asymmetry observable well suited for the study of some Beyond the SM (BSM) physics objects at the LHC. New resonances decaying to one or many leptons could constitute the first signs of BSM physics that we observe at the LHC; if these new objects carry QCD charge they may have an associated charge asymmetry in their daughter leptons. Our observable can be used in events with single or multiple leptons in the final state. We discuss this measurement in the context of coloured scalar diquarks, as well as that of $\bar{t}t$ pairs. We argue that, although a fainter signal is expected relative to other charge asymmetry observables, the low systematic uncertainties keep this particular observable relevant, especially in cases where reconstruction of the parent particle is not a viable strategy.

Finally, we propose a simple dark-sector extension to the SM that communicates with ordinary quarks and leptons only through a small kinetic mixing of the dark photon and the photon. The dark sector is assumed to undergo a series of phase transitions such that monopoles and strings arise. These objects form long-lived states that eventually decay and can account for the observed cosmic-ray positron excess observed by the PAMELA and Fermi satellites. This topological Dark Matter (DM) can account for the Universe's DM content if the coupling in the dark sector is strong.

Dedication

A mi abuelita Bertha

Acknowledgements

I am extremely grateful to my supervisor Bob Holdom for his guidance and support during my years at the University of Toronto. His unique perspective and approach to problems has been and will continue to be inspiring even outside the realm of physics and academia. I am also thankful to my office mate and collaborator Melissa Ratzlaff, whose contribution has made some of the work presented here possible. I am deeply grateful to my former fellow graduate students Simon Freedman, William Man Yin Cheung and Santiago de Lope Amigo, as well as Mohamed Anber, for endless discussions, laughs, and above all for their friendship. I would also like to extend a huge thank you to my PhD committee members Pierre Savard and Erich Poppitz for their time and support throughout these years.

A very special thank you to my good friends and companions-in-grad-school Federico Duque and Niall Ryan for being my Canadian brothers. To my wonderful fiancé Cathal I am simply grateful beyond words. I never would have made it without you. Finally, I would like to thank my family in Colombia, and especially my brother and sister who are such a huge joy in my life, and my parents who will always be at the top of my wonderful humans list, and whose hard work I owe for the privilege of education, and everything else. Thank you.

Contents

1 Introduction **1**

1.1 QCD, Walking Technicolour and the dilaton 3

1.2 Lepton based asymmetry measurements at the LHC 7

1.3 Dark Matter 8

1.4 Organization of the thesis 11

2 On the Scalar Spectrum of Walking Gauge Theories **12**

2.1 Introduction 12

2.2 The effective action and the gap equation 14

2.3 The curvature of V_{AF} and the scalar spectrum 23

2.4 The pion 36

2.5 Discussion of a simple five-dimensional model 40

2.6 Conclusions 42

2.7 Appendix 44

3 Lepton based Charge Asymmetry Measurements and Diquarks **48**

3.1 Introduction 48

3.2 A new charge asymmetry observable and scalar Diquarks 50

3.3 A_C^l and the $t\bar{t}$ Charge Asymmetry 56

3.4 The Diquark Charge Asymmetry 59

3.5 Concluding Remarks 64

4 Monopoles, strings and dark matter **65**

4.1 Introduction 65

4.2 Mixing and monopoles 68

4.3 Monopole densities 70

4.4 Lifetimes 72

4.5 More energy loss 77

4.6 Strings and $\boldsymbol{\gamma}_h$'s 80
4.7 Late times 81
4.8 Direct detection 83
4.9 Outlook 85

5 Conclusions and Future Prospects **86**

Chapter 1

Introduction

The Standard Model (SM) of particle physics has proved to be an extremely successful description of the world at the most fundamental level as we know it. However, despite its many successes there are several important issues that remain unsolved in the context of our current understanding. This has led the particle physics community at large to believe that the Standard Model as it stands can only be an effective low energy description of a more complete theory. The hope is that this more complete theory will also shed light into closely related problems from astrophysics and cosmology, as for example the particle nature of Dark Matter, one of the topics that will be discussed here, and the origin of dark energy.

One of the open questions at the core of the SM that has been the centre of attention in recent years is the nature of Electroweak Symmetry Breaking (EWSB). On July 4, 2012, the ATLAS and CMS collaborations at the Large Hadron Collider (LHC) announced that a particle resembling the SM Higgs had been discovered at a mass of 126 GeV [2,3]. Since then, both collaborations have been busy searching for discrepancies between the properties of the observed particle and the SM Higgs. To this date, all published results point towards the surprisingly simple, and yet theoretically troubling Higgs particle.

The SM Higgs is a fundamental scalar particle, the physical (electrically neutral) degree of freedom predicted from adding a complex scalar $SU(2)_L$ doublet to the SM, with a potential such that minima occur at non-zero values of the scalar field, i.e, the scalar acquires a non-zero expectation value. This scalar couples to SM matter fields via Yukawa couplings; when the scalar obtains a non-zero expectation value, these terms become mass terms for all SM fermions. At the same time, mass terms for the W and Z bosons allowed by the gauge symmetries are generated, in other words electroweak symmetry is spontaneously broken. An obvious problem with this picture appears when we consider one-loop corrections to the Higgs mass.

One-loop corrections to the Higgs mass in the SM are additive and proportional to the high energy scale at which new physics is expected to appear (e.g, the GUT scale or the Planck scale). This is in contrast with radiative corrections to fundamental fermions in the SM, where a chiral symmetry acts as a custodial symmetry guarding the "smallness" of the fermion masses, keeping all radiative corrections multiplicative. Even long prior to the discovery of the 126 GeV boson at the LHC, we have known that the mass of the Higgs should be of the order of a few hundred GeV (see e.g [4]), as dictated by precision SM measurements. But there appears to be no fundamental reason as to why a (fundamental) scalar should appear at the 10^2 GeV scale.

The most popular solution to the hierarchy problem has been that of a Supersymmetric (SUSY) extension to the SM. In this picture, all SM particles have a supersymmetric partner, of integer spin for fermions and of half-integer spin for bosons. The partners to SM fermions have just the right couplings to exactly cancel their contributions to the Higgs mass. More fundamentally, the chiral symmetry that protects the Higgs's fermionic partners is extended to protect the mass of the scalar by virtue of supersymmetry. Obviously we do not observe supersymmetric partners for SM particles in our everyday lives, hence if supersymmetry is to be an adequate description of the world, this symmetry tying SM to their partners must be broken. Weak-scale supersymmetry predicts TeV scale particles that should show signs of existence at the LHC. Hence, the search for SUSY partners of SM fields has been a large part of the LHC program in recent years. At the time of this manuscript's writing, signs of SUSY have yet to show up at the LHC. In this current state of affairs, it is reasonable to say that SUSY is unlikely to be responsible for successfully solving the SM's hierarchy problem and rendering the weak scale natural.

An alternative paradigm that has enjoyed much less popularity in the recent past is that of Dynamical EWSB due to a new strongly interacting sector. In our view this is quite a conservative approach to solving the hierarchy problem: the strong interactions in the SM have already given us a working example of how one can break EW symmetry without the need of introducing fundamental scalars, by virtue of chiral symmetry breaking (χSB) as triggered by fermion condensates in QCD. There is no hierarchy problem in QCD; the large hierarchy between Λ_{QCD} and the Planck scale arises naturally from the quantum theory itself through dimensional transmutation. The hope for a dynamical picture of EWSB is that the lessons learned from QCD could be used to understand the origin of the weak scale.

Before we proceed with the introduction, we would like to let the reader know that in this thesis we shall be studying a few complementary topics in physics Beyond the Standard Model (BSM) which are, in principle, independent of each other. However,

there is a common thread unifying this discussion, which is the presence of strongly interacting gauge theories and some of the different aspects of their phenomenology. We shall now proceed along the ideas of the previous paragraph towards introducing the background that will lead us to the discussion of the scalar spectrum of gauge theories with strong dynamics and chiral symmetry breaking. We shall then work our way back to introducing the other two main topics contained in this document. One involves possible ways of measuring collider signatures of certain BSM objects that may arise in strongly coupled extensions of the SM. The second involves a decaying DM candidate from a non-Abelian dark sector where the gauge coupling is strong.

1.1 QCD, Walking Technicolour and the dilaton

Armed with the knowledge from QCD, theorists in the 80's set out to find a dynamical theory of EWSB. The idea would be to have a new confining gauge interaction, technicolour (TC), with QCD-like dynamics at the weak scale as well as new massless chiral fermions carrying TC charge (but not necessarily colour charge, this depends on the particular model), the technifermions. In analogy with QCD, a condensate of technifermion bilinears is generated

$$\langle \bar{Q}_{iL} Q_{jR} \rangle \approx \Lambda_{TC}^3 \delta_{ij}, \tag{1.1}$$

where Λ_{TC} is the scale analogous to Λ_{QCD} of order the weak scale, v_{weak}. As a result, techniquarks acquire a (constituent) mass of order Λ_{TC}, and composite states such as technibaryons arise. There are also a number of (composite) Nambu-Goldstone bosons (NGB) resulting from the breaking of any global symmetries by the condensates. In order for EW symmetry to be broken, $SU(2)_L \times U(1)_Y$ must be a gauged subgroup of the original global chiral symmetry of the technicolour theory. In this way, when the gauge interactions are "turned on", the NGBs become the longitudinal Ws and Z bosons.

TC on its own does not address the flavour problem. In order to be able to give SM fermions their masses and mixing angles, an extension to the TC gauge group must be considered such that the new interaction couples SM fermions (that do not carry TC charge) to technifermions. The Extended Technicolour (ETC) gauge group must be broken at scales below Λ_{ETC} leaving only the TC and SM gauge groups unbroken. At low energies, the exchange of heavy ETC gauge bosons gives rise to effective contact terms between SM and TC fermions. The effective terms of greatest phenomenological importance that arise from these contact terms are as follows (see e.g. [5]):

1) "α" terms of the form

$$\alpha_{ab}\frac{\bar{Q}T^aQ\bar{Q}T^bQ}{\Lambda^2_{ETC}}, \tag{1.2}$$

where the T^a are the ETC generators, including the relevant chiral factors, and also including $T^0 \equiv \mathbb{1}$. These terms can give masses to potentially too light pseudo Nambu-Goldstone bosons (PNGB), "techniaxions" for example. This is a desirable consequence as it allows the masses of these particles to be more consistent with experimental bounds.

2) "β" terms of the form

$$\beta_{ab}\frac{\bar{Q}_LT^aQ_R\bar{\psi}_RT^b\psi_L}{\Lambda^2_{ETC}}. \tag{1.3}$$

These terms will generally give the masses to (and mixing between) SM fermions ψ, the main purpose of the ETC sector.

3)"γ" terms of the form

$$\gamma_{ab}\frac{\bar{\psi}_LT^a\psi_R\bar{\psi}_RT^b\psi_L}{\Lambda^2_{ETC}}. \tag{1.4}$$

These terms are four fermion interactions between SM fermions and will generally give rise to Flavour Changing Neutral Currents (FCNC). Assuming $\alpha \sim \beta \sim \gamma$, these terms pose a big obstacle for TC models: in order to generate the right pattern of fermion masses, and to raise PNGB masses to avoid bounds, it appears one is also necessarily generating dangerously large FCNC in the SM.

An elegant and enticing solution to this problem is found by modifying the dynamics of the theory such that the running of the TC coupling is no longer QCD-like, but is near a fixed point of the theory such that it remains strong and runs very slowly (or "walks") at scales higher than Λ_{TC}. This was first suggested in [6]. One can look at the ETC operators that give rise to the fermion mass terms in "β" type terms above. The renormalization effects due to TC, between the TC and ETC scales, for these operators can be written as [5]:

$$\langle\bar{Q}Q_{ETC}\rangle = \exp\left(\int_{\Lambda_{TC}}^{\Lambda_{ETC}} d\ln(\mu)\gamma_m(\alpha(\mu))\right)\langle\bar{Q}Q_{TC}\rangle \tag{1.5}$$

where γ_m is the anomalous dimension as a function of the running coupling. If TC is QCD-like, then the coupling $\alpha(\mu)$ falls off as $\sim 1/\ln(\mu)$ and, assuming $\gamma \sim \alpha$, we can immediately see that the exponential factor on the right-hand side (RHS) of Eq. 1.5 goes as $\left(\ln(\frac{\Lambda_{ETC}}{\Lambda_{TC}})\right)^{\gamma_m}$. If on the other hand we consider a theory near a fixed point such that

the coupling is almost constant between these two relevant scales, the exponential factor instead becomes

$$\exp\left(\int_{\Lambda_{TC}}^{\Lambda_{ETC}} d\ln(\mu)\gamma_m(\alpha(\mu)\approx const.)\right) = \exp\left(\gamma_m \ln\left(\frac{\Lambda_{ETC}}{\Lambda_{TC}}\right)\right) = \left(\frac{\Lambda_{ETC}}{\Lambda_{TC}}\right)^{\gamma_m}. \quad (1.6)$$

We can then see that for a walking type theory, it is in principle possible to enhance α and β terms by a significant amount without enhancing problematic γ terms.

Infrared fixed points (IRFP) are known to exist in gauge theories in the perturbative regime, where the gauge coupling is weak. One such IRFP, that we shall further discuss in upcoming sections, is the fixed point that appears in the (two loop) β function of an $SU(N)$ gauge theory with N_f number of flavours when the coupling $\alpha \sim -b_0/b_1$, where b_0 and b_1 are the coefficients of the first and second term in the β function, respectively. The value of the coupling at the fixed point increases as N_f decreases, which suggests that the fixed point will eventually reach the critical value for chiral symmetry breaking, as is desired for applications to EWSB. Lattice simulations have shown that gauge theories in the strongly coupled regime can indeed exhibit conformal behaviour in the IR [7, 8].

A question of great phenomenological relevance now appears. Since the walking theory is governed by the presence of a (infrared) fixed point for a significant range of momenta, there appears to be an approximate dilatation symmetry in the theory (i.e the theory is approximately scale invariant), which can be spontaneously broken along with chiral symmetry and other global symmetries. In a perfectly conformal theory, the spontaneous breaking of scale invariance should imply the presence of a massless Nambu-Goldstone boson (NGB), the dilaton. The expectation is then that in a theory with approximate scale invariance, a light pseudo-NGB (PNGB) should too appear, and its mass should be somehow proportional to the small degree of explicit breaking. This is in analogy to the pions in the SM, which are the PNGBs of approximate chiral symmetry.

The scale current for a general Lagrangian takes the following form

$$\mathcal{D}^\mu = x_\nu \theta^{\mu\nu}, \quad (1.7)$$

where $\theta^{\mu\nu}$ is the (non-symmetric) energy-momentum tensor given by Coleman and Jackiw [9]. The divergence of this current is then given by

$$\partial_\mu \mathcal{D}^\mu = g_{\mu\nu}\theta^{\mu\nu} + x_\nu \partial_\mu \theta^{\mu\nu} = \theta^\mu_\mu, \quad (1.8)$$

where the second term vanishes as required by Poincaré invariance. The above equation

implies that only when the energy-momentum tensor is traceless is the theory *classically* scale invariant. This is true for a classical Lagrangian containing no dimensionful parameters [9]. Of course in general, quantum corrections tend to spoil classical scale invariance, as is the case in QCD for example, where the scale Λ_{QCD} is dynamically generated. More explicitly, one can write $\theta^{\mu}_{\mu} = \frac{\beta(\alpha)}{4\alpha} G^{a}_{\mu\nu} G^{a\mu\nu}$ where α is the renormalized coupling constant defined at some scale μ, β is its beta function, and $G^{a}_{\mu\nu}$ is the (renormalized) field strength tensor [10]. Hence, classical scale invariance is explicitly broken by this "trace anomaly" when the coupling runs. We can see that the explicit breaking can be made small if we can justify a small β function. Then, if a dynamical mass appears in the theory, as is the case in theories where chiral symmetry is spontaneously broken, the approximate scale symmetry is also spontaneously broken.

The Schwinger-Dyson (SD) equations provide an appropriate framework for the study of non-perturbative phenomena in gauge theories. The SD equation for the fermion propagator $i(Z(p)\not{p} - \Sigma(p))^{-1}$, which is given by

$$\Sigma(p) + (1 - Z(p))\not{p} = g \int \frac{d^4k}{(2\pi)^4} \gamma^{\mu} G_{\mu\nu}(p-k) \frac{i}{Z(k)\not{k} - \Sigma(k)} \Lambda^{\nu}(p, k, p-k), \tag{1.9}$$

where $G_{\mu\nu}$ is the gauge boson propagator and Λ^{ν} is the fermion-gauge boson vertex, must be solved self-consistently and therefore allows for non-perturbative solutions. Eq. 1.9 is also known as the gap equation, given that non-trivial solutions for the function $\Sigma(p)$ indicate the appearance of a "mass gap" in the theory, i.e, the dynamical generation of mass. In fact, $\Sigma(p)$ can also be naturally understood as the order parameter for chiral symmetry breaking. We can look at the vacuum expectation value of $\bar{\psi}\psi$ which is determined by closing the (full) fermion propagator into a loop:

$$\langle \bar{\psi}\psi \rangle = -4iN_c \int \frac{d^4p}{(2\pi)^4} \frac{\Sigma(p)}{Z^2(p)p^2 - \Sigma^2(p)}. \tag{1.10}$$

If the LHS above is non-zero, then the QCD vacuum is not invariant under chiral transformations, that is, chiral symmetry has been spontaneously broken. Then, $\Sigma(p)$ will also be non-vanishing.

The argument that walking technicolour (WTC) should have a small β function over a large range of momenta as we have mentioned above, has been used since the early days of WTC to assert that indeed a light PNGB should appear in the spectrum of such theories, and that its presence would be an important low-energy signature of near-conformal dynamics [11,12]. A counter argument to this idea was presented in [13], where an integral expression for the dilaton mass was obtained involving the function $\Sigma(p)$, by

studying the change in the effective action when the order parameter $\Sigma(p)$ undergoes a chiral transformation[1]. What the authors of [13] find is that, as β becomes smaller and smaller such that one approaches the IRFP, the function inside the integral tends to peak at larger momenta. As a result, the mass integral becomes increasingly sensitive to momentum scales where the coupling is rapidly decreasing. Hence, the explicit breaking of scale invariance is not small.

It appears that the issue of whether a light dilaton should generally be present in gauge theories (exhibiting spontaneous breaking of approximate scale symmetry) is far from settled, however. Even in recent years, the debate continues [14, 15]. Most notably, in 2011 Appelquist and Bai [14] have re-sparked the debate by arguing that a dilaton parametrically light relative to the scale of χSB does appear. In their work, they turn to a partially conserved dilatation current (PCDC) analysis, in complete analogy with the partially conserved axial current (PCAC) analysis used in QCD to obtain an estimate for the mass of the pions. In their local approach, they are forced to make a subtraction procedure in order to obtain a cutoff independent expression for the vacuum expectation value of θ^{μ}_{μ}, where the contributions from high momentum scales are removed.

Being aware that non-local contributions from high momentum scales likely play an important role in this problem, we have been inspired to revisit the issue by taking a non-local effective action approach in a large N_C type theory. As a spoiler to Chapter 2, let us state in advance that our results agree with the nay-sayers; there should not be a light degree of freedom associated with the spontaneous breaking of scale invariance present in the low energy spectrum. But we do also find new qualitative features that generally apply to gauge theories with chiral symmetry breaking that could be phenomenologically relevant at the weak scale or beyond.

1.2 Lepton based asymmetry measurements at the LHC

Despite the very confusing state that we, as a high-energy physics (HEP) community, appear to find ourselves in, with an unnatural looking Higgs boson and not much else so far to light the way, we have still thought about the types of measurements one could turn to in case that anomalies do start to appear at the LHC in the coming years. In fact, hints of a possible excess in the lepton counts of some channels have recently made an appearance in the ATLAS experiment [16].

[1] As the authors of [13] point out, this procedure is analogous to finding the pion mass by studying how the vacuum energy varies after performing a chiral transformation on $\langle\bar{\psi}\psi\rangle$.

If some extended sector with strong dynamics is indeed responsible for generating the weak scale, as for example in a theory where N_C is small unlike the case that we have discussed in the previous section, looking for signatures from the lightest states expected to be present in such a picture would be a logical starting place. PNGBs with a wide array of quantum numbers can arise depending on the global symmetries being broken along with the spontaneous breaking of EW symmetry. With the model of [17] initially in mind, we became interested in the type of signatures that coloured scalars with diquark quantum numbers could generate. Coloured diquarks in fact should display a charge asymmetry from QCD analogous to that of $t\bar{t}$ pairs at the LHC. We shall discuss this in more detail later on. But unlike the case of $\bar{t}t$, diquarks are also a good illustration of a type of object that would likely be very hard to reconstruct.

Generally, diquarks will decay in complex chains often leading to final states with many high energy leptons. Fermion based asymmetry observables are then an obvious choice to explore as discriminating factors in any possible mysterious excesses that may emerge in lepton counts. Observables of this type could also be of interest for weak models of coloured scalars, that are not PNGBs and therefore even more mysterious in origin.

1.3 Dark Matter

Dark Matter (DM), as well as Dark Energy, are essential ingredients of the current Standard Cosmological model. This sophisticated picture of the Universe successfully describes many key properties, from the Universe's thermal history, to the abundance of elements and the relic background radiation, to the observed large scale structures. Although the role that these components play is crucial in this fundamental picture, their specific nature remains very much a mystery. From the particle physics standpoint, one could argue that the inability of the SM to put forth a viable DM candidate is yet another indication for the necessity to go beyond the SM. This, along with other open questions such as the origin of neutrino masses, as well as the source(s) of CP violation necessary to successfully account for Baryogenesis in the early universe, are evidence of the strong interplay between particle physics, astrophysics, and cosmology. As we search to expand our understanding of the Universe we can ultimately hope that the aforementioned questions may all share common answers.

Evidence for the existence of (non-baryonic) DM comes from various independent observations across a wide range of distance scales. At the galactic scale, one key observation comes from the rotation curves of galaxies, see, e.g, [18]. Plots of the circular

velocities of stars and gas in galaxies as a function of the distance to the galactic centre tend to become flat at large radii, even past the edge of the visible galactic disk. This behaviour is unexpected in the context of Newtonian dynamics, where the velocity curve is expected to fall off as $\sim r^{-1/2}$ past the edge of the "optical disk". Closely related to this point is also the observation of the velocity dispersions of satellites of spiral galaxies. In the case of the Milky Way, there are dwarf spheroidal galaxies and globular clusters satellites that probe the outer rotation curve of the galaxy. These curves suggest the presence of an invisible matter halo that extends well beyond the optical disk [19]. Weak gravitational lensing observed around nearby structures also indicates the presence of more matter than would appear from the object's luminosity (see for example [20]).

On larger scales, the observation and analysis of the cosmic microwave background's (CMB) power spectrum has allowed us to estimate what percentage of the total energy "budget" of the Universe is taken up by Dark Matter. WMAP (Wilkinson Microwave Anisotropy Probe) data in particular places stringent constraints on the allowed relative abundances of baryonic matter Ω_b and total matter Ω_M (and hence, of DM) in the Universe, where the Ωs are the density ratios of baryonic matter and total matter to the critical density ρ_c, respectively. These values, as presented in reference [21], are $\Omega_b = 0.0554 \pm 0.0028$ and $\Omega_M h^2 = 0.1345 \pm^{0.0056}_{0.0055}$.

The evidence for the existence of DM mentioned above, all pertains to its gravitational interactions. If we are to include a DM candidate in some extension of the SM, it is both reasonable and interesting to consider other types of interactions to SM particles. This idea has had a surge of interest from the community in the past years in light of some astrophysical anomalies that have arisen in charged cosmic-ray and γ-ray measurements [22–24].

In 2009, the PAMELA experiment observed that, between the energies of 10 GeV to about 100 GeV, there was a steep increase in the energy spectrum of the positron fraction $e^+/(e^- + e^+)$ of cosmic rays [22], a feature that is not expected in the background since high-energy electrons and positrons traveling large distances are subject to large energy losses. Hence, this type of observation points to local primary sources of the particles decaying to electron-positron pairs. It is also important to note that no corresponding excess in the anti-proton fraction was observed. The Fermi satellite later independently confirmed the positron excess observed by PAMELA and extended the measurement to a couple of hundred GeV [23]. In principle, these anomalies could possibly be explained by astrophysical objects such as pulsars [25]. Nevertheless they pose an exciting challenge to be interpreted in terms of indirect signals of Dark Matter annihilation or decay.

For a DM model to be able to explain these excesses in the local flux of charged cosmic

rays, the DM particle must have a mass of a few TeV in order to fit the "bump" in the positron fraction spectrum, but it must not also decay to anti-protons since, as noted, no such excess is observed. Additionally, if we are dealing with DM annihilations, then the DM must also have quite a large annihilation cross section in order to significantly raise the local positron flux. This is an important challenge for traditional models where the DM is a thermal relic, since the required annihilation cross section must be much larger than that required in the early universe to leave behind the right DM relic density. Several mechanisms for enhancing the DM annihilation cross section at late times have been proposed by DM model builders. However, a possibly more attractive approach would consist in considering a DM candidate that acts as a primary source of electron and positron pairs, not by annihilating, but by decaying.

Reference [26] showed in a model independent analysis, that the effective lifetime of the decaying DM particle must be of the order of 10^{26}s if it is to yield the right flux at current times to explain the PAMELA and Fermi excesses. If one can conjure up a model with a DM candidate decaying with the appropriate lifetime, that by some other independent mechanism is prevented from decaying into protons, then there are also other advantages in the form of alleviated bounds from γ-ray (and neutrino) fluxes coming from the galactic centre. For decaying DM, the γ-ray flux coming from the galactic centre where DM densities are generally largest goes linearly with the DM density, whereas for the case of annihilating DM the flux is proportional to the DM density squared. Hence, constraints that can be quite stringent on the latter scenarios become less important in the case of a decaying DM candidate.

The model that we shall present in this document does indeed satisfy all of the above requirements, but also takes a rather unusual form; let us briefly discuss the main aspects of it here. We shall consider a non-Abelian dark sector that undergoes spontaneous symmetry breaking in a pattern such that, for some period of time in the history of the Universe, an intermediate unbroken $U(1)$ gauge symmetry remains but is sequentially (spontaneously) broken. As a result of these phase transitions, a series of topological defects appear as massive degrees of freedom, which make up the dark matter candidate. As we shall see, there are several aspects of the working theory that will push us to consider a strong coupling in the dark sector. Initially, it is the right relic abundance for DM that seems to require it. Coincidentally, this choice also provides us with a mechanism to avoid Big Bang nucleosynthesis (BBN) constraints for our long-lived hidden photon in the early universe. The symmetry breaking pattern can then be assumed to be driven naturally by the dynamics of the theory, a feature we find just as desirable in the hidden sector as we did in the discussion of EWSB in the SM from

Section 1.1.

1.4 Organization of the thesis

The rest of this document shall be organized as follows. In Chapter 2 we revisit the problem of the existence of a light dilaton associated to the spontaneous breaking of scale invariance in gauge theories, as introduced in the end of Section 1.1. In Chapter 3 we shall shift gears and explore lepton based asymmetry measurements at the LHC, inspired by objects that may arise in strongly interacting extensions of the SM as previously mentioned. In Chapter 4 we turn to the second open question discussed in this introduction, namely the particle nature of Dark Matter. We propose a model of decaying dark matter based on a strongly interacting hidden sector, and intended to attempt to explain some of the astrophysical anomalies mentioned here. Finally, our concluding remarks and future prospects can be found in Chapter 5.

Chapter 2

On the Scalar Spectrum of Walking Gauge Theories

The work presented in this chapter was done in collaboration with Bob Holdom and is currently being prepared for submission.

2.1 Introduction

The existence of a light, scalar degree of freedom associated with the spontaneous breaking of approximate dilatation symmetry or scale invariance (SI) in gauge theories has been the topic of discussion for many decades now. This idea sparked much interest in the context of Technicolour (TC) extensions of the Standard Model (SM) relevant for EWSB, after early on it was realized that one of the serious shortcomings of TC, namely the generation of Flavour Changing Neutral Currents (FCNC) in conflict with precision SM observables, could be avoided if the dynamics of the theory were modified in such a way that the strong coupling responsible for the generation of (techni) quark condensates were to walk, i.e. run very slowly [27]. In this regime, the divergence of the dilatation current, given by

$$\partial_\mu \mathcal{D}^\mu = \frac{\beta(\alpha)}{3\alpha} G^{a\ \mu\nu} G^a_{\mu\nu}, \tag{2.1}$$

where $\mathcal{D}^\mu = \theta^{\mu\nu} x_\nu$, can become arbitrarily small such that it is partially conserved, and the approximate symmetry spontaneously broken along with other (exact or approximate) global symmetries of the theory such as chiral symmetry.

This argument has been often used, along with a Partially Conserved Dilatation Current (PCDC) analysis analogous to the Partially Conserved Axial Current (PCAC) one used to estimate the pion's mass in QCD, to ascertain that a dilaton parametrically

light relative to the confinement scale Λ is expected in theories with walking dynamics [14], [28].

We have revisited this problem by studying the effective action for the scalar modes that would be present in an $SU(N)$ gauge theory with N_f number of flavours, starting from a *non-local* effective action derived using the auxiliary field (AF) method [29,30], and working in the renormalization-group improved ladder approximation where the running coupling is adopted from the two-loop perturbative result known to possess an infrared fixed point. We are going beyond previous studies by adapting the systematic method suggested by Fraser in [31] to determine the kinetic terms that should appear in the scalar (and pseudo-scalar) field's effective action, which also allows us to include effects of the interaction term in the effective action into our solutions. As we shall see, our results point to the fact that there are important non-local contributions to the "dilaton" mass coming from UV physics that are naturally included in our approach, but that are absent from (more common) purely local analyses, that lift the mass of the lightest scalar excitation to be of order the dynamical fermion mass scale.

For theories of interest for EW physics, we require that the coupling be strong enough to generate a quark condensate and hence trigger chiral symmetry breaking.[1] As we advance towards our goal of predicting the mass for the lowest lying scalar state in the theory, we will indeed be forced to make a series of approximations in order to obtain useful results, and to ultimately obtain numerical solutions for the fermion and scalar mass functions $\Sigma(p)$ and $\Delta(p)$. We shall present plots of our solutions $p\Delta$ and $p\Sigma$, the quantities that appear inside of the integral equations that determine the mass spectrum of the theory, in order to illustrate the behaviour of the solutions across a large range of momenta. We hope that it will become clear to the reader that our results suggest a robust qualitative picture that we expect should survive beyond the approximations we have worked in, and that furthermore, these non-local contributions to the scalar's mass that we have mentioned should not tend to vanish as the theory approaches the fixed point.

This chapter is organized as follows: in Section 2.2 we derive an effective action that is a functional of the momentum dependent fermion mass function Σ, and obtain non-trivial numerical solutions for Σ via a differential form of the gap equation. In Section 2.3 we derive an effective action for the scalar fields, and we solve the differential equation that determines the mass spectrum including both terms in the original effective action. In Section 2.4 we discuss the Goldstone bosons and obtain an integral expression for the

[1] Strictly speaking, this is not necessarily true if one is willing to consider a particular limit, which we shall briefly discuss towards the end of Section 2.3.

pion's decay constant. The idea that a strongly coupled, near-conformal theory could be responsible for EWSB along with the AdS/CFT correspondence have also brought the dilaton, which is the dual of the radion in the holographic picture, to the spotlight in recent years, in particular in light of the 126 GeV scalar Higgs discovery. While we have nothing to add to the holographic description from our gauge theory context, we shall comment on some of the similarities in the equations on either side of this duality in Section 2.5. Concluding remarks can be found in Section 2.6.

2.2 The effective action and the gap equation

In order to study the dynamical generation of mass and chiral symmetry breaking in gauge theories, we shall now turn to the effective action formalism. This approach allows us to derive the Schwinger-Dyson equation for the full quark propagator or the "gap equation", that we can solve using a series of approximations, allowing us to observe non-perturbative phenomena.

Let us start by considering the path integral for an $SU(N)$ gauge theory with N_F flavours of massless fermions in the fundamental representation. We will use the auxiliary field (AF) method to derive an effective action. This consists in adding a Gaussian term with a bilocal auxiliary composite field to the action, such that the actual dynamics of the theory remains unchanged. This can be achieved by inserting a constant into the path integral of the form:

$$c = \int [dT] e^{\frac{1}{2}\mathrm{Tr}(T-\psi\bar{\psi})G(T-\psi\bar{\psi})}, \tag{2.2}$$

Then, by coupling a source J to this composite field $T(x,y)$ we can derive an expression for the effective action, to a given order in T loop expansion,

$$e^{iW_{AF}[J]} = \int [d\psi][d\bar{\psi}][dT] \exp[i(i\psi S_0^{-1}\bar{\psi} + I_{int} - \frac{i}{2}\mathrm{Tr}(T-\psi\bar{\psi})G(T-\psi\bar{\psi}) + \mathrm{Tr}JT)]. \tag{2.3}$$

Here, G is so far an arbitrary function and I_{int} includes the integration over the gauge fields. Note that we are using matrix notation which replaces integration over space-time coordinates. For non-Abelian gauge theories, integration over the gauge fields cannot be performed exactly due to self-interactions. However, if we ignore self-interaction vertices,

at least for now, we can perform the integral over the gauge fields to obtain:

$$I_{int} = D_{\mu\nu}(x-y)\left[\overline{\psi}^i_\alpha(x)\gamma^\mu\left(\frac{\lambda^a}{2}\right)_{\alpha,\beta}\psi^i_\beta(x)\right]\left[\overline{\psi}^j_\delta(y)\gamma^\nu\left(\frac{\lambda^a}{2}\right)_{\delta,\sigma}\psi^j_\sigma(y)\right] \tag{2.4}$$

where the λ^a are the generators of the gauge group and $D^{\mu\nu}$ is the (tree level) gauge boson propagator. The AF method is particularly useful when these types of quartic interactions are involved. We can make the following choice for the function G

$$G_{\alpha\beta,\delta\sigma} = D_{\mu\nu}(x,y)\gamma^\mu\left(\frac{\lambda^a}{2}\right)_{\alpha,\beta}\gamma^\nu\left(\frac{\lambda^a}{2}\right)_{\delta,\sigma} \tag{2.5}$$

such that the four-fermion term in I_{int} cancels. Then, we can proceed to integrate out the fermions fields to obtain

$$e^{iW_{AF}[J]} = \int [dT]\exp\left[i(-i\mathrm{Tr}\ln(S_0^{-1}-DT) - \frac{i}{2}\mathrm{Tr}TDT + \mathrm{Tr}JT)\right]. \tag{2.6}$$

where D is given in Eq. 2.11 below. We will now take the tree level approximation in the T field. The resulting expression for the effective action $\Gamma_{AF}[T]$ is

$$\Gamma_{AF}[T_c] = W[J] - \mathrm{Tr}(JT_c) = -i\mathrm{Tr}\ln(S_0^{-1}-DT_c) - \frac{i}{2}\mathrm{Tr}(T_cDT_c) \tag{2.7}$$

where T_c is T such that it satisfies the equation for the stationary phase condition:

$$\frac{\delta\Gamma_{AF}[T]}{\delta T} = -J = iD(S_0^{-1}-DT)^{-1} - iDT. \tag{2.8}$$

We can now define the self energy Σ and eliminate T

$$\Sigma = iDT_c. \tag{2.9}$$

Fourier transforming the RHS of Eq. 2.7, where as before the integrals (now over four-momenta) are implicit in the trace, we finally obtain:

$$\Gamma_{AF} = -i\mathrm{Tr}\ln(\gamma\cdot p - \Sigma) + \frac{i}{2}\mathrm{Tr}(\Sigma D^{-1}\Sigma). \tag{2.10}$$

Here we give the expression for the kernel D in momentum space, with the gauge boson propagator in Landau gauge

$$D(k)_{\alpha\beta,\gamma\delta} = ig^2(k)(\gamma^\mu)_{\alpha\delta}(\gamma^\nu)_{\gamma\beta}\frac{1}{k^2}\left(\eta_{\mu\nu} - \frac{k_\mu k_\nu}{k^2}\right). \tag{2.11}$$

Our choice of gauge can be motivated as follows: while the most general expression for the full fermion propagator (allowed by Lorentz and parity invariance) is of the form

$$S = \frac{i}{Z(p)\gamma \cdot p - \Sigma(p)}, \tag{2.12}$$

in Landau gauge we know that the wave function renormalization vanishes at lowest order, and hence $Z(p) \to 1$ for $p \gg \Sigma(p)$. More importantly, however, one can show that in the ladder approximation, that we believe is equivalent to that which we have taken above, $Z(p)$ is exactly equal to 1 for every $\Sigma(p)$ [32], and will therefore not appear in our final expression for the effective action.

As pointed out by the authors of [33] this approximation in the AF formalism is equivalent, up to first derivatives of the effective action Γ, to taking the two loop approximation of the Cornwall-Jackiw-Tomboulis (CJT) effective action (which in the latter, constitutes the lowest non-trivial order.) They have in fact shown that all chiral symmetry breaking, i.e. non-zero, solutions to the gap equation in the CJT formalism are in reality at a saddle point meaning that the effective potential does not give a functional that is bounded from below. The AF formalism solves this problem: the introduction of the T field to the action simply has the effect of modifying W_{CJT} by adding a new term proportional to the square of the source J, and it is this term that is responsible for changing the boundedness properties of the effective potential V such that all solutions now lie in a stable local minima.

We are now ready to derive an expression for the effective potential V, that we shall give in 4-dimensional Euclidean space, and finally the gap equation. Starting from Eq. 2.10 above, we can simplify the first term on the RHS by using $\mathrm{Tr}(\ln A) = \ln(\det A)$ to remove the logarithm from inside the trace. Next, we can make use of the Cayley-Hamilton theorem to re-write the determinant of A as:

$$\det A = \frac{1}{24}[(\mathrm{Tr}A)^4 - 6\mathrm{Tr}(A^2)(\mathrm{Tr}A)^2 + 3(\mathrm{Tr}(A^2))^2 + 8\mathrm{Tr}(A^3)\mathrm{Tr}(A) - 6\mathrm{Tr}(A^4)]. \tag{2.13}$$

Here, $A = \gamma \cdot p - \Sigma$, and so we find:

$$\begin{aligned} \mathrm{Tr}A &= -4\Sigma, \\ \mathrm{Tr}(A^2) &= 4(p^2 + \Sigma^2), \\ \mathrm{Tr}(A^3) &= -12\Sigma p^2 - 4\Sigma^3, \\ \mathrm{Tr}(A^4) &= 4p^4 + 24\Sigma^2 p^2 + 4\Sigma^4. \end{aligned} \tag{2.14}$$

Transforming all momenta to Euclidean space, and integrating over angular coordinates we finally obtain an expression for the effective potential:

$$V[\Sigma] = \frac{1}{2\pi^2}\left(-\frac{1}{2}\int dpp^3 \ln\left(1+\frac{\Sigma^2(p)}{p^2}\right)+\frac{1}{2}\int dpdqp^3q^3\Sigma(p)M^{-1}(p,q)\Sigma(q)\right), \quad (2.15)$$

where p and q denote the magnitudes of Euclidean 4-momenta. $M(p,q)$ is the fermion-antifermion scattering kernel, the inverse of which is defined as:

$$\int r^3 dr M^{-1}(p,r)M(r,q) = \frac{1}{p^3}\delta(p-q) \quad (2.16)$$

following [33].

Before proceeding to deriving the gap equation, it will be useful to first find an explicit form for the kernel $M(p,q)$. Let us do so by considering the following expression:

$$V_D \equiv -\frac{i}{2}\mathrm{Tr}S(p)D(p-q)S(q) \quad (2.17)$$

where, again, the integration over momenta is implied in the trace. We can now insert the expression from Eq. 2.11 into Eq. 2.17 and, assuming that the solution to the gap equation is spherically symmetric in 4-d Euclidean momentum space such that we can integrate over angular variables, we can replace $(p-q)_\mu(p-q)_\nu$ by $\eta_{\mu\nu}(p-q)^2/4$. Then, the term inside the parentheses of Eq. 2.11 becomes $\frac{3}{4}\eta_{\mu\nu}$. We will also need to make an approximation for the gauge boson propagator. We will replace the momentum dependence by the following expression

$$D(p-q)_{\alpha\beta,\gamma\delta} \to D(\max[p,q])_{\alpha\beta,\gamma\delta}. \quad (2.18)$$

Transforming all momenta to Euclidean space, we are now able to perform the angular portion of the 4-momentum integral to obtain

$$V_D = -\frac{1}{2}\frac{1}{2\pi^2}\int dpp^3\int dqq^3\frac{3}{8\pi^2}2C_2\frac{\Sigma(p)}{p^2+\Sigma^2(p)}\left(\frac{g^2(p)}{p^2}\theta(p-q)+\frac{g^2(q)}{q^2}\theta(q-p)\right)\frac{\Sigma(q)}{q^2+\Sigma^2(q)}. \quad (2.19)$$

This yields the desired result, up to the momentum dependence of the running coupling g. We can now define

$$M(p,q) = \frac{r(p)}{p^2}\theta(p-q)+\frac{r(q)}{q^2}\theta(q-p) \quad (2.20)$$

where the running coupling is included in the definition of r,

$$r(p) = \frac{3C_2 g^2(p)}{8\pi^2} = \frac{3C_2\alpha(p)}{2\pi}. \tag{2.21}$$

We have also included some additional factors that appear in the integrals into this definition for convenience. Now, in order to include the effects of the running coupling we shall adopt $\alpha(p)$ from the perturbative result for two-loop $SU(N_c)$ gauge theory with N_f number of flavours, whose beta function is given by:

$$\mu\frac{d\alpha}{d\mu} = -b_0\alpha^2 - b_1\alpha^3 \tag{2.22}$$

where

$$\begin{aligned} b_0 &= \frac{1}{6\pi}(11N_c - 2N_f) \\ b_1 &= \frac{1}{24\pi^2}(34N_c^2 - 10N_cN_f - 3\frac{N_c^2-1}{N_c}N_f). \end{aligned} \tag{2.23}$$

The hope is that, by doing this, we are introducing some of the essential physics coming from corrections to the gauge coupling that we have ignored through the approximations used to derive the effective action above. This theory is known to possess an infrared fixed point with critical $N_f \sim 4N_c$. By treating N_f as a continuous variable we are able to explore the walking (close to conformal) regime expected to appear as we approach the IR fixed point from lower values of N_f towards the critical value.

Solving the Gap Equation

Having found an explicit expression for $M(p,q)$, we can continue to taking the first variation of Eq. 2.15 with respect to Σ. We've finally arrived at the gap equation:

$$\frac{\delta V[\Sigma]}{\delta\Sigma(p)} = \frac{1}{2\pi^2}\bigg(- p^3\frac{\Sigma(p)}{p^2+\Sigma^2(p)} + \int p^3 M^{-1}(p,q)\Sigma(q)q^3 dq\bigg) = 0. \tag{2.24}$$

Using Eq. 2.16 and the fact that $M(p,q)$ is symmetric under p and q exchange, we can re-write Eq. 2.24 as

$$\Sigma(p) - \int M(p,q)q^3\frac{\Sigma(q)}{q^2+\Sigma(q)^2}dq = 0. \tag{2.25}$$

It may be interesting to the reader to note that this is the same gap equation found via Γ_{CJT} in [33].

Eq. 2.25 can of course be solved in its integral form as we have written it above. We can

use matrix notation to turn this into a linear algebra problem, where the non-linear effect in the denominator of the integrand can be built in by iteration, until $\Sigma(p)$ converges to a solution. Alternatively, one can turn this integral equation into a differential one, with its corresponding boundary conditions. This may seem like an unnecessary complication at this stage, as it is not hard to verify that the first method converges after a few iterations. However, as will become evident in the next section once we start to look at fluctuations of the order parameter Σ, the expressions inside the integral analogous to Eq. 2.25 become quite complicated and the first method stops being useful. We therefore opt to take the second approach and transform Eq. 2.25 into a differential equation.

Inserting Eq. 2.20 into Eq. 2.25 we can write the latter as

$$\Sigma(p) = \frac{r(p)}{p^2}\int_0^p dqq^3\frac{\Sigma(q)}{q^2+\Sigma(q)^2} + \int_p^\infty dqr(q)q\frac{\Sigma(q)}{q^2+\Sigma(q)^2}. \tag{2.26}$$

We now differentiate once with respect to p, which shall be indicated by primes below, to obtain

$$\Sigma'(p) = \left(\frac{r'(p)}{p^2} - \frac{2r(p)}{p^3}\right)\int_0^p dqq^3\frac{\Sigma(q)}{q^2+\Sigma(q)^2} \tag{2.27}$$

where the term with a derivative of the integral in the first term of Eq. 2.26 has cancelled against the derivative of the second term. We now multiply all terms by p^3 for convenience and differentiate once more, to obtain

$$p^3\Sigma''(p) + 3p^2\Sigma'(p) = (pr''(p) - r'(p))\int_0^p dqq^3\frac{\Sigma(q)}{q^2+\Sigma(q)^2} + (pr'(p) - 2r(p))p^3\frac{\Sigma(p)}{p^2+\Sigma(p)^2} \tag{2.28}$$

We can make use of Eq. 2.27 to eliminate the integral from the above expression. The resulting differential equation for Σ becomes

$$p^3\Sigma'' + \frac{-r''p^2+4r'p-6r}{r'p-2r}p^2\Sigma - (r'p-2r)\frac{p^3\Sigma}{p^2+\Sigma^2} = 0. \tag{2.29}$$

Before we continue on to defining the boundary conditions required to solve this equation, it will be useful to define the quantity κ as the value of p such that $\kappa\Sigma(\kappa) = \kappa^2$. It will be convenient also to convert to logarithmic coordinates, $t = \ln(p/\kappa)$, in order to study the deep infrared behaviour of Σ. In t coordinates, $p\Sigma$ will intersect the $t = 0$ axis at precisely κ^2. For simplicity we shall, from now on, redefine Σ and p to be dimensionless quantities by dividing each by κ, i.e $p \to p/\kappa$ and $\Sigma \to \Sigma/\kappa$. In this notation, $\Sigma(t = 0)$ must be equal to 1.

Boundary Conditions

In order to solve Eq. 2.29 we must specify two sets of boundary conditions: the IR (initial) condition for both Σ and Σ', and a UV condition for Σ. Let us first consider the IR condition for Σ', as it can be immediately read off from Eq. 2.27: $\Sigma'(p=0)=0$, which becomes $\Sigma'(t\to-\infty)\to 0$ in t coordinates. The IR condition for Σ is given by demanding that at $t=0$, $\Sigma=1$ as we have discussed above.

In the case of a running coupling, the UV condition for $\Sigma(t)$ is simply given by $\Sigma(t\to\infty)\to 0$. In the case of a constant coupling such that r' and r'' terms in Eq. 2.29 vanish, a cutoff Λ must be introduced at high momenta in order to obtain a solution for Σ. The UV condition for Σ will then be given by Eq. 2.26 when $p=\Lambda$, which in t coordinates becomes

$$\Sigma(\ln\Lambda)=\frac{r}{\Lambda}\int_{-\infty}^{\ln\Lambda}\frac{\Sigma(t)}{1+e^{-4t}\Sigma(t)^2}e^t dt. \tag{2.30}$$

Demanding that the above condition be satisfied for a given value of the cutoff Λ will determine the value of r.

We shall now present plots of our numerical solutions of Eq. 2.29 satisfying the boundary conditions described above. Fig. 2.1 is obtained for the case of a constant coupling for three different values of the cut-off $\ln(\Lambda)$, while in Fig. 2.2 and Fig. 2.3 we use the running coupling of Eq. 2.22 with $N_f=11.5$ and $N_f=9$, respectively. The procedure whereby we obtain these solutions is described in detail below.

Solving Eq. 2.29 with a constant coupling

We begin by choosing a (large) value for the cutoff Λ. In theory, since we have already determined the IR conditions for Σ and Σ', all that is left to adjust is the value of the coupling r such that Eq. 2.30 is satisfied. In practice, when searching for numerical solutions to a second order differential equation, the initial conditions for Σ and its first derivative must both be specified at the *same* value of t. If we choose to keep the simple IR condition for Σ' given at $t\to-\infty$ (in practice this will become $t=t_0$ where t_0 takes an arbitrary large negative value[2]) then the initial condition for Σ must be translated to $t\to-\infty$ (t_0 in practice) as well.

We will then start by fixing the IR condition for Σ' as determined already, which now leaves two quantities that must be adjusted in order to obtain the solution for Σ, namely the value of the coupling r and the value of the IR condition $\Sigma(t\to-\infty)$, such that the

[2]For the interested reader, we have chosen $t_0=\ln(0.01)$ and validated this approximation by comparing the solutions obtained this way to the solution obtained in p coordinates, where the IR condition is enforced at exactly $p=0$. We find that both solutions agree extremely well and, in fact, the solution is not sensitive to small changes in the specific choice for t_0.

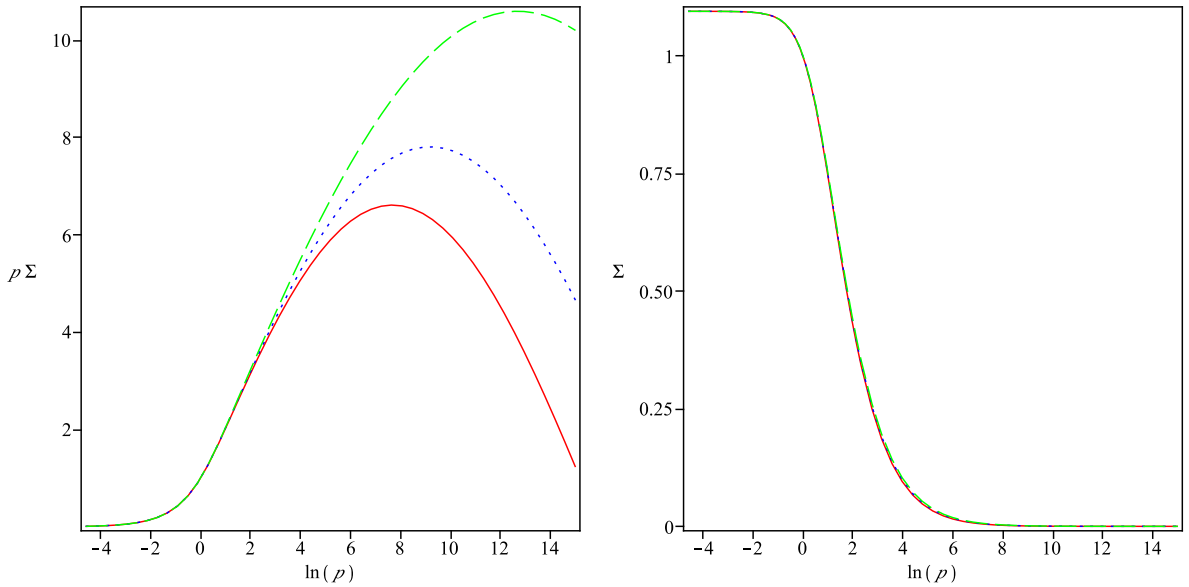

Figure 2.1: Numerical solution for $p\Sigma$ (left) and Σ (right) vs. $t = \ln(p)$ in the case of a constant coupling, with cutoff $\ln \Lambda = 15$ (red line), 18 (blue dots) and 25 (green dotted line). The corresponding values of the coupling r for these three cases are 0.517, 0.513, and 0.507 respectively.

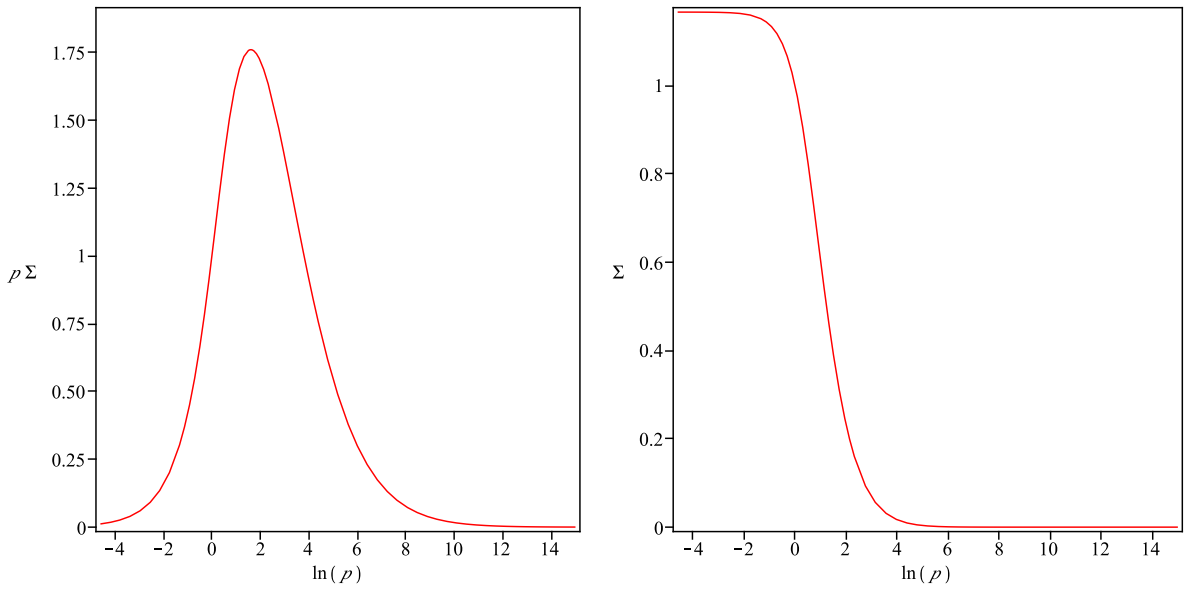

Figure 2.2: Numerical solution for $p\Sigma$ (left) and Σ (right) vs. $t = \ln(p)$ in the case of the running coupling of Eq. 2.22, with $N_f = 11.5$ and $N_c = 3$.

conditions Eq. 2.30 and $\Sigma(t = 0) = 1$ are both satisfied to the desired degree of accuracy. This must be done iteratively starting from arbitrary values until the solution converges. This method is referred to as "shooting".

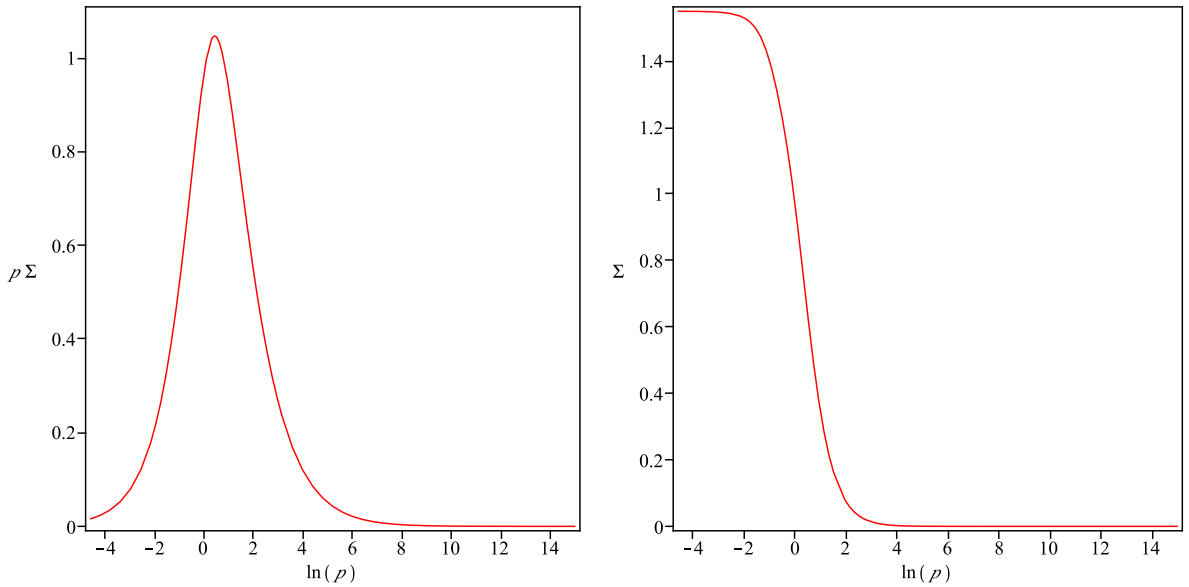

Figure 2.3: Numerical solution for $p\Sigma$ (left) and Σ (right) vs. $t = \ln(p)$ in the case of the running coupling of Eq. 2.22, with $N_f = 9$ and $N_c = 3$.

We would like to note that, given that Eq. 2.29 is nonlinear, once the first condition is satisfied one cannot simply scale the resulting Σ such that the second condition is also satisfied. Here the reader may be questioning why we have not chosen $t = 0$ to be the value of t at which we impose the IR conditions for Σ and Σ'; this would of course be a perfectly valid choice. In that case however, the IR condition for Σ' (now $\Sigma'(t = 0)$) is no longer vanishing and would need to be determined by satisfying the integral equation that results from making $p = 1$ in Eq. 2.27; the IR condition for Σ does become more trivial. We would be neither winning nor losing much by making this alternative choice.

Solving Eq. 2.29 with a running coupling

Similarly to the constant coupling case, in theory the IR conditions have been determined and now only one parameter must be varied, namely the initial condition for r, $r(t \to -\infty)$, such that the boundary condition for Σ is satisfied. In practice, in order to obtain the numerical solutions we will again be varying two parameters, $r(t = t_0)$ and $\Sigma(t = t_0)$ such that the two conditions $\Sigma(t \to \infty) \to 0$ and $\Sigma(t = 0) = 1$ are satisfied. The two parameters are again varied iteratively until the solution converges. Notice that in this case, every iteration requires that we solve Eq. 2.22 using the new initial condition for r.

2.3 The curvature of V_{AF} and the scalar spectrum

Now that we have found non-trivial solutions for Σ, we turn to the study of local fluctuations around these solutions. Σ is not only the dynamical fermion mass function in our theory, but also a natural order parameter for the spontaneous breaking of Chiral Symmetry (χSB). Local fluctuations around Σ are in turn a natural description of the low energy degrees of freedom remaining in the theory after having integrated out the fermions. Our goal in this section is to obtain an effective description of the lightest *scalar* degrees of freedom in the theory. We shall derive a low-energy effective action containing both kinetic and mass terms for these scalars in order to obtain their pole masses. The effective description of pseudo-scalar degrees of freedom, the Goldstone bosons in the theory, will be the focus of the next section.

Let us then begin by considering fluctuations $\Sigma + \delta\Sigma$ of the form $\delta\Sigma = \frac{\Delta(p)}{f}\phi(x)$, where $\phi(x)$ is a (up to now arbitrary) scalar field, f a dimension one decay constant, and Δ is a momentum dependent form factor analogous to the momentum dependent mass function Σ. Notice that, unlike the analysis of reference [33], we have introduced explicit x dependence in the field ϕ: we demand that ϕ be a slowly varying function of x relative to the typical momentum scale of Σ and Δ such that an expansion in powers of $\partial_\mu\phi(x)$ is justified. Following reference [31], we start by schematically writing out this expansion as:

$$\begin{aligned}\Gamma\left(\Sigma+\frac{\Delta}{f}\phi\right) &= \int d^4x\left(-V\left(\Sigma,\Delta\right)+\frac{1}{2}Z\left(\Sigma,\Delta\right)\left(\partial_\mu\phi\right)^2+\mathcal{O}((\partial_\mu\phi)^4)\right)\\ &= \int d^4x\Bigg(-V(\Sigma)-\int dp\frac{\delta V}{\delta\Sigma(p)}\frac{\Delta(p)}{f}\phi(x)-\frac{1}{2!}\int dpdq\frac{\delta^2V}{\delta\Sigma(p)\delta\Sigma(q)}\frac{\Delta(p)}{f}\frac{\Delta(q)}{f}\phi(x)^2\\ &+ \frac{1}{2}Z\left(\Sigma,\Delta\right)\left(\partial_\mu\phi\right)^2+\mathcal{O}(\partial_\mu\phi)^4\Bigg)\end{aligned} \tag{2.31}$$

We will be using the method outlined by Fraser in [31], adapted to our particular theory, in order to obtain an expression for the kinetic term above.

Notice that the second term on the second line of Eq. 2.31 must vanish, by definition. An explicit expression for the third term can be obtained from taking the variation of Eq. 2.24:

$$\frac{\delta^2V}{\delta\Sigma(p)\delta\Sigma(q)}=\frac{1}{2\pi^2}\left(p^3M^{-1}(p,q)q^3-p^3\frac{p^2-\Sigma(p)^2}{(p^2+\Sigma(p)^2)^2}\delta(p-q)\right). \tag{2.32}$$

We can now write an expression for the effective action of the scalar ϕ in momentum

space, up to second order in the scalar's momentum Q^2, as

$$\Gamma_{AF}\left(\Sigma+\frac{\Delta}{f}\phi\right)-\Gamma_{AF}(\Sigma)= \tag{2.33}$$
$$\int d^4x\Bigg\{-\frac{1}{2}\frac{1}{2\pi^2}\int dp\frac{\Delta(p)}{f}\int dq\Bigg(p^3M^{-1}(p,q)q^3-p^3\frac{(p^2-\Sigma(p)^2)}{(p^2+\Sigma(p)^2)^2}\delta(p-q)$$
$$+Q^2\delta(p-q)Z_O(\Sigma(q))\Bigg)\frac{\Delta(q)}{f}\Bigg\}\phi^2$$

where $Z_O(\Sigma)$ is defined in relation to $Z(\Sigma,\Delta)$ which appears in Eq. 2.31 as

$$Z(\Sigma,\Delta)=\frac{1}{2\pi^2}\int dp\int dq\frac{\Delta(p)}{f}\delta(p-q)Z_O(\Sigma(q))\frac{\Delta(q)}{f}. \tag{2.34}$$

The subscript "O" indicates that Z_O is a differential operator. More specifically, Z_O should be of the form

$$Z_O=C_0\left(\Sigma,\frac{\partial\Sigma}{\partial q},\frac{\partial^2\Sigma}{\partial q^2}\right)+C_1\left(\Sigma,\frac{\partial\Sigma}{\partial q}\right)\frac{\partial}{\partial q}+C_2(\Sigma)\frac{\partial^2}{\partial q^2}. \tag{2.35}$$

The reason behind this will become clear shortly.

We now turn our attention to deriving an equation for $\Delta(p)$ as we did for $\Sigma(p)$ in the previous section. It will be convenient to normalize Δ by making the choice $f=f_\pi$, where f_π is the pseudo-scalar pion's decay constant that we shall define in the next section. Since Δ is always accompanied by a factor of $1/f$ in all expressions, here we wish to re-define the symbol Δ to include this factor, that is, Δ will refer to $\frac{\Delta}{f}$ in the definition of $\delta\Sigma$ from now on.

From Eq. 2.34 above we can determine the inverse propagator of the scalar field, which must vanish at the pole mass:

$$\int dq(p^3M^{-1}(p,q)q^3-p^3\frac{(p^2-\Sigma(p)^2)}{(p^2+\Sigma(p)^2)^2}\delta(p-q)+Q^2\delta(p-q)Z_O(q))\Delta(q)=0. \tag{2.36}$$

The resulting Q^2 here defines the pole mass squared.

Notice that so far we have referred to ϕ as an arbitrary scalar. However, the fluctuations around our order parameter Σ should correspond to a whole tower of states $\delta\Sigma=\Delta_i(p)\phi_i(x)$. Allow us for a moment to rewrite Eq. 2.36 in the following form:

$$\int dq(p^3M^{-1}(p,q)q^3-p^3\frac{(p^2-\Sigma(p)^2)}{(p^2+\Sigma(p)^2)^2}\delta(p-q))\Delta_i(q)=m_i^2Z_O(p)\Delta_i(p), \tag{2.37}$$

where we have re-written the $Q_i^2=-m_i^2$. This has the form of a *generalized* eigenvalue

equation. By solving this generalized eigenvalue problem we would then be diagonalizing the quadratic fluctuations of the effective action and finding the mass of each eigenmode.

Before we can continue towards deriving a differential equation for Δ, we shall first seek to obtain an explicit expression for $Z_O(p)$.

Determination of Z_O

Let us begin by explicitly expanding our AF action Eq. 2.10 around the solution to the gap equation, Eq. 2.29, by replacing $\Sigma(p)$ by $\Sigma(p)+\Delta(p)\phi(x)$. For the sake of clarity, we shall treat each of the two terms that contribute to the effective action separately. Starting with the first term on the RHS of Eq. 2.10, which we shall refer to as $\Gamma_{\log}$, we have

$$\Gamma_{\log}(\Sigma+\Delta\phi)-\Gamma_{\log}(\Sigma)=-i\mathrm{Tr}\ln\left(1-(\gamma\cdot p-\Sigma)^{-1}\Delta\phi\right). \tag{2.38}$$

We can re-write the RHS of this expression as:

$$-i\mathrm{Tr}\left[\ln\left(1-\frac{\gamma\cdot p+\Sigma}{p^2-\Sigma^2}\Delta\phi\right)\right]=-i\mathrm{Tr}\left[-\frac{\gamma\cdot p+\Sigma}{p^2-\Sigma^2}\Delta\phi-\frac{1}{2}\frac{\gamma\cdot p+\Sigma}{p^2-\Sigma^2}\Delta\phi\frac{\gamma\cdot p+\Sigma}{p^2-\Sigma^2}\Delta\phi+...\right], \tag{2.39}$$

where we have also expanded the logarithm.

The main idea of Fraser's method [31] consists on treating the different functions of p and x inside the trace above as functions of the $\hat{x}$ and $\hat{p}$ operators. (However, we will not continue to write the hats from now on.) With this in mind, we can see that if we attempt to compute the functional trace in Eq. 2.39, we are faced with the difficulty that, given the x dependence of ϕ, the operators inside this trace are not diagonal in momentum space. The same will be true of the second term in Eq. 2.10 which we will refer to as Γ_{int}. In order to overcome this difficulty, we must use the appropriate commutation relations for functions of p and x to bring all functions of x to the right of all functions of p. Here is the relation in question:

$$\phi(x)F(p)=F(p)\phi(x)+i\frac{\partial F}{\partial p_\mu}\partial_\mu\phi+\frac{i^2}{2}\frac{\partial^2 F}{\partial p_\nu\partial p_\mu}\partial_\nu\partial_\mu\phi+\frac{i^3}{3}\frac{\partial^3 F}{\partial p_\alpha\partial p_\nu\partial p_\mu}\partial_\alpha\partial_\nu\partial_\mu\phi+..., \tag{2.40}$$

which we have derived from the familiar relations

$$\begin{aligned}[x_i,F(\vec{p})] &= i\hbar\frac{\partial F(\vec{p})}{\partial p_i},\\ [p_i,F(\vec{x})] &= -i\hbar\frac{\partial F(\vec{x})}{\partial x_i},\end{aligned} \tag{2.41}$$

and generalized to four dimensions (in Minkowski space)[3]. This commutation procedure will result in an expansion of our AF action in powers of ϕ and $\partial_\mu\phi$, exactly what we are after. We then should be able to "match" the coefficients of this expansion to those of Eq. 2.31 therefore giving us an explicit expression for Z_O.

Here we would like to point out that we have found some sign problems in the relations (Eq. 2.8 and 2.9) given by reference [31]. However their final result is unaffected by them as the terms we find a problem with do not contribute to Z there; below are these equations with the correct signs, which follow from Eq. 2.40:

$$\begin{aligned} [p^2,\phi] &= \Box\phi - 2ip^\mu\partial_\mu\phi \\ [p^2,[p^2,\phi]] &= \Box\Box\phi - 4ip^\mu\partial_\mu\Box\phi - 4p^\mu p^\nu\partial_\mu\partial_\nu\phi. \end{aligned} \tag{2.42}$$

Using the commutation relation Eq. 2.40, we now rewrite Eq. 2.39 as

$$\begin{aligned} -i\mathrm{Tr}\left[\ln\left(1-\frac{\gamma\cdot p+\Sigma}{p^2-\Sigma^2}\Delta\phi\right)\right] &= -i\mathrm{Tr}\Big[-\frac{\gamma\cdot p+\Sigma}{p^2-\Sigma^2}\Delta\phi \\ &- \frac{1}{2}\frac{\gamma\cdot p+\Sigma}{p^2-\Sigma^2}\Delta\left[\frac{\gamma\cdot p+\Sigma}{p^2-\Sigma^2}\Delta\phi + i\frac{\partial}{\partial p_\mu}\left(\frac{\gamma\cdot p+\Sigma}{p^2-\Sigma^2}\Delta\right)\partial_\mu\phi\right. \\ &+ \left.\frac{i^2}{2}\frac{\partial^2}{\partial p_\mu\partial p_\nu}\left(\frac{\gamma\cdot p+\Sigma}{p^2-\Sigma^2}\Delta\right)\partial_\mu\partial_\nu\phi + \mathcal{O}(\partial^3\phi)\right]\phi + ...\Big] \end{aligned} \tag{2.43}$$

We can immediately see that it is the first term on the third line of Eq. 2.43 which will contribute to $Z(\Sigma,\Delta)$. It is now straightforward, albeit tedious, to write down an explicit expression for Z_O in the form of Eq. 2.35. There will be many terms involving zeroth, first, and second derivatives of Δ. Here we present the first (zeroth derivative) of such terms for illustrative purposes:

$$\begin{aligned} C_0 = &- \frac{1}{2}\frac{q^3}{(q^2+\Sigma^2)^4}\Big(-3q^2\Sigma^2 - q^4 + 2\Sigma^4 + 2\Sigma^5(\partial\Sigma) - 2(\partial\Sigma)^2q^6 - 3\Sigma(\partial^2\Sigma)q^6 \\ &- 2\Sigma^3(\partial^2\Sigma)q^4 + \Sigma^5(\partial^2\Sigma)q^2 + 2\Sigma(\partial\Sigma)q^4 - 12\Sigma^3(\partial\Sigma)q^2 + 12\Sigma^2(\partial\Sigma)^2q^4 - 2\Sigma^4(\partial\Sigma)^2q^2\Big). \end{aligned} \tag{2.44}$$

The complete expression including C_1 and C_2 can be found in the Appendix. In the equation above, we have converted all p^μ derivatives coming from Eq. 2.40 to derivatives of q^2 in Euclidean space, and we have defined $\partial \equiv \frac{\partial}{\partial q^2}$ to avoid overcrowded notation.

We now turn our attention to the second term in the effective action for the scalar,

[3] Applying our result to the case of one spatial dimension agrees with the result obtained by the authors of [34]. (See Eq. 18 therein, with $x_1 = p$, $x_2 = x$, and therefore $c = -i$).

Γ_{int}. Proceeding similarly as we did for $\Gamma_{\log}$ let us write this as:

$$\Gamma_{int}\left(\Sigma+\Delta\phi\right)-\Gamma_{int}(\Sigma)=\frac{i}{2}\mathrm{Tr}\left(\Sigma(p)M^{-1}\Delta\phi+\Delta\phi M^{-1}\Sigma(q)+\Delta\phi M^{-1}\Delta\phi\right). \quad (2.45)$$

Again using Eq. 2.40 we commute all functions of x to the right. We can see that the term that will contribute to $Z(\Sigma,\Delta)$, which must have two factors of ϕ and two derivatives, will come from the third term in Eq. 2.45, and we write this as:

$$\int d^4x\frac{1}{2}Z(\Sigma,\Delta)_{int}(\partial_\mu\phi)^2=2\int d^4x\int\frac{d^4p}{(2\pi)^4}\frac{i^2}{2}\Delta(p)\frac{\partial^2}{\partial p_\mu\partial p_\nu}\left[\int\frac{d^4q}{(2\pi)^4}M^{-1}(p,q)\Delta(q)\right](\partial_\mu\partial_\nu\phi)\phi. \quad (2.46)$$

Unlike the case of $\Gamma_{\log}$, the presence of $M^{-1}(p,q)$ inside the derivatives in this expression is a major complication to our problem, as we do not have an explicit expression for the kernel in this form except through the relation Eq. 2.16. To overcome this difficulty we will have to get somewhat creative. In order to simplify our notation a bit, allow us to define

$$\tilde{\Delta}(p)=\int dqM^{-1}(p,q)q^3\Delta(q), \quad (2.47)$$

where we have now converted all four momenta to Euclidean space. We can write the two derivative term in Eq. 2.46 above as

$$\frac{\partial^2}{\partial p_\mu\partial p_\nu}\tilde{\Delta}=-\left(p^2\partial^2\tilde{\Delta}+2\partial\tilde{\Delta}\right)g^{\mu\nu}. \quad (2.48)$$

Then, in order to include the effect of Γ_{int} in Z_O as we did for $\Gamma_{\log}$, we must find some kind of expression for Eq. 2.47 above. We will continue to make progress in this direction further down in this section, but for now allow us to take a hiatus to put what we have done to determine Z_O so far in more familiar terms.

Here we would like to note that our calculation of $\Gamma_{\log}$'s contribution to $Z(\Sigma,\Delta)$ as performed above is in fact equivalent to the result one would obtain from a diagrammatic approach, that is, that the coefficient of the kinetic term in the scalar field's effective action should be given by the p^2 term in the two point function, which we write as

$$Z(\Sigma,\Delta)_{\log}=-i\Gamma^{(2)}_{p^2}(p,-p,\Sigma,\Delta). \quad (2.49)$$

Looking at Fig. 2.4 we can write

$$\Gamma^{(2)}=\int\frac{d^4k}{(2\pi)^4}\frac{i(\not{k}+\Sigma(k))}{(k^2-\Sigma^2(k))}\frac{i(\not{k}-\not{p}+\Sigma(k-p))}{(k-p)^2+\Sigma^2(k-p)}(-i\Delta(k))(-i\Delta(k-p)), \quad (2.50)$$

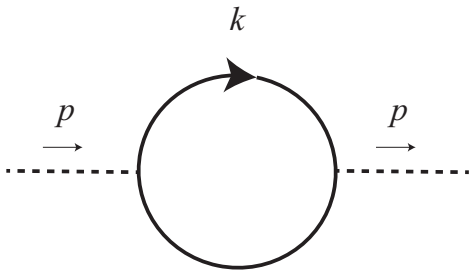

Figure 2.4: Quadratic term in the effective action.

and taking the trace to get rid of the γs in the fermion propagators, and defining $q = k - p$, we find

$$\Gamma^{(2)} = \int \frac{d^4k}{(2\pi)^4} \Delta(k)\Delta(q) 4 \frac{k^2 - k \cdot p + \Sigma(k)\Sigma(q)}{(k^2 - \Sigma^2(k))(q^2 - \Sigma^2(q))}. \tag{2.51}$$

We can now straightforwardly expand the integrand of Eq. 2.51 in powers of p in order to isolate the term proportional to p^2. The complete result for this expression can be found in the Appendix, where we explicitly show that the it perfectly agrees with our calculation of Eq. 2.45 using Fraser's method. Note that to obtain this agreement we have made a particular choice for the Feynman rule for the fermion-scalar vertex; rather than for example the symmetric combination $(\Delta(k) + \Delta(q))/2$ instead. Interestingly, this latter choice yields additional terms proportional to Δ' which do not appear in our previous calculation of $Z_{\log}$. Thus, our results have resolved this potential ambiguity.

Solving the curvature equation

We shall now proceed to derive a differential equation for Δ. First, it will be useful however to transform Eq. 2.36 into one without M^{-1} by making use of Eq. 2.16:

$$\Delta(p) = \int dq \left[q^3 \frac{q^2 - \Sigma(q)^2}{(q^2 + \Sigma(q)^2)^2} M(q,p) - Q^2 M(q,p) Z_O(\Sigma) \right] \Delta(q). \tag{2.52}$$

Following a similar procedure as that used to transform Eq. 2.25 into a differential equation for $\Sigma(p)$ with its corresponding IR and UV conditions, we shall now derive the differential version of Eq. 2.52. Let us first differentiate once with respect to p:

$$\Delta_i'(p) = \left(\frac{r'(p)}{p^2} - \frac{2r(p)}{p^3} \right) \int_0^p \left(\frac{q^3(q^2 - \Sigma(q)^2)}{(q^2 + \Sigma^2(q))^2} + m_i^2 Z_O(\Sigma) \right) \Delta_i(q) dq. \tag{2.53}$$

Multiplying both sides in Eq. 2.53 by a factor of p^3, and once more differentiating with

respect to p, we obtain

$$\begin{aligned} 3p^2\Delta_i'(p) + p^3\Delta_i''(p) &= (pr''(p) - r'(p)) \int_0^p \left(\frac{q^3(q^2 - \Sigma(q)^2)}{(q^2 + \Sigma^2(q))^2} + m_i^2 Z_O(\Sigma) \right) \Delta_i(q) dq \\ &+ (pr'(p) - 2r(p)) \left(\frac{p^3(p^2 - \Sigma^2(p))}{(p^2 + \Sigma^2(p))^2} + m_i^2 Z_O(\Sigma) \right) \Delta_i(p). \quad (2.54) \end{aligned}$$

Making use of Eq. 2.53 we can rewrite the remaining integral on the RHS as a term proportional Δ'. The result is then:

$$p^3\Delta_i'' + \left(3p^2 - p^3 \frac{pr'' - r'}{pr' - 2r} \right) \Delta_i' - (pr' - 2r) \left(\frac{p^3(p^2 - \Sigma^2)}{(p^2 + \Sigma^2)^2} + m_i^2 Z_O(\Sigma) \right) \Delta_i = 0 \quad (2.55)$$

where Σ, Δ, and r are all understood to be functions of p. Notice that, as in the derivation of Eq. 2.29, the functions of q in the integrand of Eq. 2.52 do not pick up any derivatives, and appear intact as functions of p in the differential equation above. But more importantly here, notice that Z_O acting on Δ_i in the third term of Eq. 2.55 will generate new terms proportional to Δ_i' and Δ_i'', in addition to the linear term in Δ.

Boundary Conditions

In order to solve Eq. 2.55 we must specify two sets of boundary conditions: the IR (initial) condition for both Δ and Δ', and a UV condition for Δ. The IR condition for Δ' can be immediately read off from Eq. 2.53: $\Delta'(p = 0) = 0$, which in t coordinates this becomes $\Delta'(t \to -\infty) \to 0$. The initial condition for Δ, $\Delta(t \to -\infty)$ is determined by the requirement that the kinetic term in the scalar's effective action be canonical. Inspecting Eq. 2.31, we can see that this then implies

$$Z(\Sigma, \Delta) = 1. \quad (2.56)$$

In the case of the running coupling of Eq. 2.22 the UV condition for Δ is given by $\Delta(p \to \infty) \to 0$. In the case of a constant coupling, the UV condition for Δ is given by Eq. 2.52 evaluated at $p = \Lambda$:

$$\Delta(\Lambda) = \frac{r}{\Lambda^2} \int_0^\Lambda dq \left[q^3 \frac{q^2 - \Sigma(q)^2}{(q^2 + \Sigma(q)^2)^2} - Q^2 Z_O \right] \Delta(q). \quad (2.57)$$

Demanding that the above conditions be satisfied determines the value of m^2.

We shall now present plots of our numerical solution for the lightest scalar's $p\Delta(t)$ (left) and $\Delta(t)$ (right), first considering *only* the effect of the $\Gamma_{\log}$ term in Z_O, for a variety

of cases. In Fig. 2.5 we present the case of a constant coupling $r = 0.517$ compatible with the first solution for Σ presented above; the resulting value of the mass for the scalar is $m = 1.52$. Here we would like to remind the reader that all masses are given in units of the dynamical fermion mass. Fig. 2.6 and Fig. 2.7 show the solutions for the case of the running coupling from the previous section for two different values of N_f, $N_f = 11.5$ and $N_f = 9$ respectively; here we obtain $m = 1.53$ and $m = 1.45$ respectively. In Fig. 2.8 we also present plots for $p\Delta$ and Δ of a higher mass scalar in the constant coupling regime for illustrative purposes; the value of the mass for this particular scalar is $m = 6.72$. This latter mass is clearly above the scale where our effective description makes sense.

More details on how we have obtained these solutions will be provided below. We also present plots for the solutions to $p\Delta$ and Δ considering *also* the effect of Γ_{int} in Z_O for two cases: that of the constant coupling $r = 0.517$ from above which can be found in Fig. 2.9, and that of the running coupling with $N_f = 9$ which can be found in Fig. 2.10. The corresponding values of the lightest scalar's mass are $m = 1.46$ and $m = 1.43$ respectively. We have not yet explained how we have included the Γ_{int} effect into our equations, this will be done in detail below.

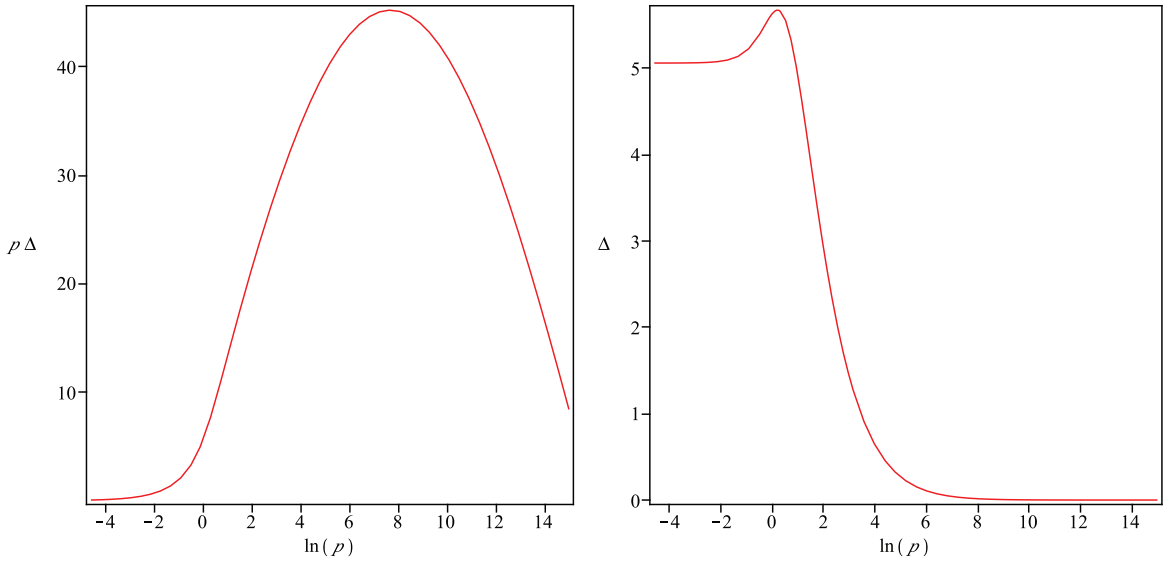

Figure 2.5: Numerical solution of $p\Delta$ (left) and Δ (right), considering *only* the effect of $\Gamma_{\log}$ in the effective action, for the lightest mass scalar (mass $m = 1.52$) in the case of a constant coupling $r = 0.517$ and UV cutoff at $t = \ln(\Lambda) = 15$.

Solving Eq. 2.55

We now proceed to explain how we have obtained numerical solutions to Eq. 2.55 presented here. We shall initially concentrate on the effect of $\Gamma_{\log}$ only. The procedure that we follow in this case closely follows that used for solving for Σ in the previous section. In

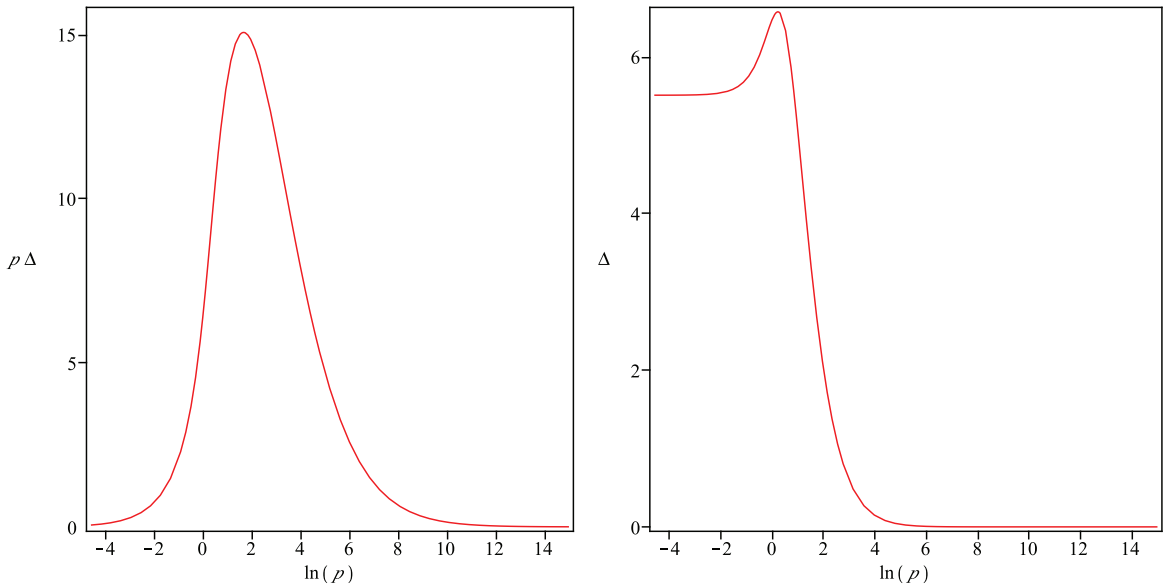

Figure 2.6: Numerical solution of $p\Delta$ (left) and Δ (right), considering *only* the effect of $\Gamma_{\log}$ in the effective action, for the lightest mass scalar ($m = 1.53$) in the case of the running coupling from Eq. 2.22, with $N_f = 11.5$.

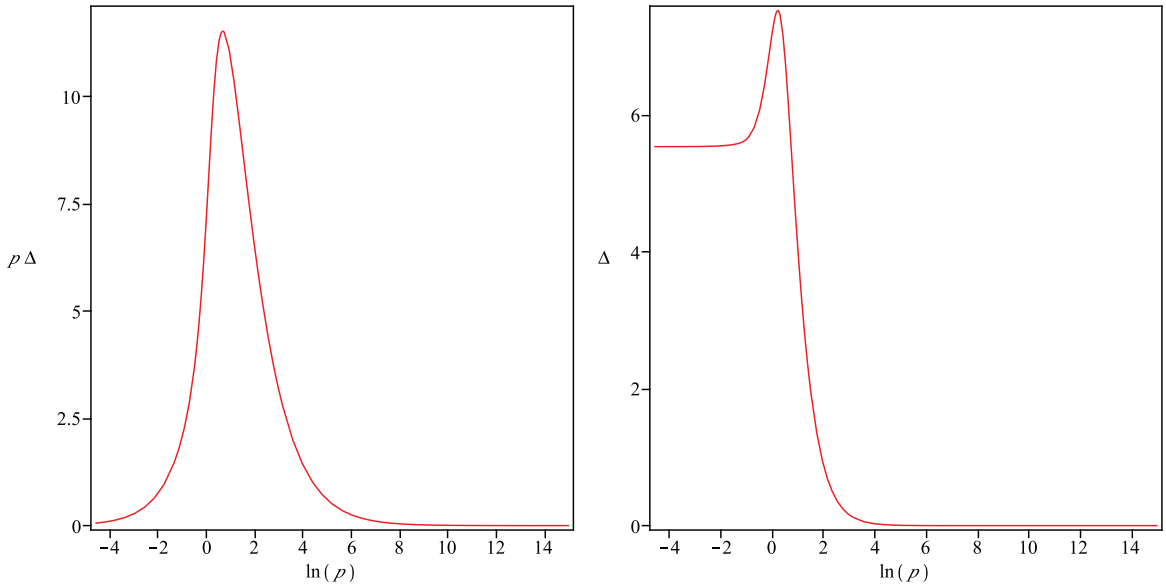

Figure 2.7: Numerical solution of $p\Delta$ (left) and Δ (right), considering *only* the effect of $\Gamma_{\log}$ in the effective action, for the lightest mass scalar ($m = 1.45$) in the case of the running coupling from Eq. 2.22, with $N_f = 9$.

principle, the only parameter left to vary is m^2 such that the boundary condition for Δ is satisfied. In practice, the two quantities that we shall vary are $\Delta(t = t_0)$ and of course m^2; the two conditions that we seek to satisfy are Eq. 2.56 and Eq. 2.57 in the case of a constant coupling, and Eq. 2.56 along with $\Sigma(t \to \infty) \to 0$ in the case of a running

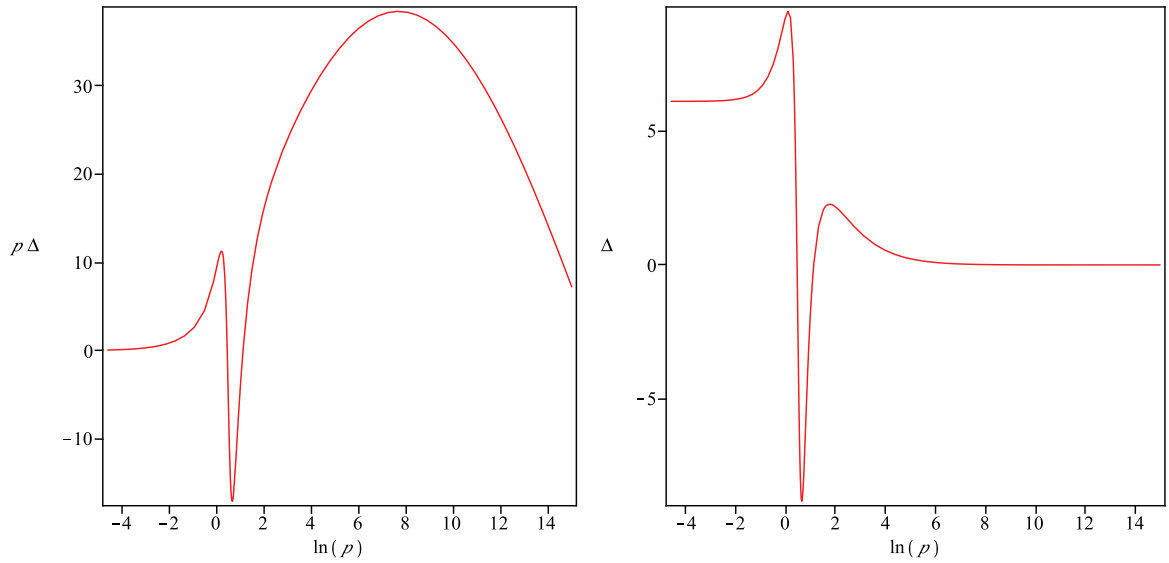

Figure 2.8: Numerical solution of $p\Delta$ (left) and Δ (right), considering *only* the effect of $\Gamma_{\log}$ in the effective action, for a higher mass scalar in the spectrum ($m = 6.72$) in the case of a constant coupling $r = 0.517$ and UV cutoff at $t = \ln(\Lambda) = 15$.

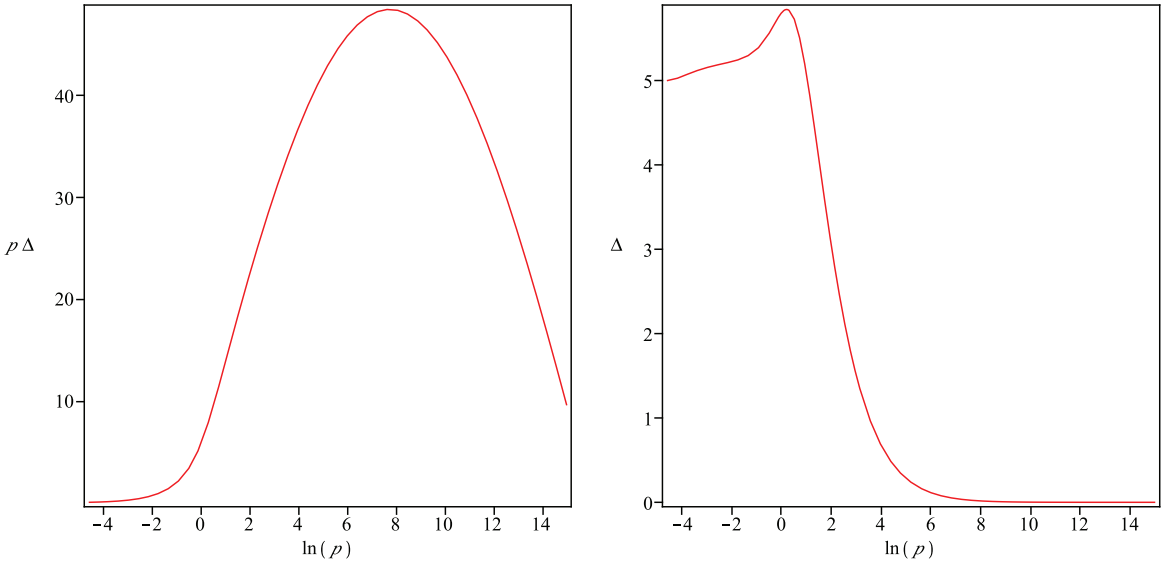

Figure 2.9: Numerical solution of $p\Delta$ (left) and Δ (right), considering the effect of both $\Gamma_{\log}$ *and* Γ_{int} in the effective action, for the lightest mass scalar ($m = 1.46$) in the case of a constant coupling with a cut-off at $t = 15$.

coupling. We shoot from small and initially arbitrary values of both parameters, and proceed recursively until a solution for Δ converges. The resulting value of m determines the physical mass of our lightest scalar, the "dilaton". Note that, unlike the differential equation for Σ, Eq. 2.55 up to this point is linear. Therefore we can focus solely on satisfying the second condition, Eq. 2.57, for an arbitrary value of $\Delta(t = t_0)$ and then scale the

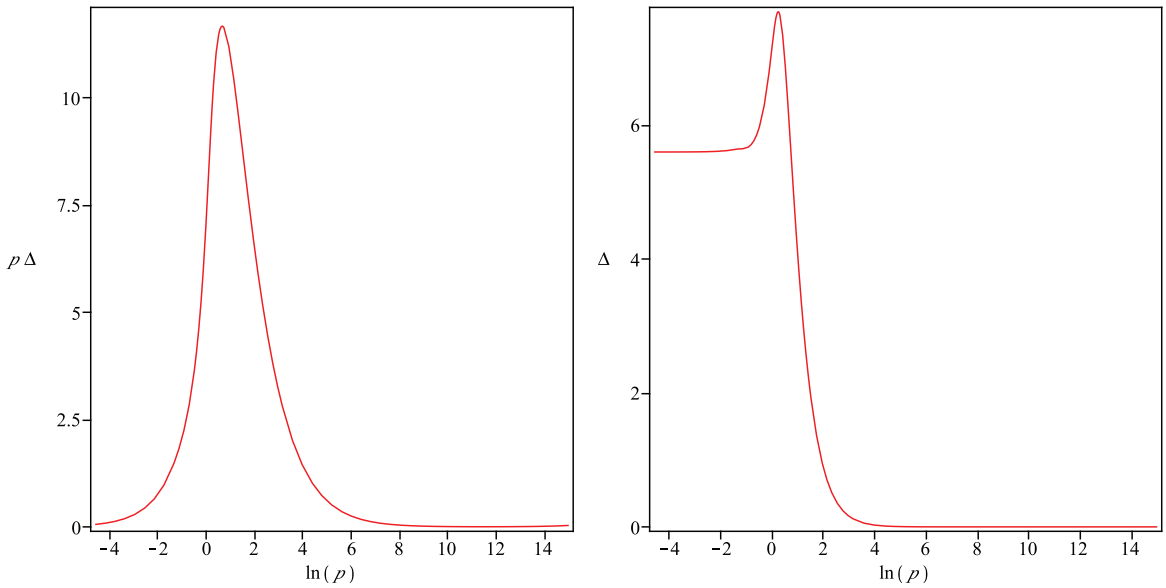

Figure 2.10: Numerical solution of $p\Delta$ (left) and Δ (right), considering the effect of both $\Gamma_{\log}$ *and* Γ_{int} in the effective action, for the lightest mass scalar ($m = 1.43$) in the case of the running coupling from Eq. 2.22, with $N_f = 9$.

obtained solution by a multiplicative constant such that Eq. 2.56 is satisfied. This will not remain true once we introduce the contribution from Γ_{int}, as will become clear shortly.

Incorporating Γ_{int} effects

Now that we have an idea of what our solutions should look like, we can use what we know about $M(p,q)$ to numerically obtain a discrete number of points for the function $\tilde{\Delta}(p)$, which can be used to incorporate the effect of the interaction term into Z_O. We begin by defining a dimensionless, discrete version of the kernel $M(p,q)$ as a $n \times n$ matrix:

$$\mathcal{M} = pM(p,q)q \tag{2.58}$$

where both p and q run from 0.01 (where our solutions begin when we translate t_0 to p coordinates) to exp(15), the cut-off for our constant coupling solution; we have chosen $n = 500$. From Eq. 2.15, we can see that the dimensionless expression containing the inverse of $M(p,q)$ is $p^3 M^{-1}(p,q)q^3$. Hence, in matrix notation, we can invert $\mathcal{M}$ to find

$$\mathcal{M}^{-1} = p^3 M^{-1}(p,q)q^3. \tag{2.59}$$

In log coordinates where t, s are related to p, q respectively, we can write

$$\tilde{\Delta}(t) = \mathcal{M}^{-1}(t,s)\Delta(s)\exp(-3t). \tag{2.60}$$

We can now numerically compute the first and second derivatives of $\tilde{\Delta}$ as required by Eq. 2.48. The result may be fit to a function that yields the contribution of Γ_{int} to $Z_O\Delta_i$ in Eq. 2.55.

We now proceed as follows. We include this new term as an inhomogeneous term in Eq. 2.55, and solve for Δ as usual. Notice that now, the initial condition that gives the proper normalization for Δ (such that the kinetic term remains canonical) must now be input correctly from the beginning. We can iterate the above described procedure a few times, in this way we are building in the non-linear effect of the interaction term into our equation. Starting with the solution presented in Fig. 2.5 we iterate this procedure twice, which is sufficient for the desired accuracy. The corresponding new resulting $p\Delta$ and Δ can be found in Fig. 2.9. The same has been done for the solution with Γ_{int} omitted, as presented in Fig. 2.7, to be compared with that of Fig. 2.10. As evidenced by comparing these two sets of figures, the effect of Γ_{int} is not dramatic at all, but there is a slight change in the values of the lightest scalar's mass: $m = 1.46$, compared to 1.52, in the first and $m = 1.43$, compared to 1.45, in the second. The interaction term clearly does not play a leading role in our analysis.

Discussion

It has now become apparent that the lightest scalar state in our theory is not expected to be light relative to the dynamical fermion mass scale, regardless of the near-conformal dynamics we have considered here. This result appears to directly contradict the conclusion of well-read papers on the subject (see [14] and [28] for example) that predict a parametrically light scalar associated with the spontaneous breaking of dilatation symmetry for gauge theories with an (approximate) infrared fixed point.

Inspired by applications to holography where the dilaton can be identified with the radion, literature from recent years on the dilaton in the context of Conformal Field Theory (CFT) suggests that, in general, a quasi-conformal theory will not produce a light dilaton unless, among other conditions, there is a flat direction available in the theory, which would correspond to fine tuning unless supersymmetry is invoked (see [35], [36] for example). While a clear connection between a gauge theory like we have considered here and the types of theories studied in this context is not apparent to us at this time, we still find tension between the result (see [35], Eq. 5.12)

$$\frac{m^2}{\Lambda^2} \sim \frac{\beta}{\pi}, \tag{2.61}$$

and our own analysis. We illustrate the issue by taking a special limit of our gauge theory

in what follows.

Let us consider the beta function from Eq. 2.22

$$\frac{\beta(\alpha)}{\alpha} = -b_0\alpha + ... \tag{2.62}$$

We first re-write b_0 from Eq. 2.23 in the more general form

$$b_0 = \frac{11}{6\pi}C_2(G) - \frac{4}{6\pi}N_f C(r), \tag{2.63}$$

where G denotes the representation of the gauge generators (the adjoint representation) and r denotes the representation under which the fermions transform. It will be useful to re-write $C(r)$ above as

$$C(r) = \frac{d_r}{d_G}C_2(r). \tag{2.64}$$

We consider fermions in a d_r dimensional fermion representation of $SU(N)$ such that $C_2(r)$ is large compared to N_c, and simultaneously we have a small number of flavours $N_f \ll \frac{N^2}{d_r}$. This limit, although unphysical given that N_f is less than 1, is well defined and has been used in the past to study χSB in Monte Carlo calculations; see e.g., [37]. Here, χSB occurs at a value of $\alpha \sim 1/C_2(r)$ such that it is much less than one. We can then see that the pure gauge boson contribution to Eq. 2.62 will be dominated by a term $\sim N/C_2(r) \ll 1$, while the fermonic term is $\sim N_f d_r/(N^2-1)$, also much less than 1 given the condition on N_f. Hence, in this limit the beta function can be made arbitrarily small to all orders in α, and Eq. 2.61 would imply $m^2/\Lambda^2 \ll 1$. This is not the case for us at all however. We have found that a small (but non-zero) beta function will allow for large contributions to the scalar's mass coming from a large range of scales up to high momenta, a non-local effect not captured by a local analysis. Even in the case of a constant coupling where β is exactly 0, we do not expect the scalar to be light. It is in fact the boundary condition at the cutoff, necessary to obtain a solution in this case, which breaks the scale invariance and generates a non-zero mass for the dilaton.

Something striking about our results for the momentum dependent mass function $\Sigma(t)$ and form factor of our lightest scalar $\Delta(t)$, and perhaps the most interesting qualitative result that we observe here, is how similar they are to each other away from the IR where the terms that cut off the loop integrals become dominant. There are two reasons why we believe this is interesting. The first is in fact related to to the nature of our scalar: if the lightest scalar in the theory is indeed associated with the spontaneous breaking of scale invariance, one would expect its mass function to be quite distinct from $\Sigma(p)$. In fact, we would expect it to be proportional to $\Sigma(p) - \Sigma'(p)p$. This can be understood by

performing a scale transformation of the order parameter $\Sigma(p)$, as done by the authors of [13]. This result is in direct contrast with our findings for Δ, which closely resembles Σ throughout. The second is that in the limit where Δ approaches Σ, up to a factor of $i\gamma^5$, attaching an additional scalar to a fermion loop will have an amplitude that is the same as attaching a pion. This will become more clear in the next section when we study pseudo-scalar excitations of the order parameter Σ. Therefore, it appears that upon integrating out the fermions, a linear sigma model remains where f (which is equal to f_π) gives both the vacuum expectation value (VEV) and the decay constant. This suggests that the coupling of our scalar to the Goldstone bosons, and thus to the W and Z bosons, will be similar to that of a SM Higgs doublet.

Finally, we believe it is worthwhile noting that, even as we move away from the walking regime, we continue to find values for the pole mass of the lowest lying scalar particle of approximately 1.5 times the value of the dynamical fermion mass. This result is interesting when interpreted in the context of QCD, where 1.5 times $\sim$ 330 MeV is $\sim$ 500 MeV, the location of the σ resonance.

In order to obtain concrete results, we have made quite a few approximations. The one that we believe carries the most implications is the tree level truncation in T of the AF action, Eq. 2.6, which should correspond to working in the large N_c limit. While we have initially dropped gauge boson self interactions, we have re-introduced the effect through the running coupling in the kernel; we are essentialy working in the standard renormalization-group-improved ladder approximation. We believe that the qualitative behaviour observed in our solutions for Eq. 2.29 and Eq. 2.55 should survive beyond our approximations and that the mass of the lightest scalar always receives important contributions that arise from a large range of momenta. One way to understand this is by observing that it is the scale invariance of the kernel that is responsible for the weighting of the integral equation for Σ in the UV, where the significant drop in the coupling becomes a large explicit source of breaking of scale invariance (see e.g., [38]).

2.4 The pion

We now turn to study pseudo-scalar fluctuations around the order parameter Σ. Much of what we have done in the previous section to obtain an effective description of the scalar field ϕ will follow through very similarly here. An important difference to note here however is that, in contrast to the scalar case, there will be no separate momentum dependent form factor analogous to Δ involved for pseudo-scalars; as required by chiral symmetry, the pion fields' form factor must be proportional to Σ. Then, having already

solved for Σ and determined its normalization, we can simply demand that the pion's kinetic term in the effective action be canonical in order to obtain an integral expression for the constant f_π. Any contributions to f_π coming from terms involving $M^{-1}(p,q)$ can also now be calculated in a pretty straightforward way, as will soon become clear. Towards the end, we shall compare our results to the well known result for f_π by Pagels and Stokar [39].

Let us then begin by looking at fluctuations of the order parameter of the form $\delta\Sigma = \Sigma(p)(e^{-\frac{i}{f_\pi}\pi(x)\gamma^5} - 1)$. Here, $\pi = \lambda^a\pi^a$ where the λ are the $SU(3)$ generators with normalization $\mathrm{Tr}(\lambda^a\lambda^b) = \delta^{ab}/2$. We schematically expand the effective action in terms of the slowly varying field $\pi(x)$ as

$$\begin{aligned}\Gamma(\Sigma+\delta\Sigma) - \Gamma(\Sigma) &= \int d^4x\Bigg[- \int dp \frac{\delta V}{\delta\Sigma(p)}\Sigma(p)(e^{-\frac{i}{f_\pi}\pi(x)\gamma^5} - 1) \\ &- \frac{1}{2}\int dpdq \frac{\delta^2 V}{\delta\Sigma(p)\delta\Sigma(q)}\Sigma(p)\Sigma(q)(e^{-\frac{i}{f_\pi}\pi(x)\gamma^5} - 1)^2 + \frac{1}{2}Z(\Sigma)(\partial_\mu\pi^a(x))^2 + ...\Bigg].\end{aligned} \tag{2.65}$$

Notice that now, both the first and the second term in this expansion will give rise to π^2 terms that could in principle give the pions a non-zero mass. Of course in the chiral limit that we are studying, the Goldstone bosons should remain exactly massless; we must verify that these contributions are indeed vanishing. Also, while it remains true that $\frac{\delta V}{\delta\Sigma(p)}$ alone should vanish when both terms in Eq. 2.10 are considered together, we will show that, when combined with the π^2 contributions from $\frac{\delta^2 V}{\delta\Sigma(p)\delta\Sigma(q))}$, the contribution from each $\Gamma_{\log}$ and Γ_{int} vanish independently of each other.

Let us first consider the contribution to the pions' effective action coming from $\Gamma_{\log}$:

$$\begin{aligned}\Gamma(\Sigma+\delta\Sigma) - \Gamma(\Sigma) &= -i\mathrm{Tr}\left[\ln\left(1 + \frac{\gamma\cdot p + \Sigma}{p^2-\Sigma^2}\Sigma\left(\frac{i}{f_\pi}\gamma^5\pi - \frac{i^2}{2f_\pi^2}\pi^2 + ...\right)\right)\right] \\ &= -i\mathrm{Tr}\Bigg[\frac{\gamma\cdot p + \Sigma}{p^2-\Sigma^2}\Sigma\left(\frac{i}{f_\pi}\gamma^5\pi - \frac{i^2}{2f_\pi^2}\pi^2 + ...\right) \\ &- \frac{1}{2}\frac{\gamma\cdot p + \Sigma}{p^2-\Sigma^2}\Sigma\left(\frac{i}{f_\pi}\gamma^5\pi - \frac{i^2}{2f_\pi^2}\pi^2 + ...\right)\frac{\gamma\cdot p + \Sigma}{p^2-\Sigma^2}\Sigma\left(\frac{i}{f_\pi}\gamma^5\pi - \frac{i^2}{2f_\pi^2}\pi^2 + ...\right) + ...\Bigg].\end{aligned} \tag{2.66}$$

We can immediately write an expression for the (non-derivative) π^2 term, let us call it L_{π^2}, as

$$L_{\pi^2} = -i\mathrm{Tr}\left(\frac{1}{2f_\pi^2}\frac{\gamma\cdot p + \Sigma}{p^2-\Sigma^2}\Sigma\pi^2 - \frac{i^2}{2f_\pi^2}\frac{\gamma\cdot p + \Sigma}{p^2-\Sigma^2}\Sigma\pi\frac{-\gamma\cdot p + \Sigma}{p^2-\Sigma^2}\Sigma\pi\right) \tag{2.67}$$

$$= -i\left(\frac{1}{2f_\pi^2}\frac{4\Sigma^2}{(p^2-\Sigma^2)}\pi^2 + \frac{1}{2f_\pi^2}4\frac{-p^2+\Sigma^2}{(p^2-\Sigma^2)^2}\Sigma^2\pi^2\right) + deri. = 0, \tag{2.68}$$

which vanishes as promised. Note that in the second line, we have ignored the derivative terms that arise from commuting π to the right as they are not relevant for us here.

We can now determine $Z_{\log}(\Sigma)$, by using Eq. 2.40 to bring all pion fields in Eq. 2.67 to the right and isolating the terms with two π fields and two derivatives. Here we present the leading term containing no derivatives of Σ:

$$Z(\Sigma)_{\log} = \int \frac{d^4p}{(2\pi)^4} \frac{1}{f_\pi^2} \frac{\Sigma^2(p)p^2 + 2\Sigma^4(p)}{(p^2+\Sigma^2(p))^3} + ... \tag{2.69}$$

For the full expression of $Z_{\log}$ including Σ' and Σ'' terms, please refer to the Appendix. Demanding that the kinetic term for the pion effective action be canonical, we find an expression for the decay constant

$$f_\pi^2 = \frac{N_c}{16\pi^2} \int dq^2 q^2 \frac{\Sigma^2(p)p^2 + 2\Sigma^4(p)}{(p^2+\Sigma^2(p))^3} + ... \tag{2.70}$$

Before we proceed to the discussion of the interaction term, let us first use our solutions for Σ from Section 2.1 to find the numerical values of f_π in the case of a constant and running coupling. For the first case, with $r = 0.517$ and cutoff at $t = \ln\Lambda = 15$, we find $f_\pi = 0.17$. For the second case, and using $N_f = 11.5$ we find $f_\pi = 0.16$.

We can compare the above results to the calculation by Pagels and Stokar [39] obtained by calculating the amplitude for the annihilation of a Goldstone through an axial-vector current:

$$\begin{aligned} f_\pi^2 &= \frac{N_c}{16\pi^2} \int dq^2 q^2 \frac{\Sigma^2(q) - \frac{1}{2}q^2\Sigma(q)\partial\Sigma(q)}{(q^2+\Sigma^2(q))^2} \\ &= \frac{N_c}{16\pi^2} \int dq^2 q^2 \frac{\Sigma^2(q)q^2 + \Sigma^4(p)}{(q^2+\Sigma^2(p))^3} + ..., \end{aligned} \tag{2.71}$$

where $\partial \equiv \frac{\partial}{\partial q^2}$ as defined in the previous section. In the second line, we have re-written in a similar form as our result Eq. 2.70 above. Notice that at large p, the leading term in our result agrees with the Pagels-Stokar result. The numerical values for the decay constant from Pagels-Stokar, corresponding to the same cases discussed by us above are: $f_\pi = 0.14$ for the constant coupling, and $f_\pi = 0.13$ for the running coupling.

Let us now turn to the interaction term Γ_{int},

$$\Gamma_{int}[\Sigma+\delta\Sigma] = \frac{i}{2}\mathrm{Tr}\left[\Sigma\left(1 - \frac{i}{f_\pi}\pi\gamma^5 + \frac{i^2}{2}\frac{\pi^2}{f_\pi^2} + ...\right) D^{-1} \Sigma \left(1 + \frac{i}{f_\pi}\pi\gamma^5 + \frac{i^2}{2}\frac{\pi^2}{f_\pi^2} + ...\right)\right], \tag{2.72}$$

where the expansions inside the rounded parentheses correspond to $e^{-\frac{i}{f_\pi}\pi(x)\gamma^5}$ and $e^{+\frac{i}{f_\pi}\pi(x)\gamma^5}$

respectively.

We can immediately isolate the (non-derivative) terms that are quadratic in π which can potentially contribute to a non-zero pion mass, let us call them I_π:

$$\begin{aligned} I_\pi &= \mathrm{Tr}\left[\Sigma D^{-1}\Sigma\frac{i^2}{2}\frac{\pi^2}{f_\pi^2} + \Sigma\left(-\frac{i}{f_\pi}\pi\gamma^5\right)D^{-1}\Sigma\left(-\frac{i}{f_\pi}\pi\gamma^5\right) + \Sigma\frac{i^2}{2}\frac{\pi^2}{f_\pi^2}D^{-1}\Sigma\right] \quad (2.73)\\ &= \mathrm{Tr}\left[i^2\Sigma D^{-1}\Sigma\frac{\pi^2}{f_\pi^2} - i^2\Sigma D^{-}1\Sigma\frac{\pi^2}{f_\pi^2} + deri.\right] = 0 \quad (2.74)\end{aligned}$$

which also vanishes, as promised. Here, we have also ignored all the derivative terms that arise from commuting the pion fields to the right since they are not relevant to the mass term.

We can now comment on the effect of Γ_{int} in the result of f_π, the pion decay constant. Proceeding in the same way as we did for $\Gamma_{\log}$, we can start from Eq. 2.72 above and compute $\Gamma_{int}(\Sigma+\delta\Sigma) - \Gamma_{int}(\Sigma)$. We again make use of Eq. 2.40 to commute all pion fields to the right of all function of p and q. It is then straightforward to isolate the term containing two pion fields and two derivatives:

$$\begin{aligned} &\int d^4x\frac{1}{2}Z_{int}(\Sigma)(\partial_\mu\pi^a)^2 = \frac{i}{2}\mathrm{Tr}\left[\frac{i^2}{2}\Sigma(p)\frac{\partial^2}{\partial p_\mu\partial p_\nu}\left(M^{-1}\Sigma(q)\right)\frac{i^2}{f_\pi^2}\partial_\mu\pi\partial_\nu\pi\right] \quad (2.75)\\ =\ &-\int d^4x\frac{1}{f_\pi^2}\frac{i}{2^3\pi^2}\int dpp^3\Sigma(p)\left(-p^2\partial^2 - 2\partial\right)\left(\int dqq^3M^{-1}(p,q)\Sigma(q)\right)(\partial_\mu\pi)^2\end{aligned}$$

where we have converted all momenta to $4-d$ Euclidean space. Notice the big difference here is that it is Σ inside of the derivative with M^{-1}; while we may not have an explicit expression for M^{-1}, we certainly know how M^{-1} acts on Σ in the equation above from Eq. 2.24. We can then replace the integral in parenthesis on which the derivatives are acting by $\frac{\Sigma(p)}{p^2+\Sigma^2(p)}$. It is now straightforward to add this contribution to our previous expression for $Z(\Sigma)$. The numerical results for the cases discussed above, including the effect of Γ_{int}, are then $f_\pi = 0.22$ for the constant coupling and $f_\pi = 0.21$ for the running coupling.

Before closing off this section, we would like to mention that, as we did for the case of the scalar, we have also verified our result for $Z(\Sigma)$ here by calculating the diagram of Fig. 2.4 with pseudo-scalars instead of scalars attached to the fermion loop. In order to find the p^2 coefficient of the two point function above, we proceed as in the previous

section

$$\Gamma^{(2)} = \int \frac{d^4k}{(2\pi)^4} \frac{-1}{f_\pi^2} \Sigma(q)\Sigma(k) 2 \frac{-k^2 + k \cdot p + \Sigma(k)\Sigma(q)}{(k^2 - \Sigma^2(k))(q^2 - \Sigma^2(q))}. \tag{2.76}$$

Except for the replacement of Δ by Σ and a few signs, everything else follows through in the same way. We have expanded the above integrand in powers of p and checked that indeed, the result exactly agrees with our result Eq. 2.70 including all derivative terms. The full result and comparison can be found in the Appendix.

2.5 Discussion of a simple five-dimensional model

In this section we would like discuss the dynamic AdS/QCD model of walking gauge theories of Alho, Evans, and Touminen in [1], which they use to give an example of a holographic description of an $SU(3)$ gauge theory which approaches the conformal window in the walking regime. This is achieved by varying N_f as a continuous parameter in the same way we have done above. The dynamics for the gauge field is included through the running of γ, the anomalous dimension of the quark bilinear which, in the holographic picture, is related to the mass of a canonical scalar in AdS_5, which suffers an instability as it passes through what is known as the Breitenlohner-Freedman bound. This occurs when $\gamma = 1$ or holographically, when the mass of the scalar $m^2 = -4$. Our interest in exploring this model lies in the claim by the authors of [1], that these walking gauge theories possess a Higgs-like excitation, presumably associated with the spontaneous breaking of dilatation symmetry.

Let us then briefly look at the model. For details please refer to the original reference cited above. The holographic coordinate is denoted by ρ, and it is such that $\rho = 0$ is the IR and $\rho = \infty$ is the UV. The scalar meson is described by x dependent fluctuations around the vacuum configurations of a dimension one field $X = L(\rho)e^{2i\pi^a T^a}$, $|X| = L$. Notice then that L is analogous to our momentum dependent fermion mass function, Σ. The effective radial coordinate (in the bulk) is given by $r^2 = \rho^2 + |X|^2$, such that a non-zero value of L implies that, at $\rho = 0$, $r \to 0$ is excluded. In this way, the quark condensate gives rise to a "soft" IR wall.

The $5 - d$ metric is

$$ds^2 = \frac{d\rho^2}{(\rho^2 + |X|^2)} + (\rho^2 + |X|^2)dx^2, \tag{2.77}$$

and the five dimensional action (Eq. 3 in [1] where we have set the F_A and F_V vector

fields to 0) is

$$S_5 = \int d^4x d\rho \mathrm{Tr}\left[\rho^3\left(\frac{1}{\rho^2+|X|^2}|DX|^2 + \frac{\Delta m^2}{\rho^2}|X|^2\right)\right] \tag{2.78}$$

where Δm^2 is related to the canonical scalar's mass[4], and hence to γ. From this action we can immediately find the equation of motion for L, assuming that Δm^2 is a constant:

$$\partial_\rho(\rho^3\partial_\rho L) - \rho\Delta m^2 L = 0. \tag{2.79}$$

Of course an $r(L)$ dependent Δm^2 will be used to describe the running of γ, but only at the level of the equation of motion above. The boundary conditions are $L'(0) = 0$ and $L(0)$, which is interpreted as the effective IR quark mass, such that $L(\infty) = 0$ (only in the chiral limit).

Δm^2 will be given by -2γ, and γ in turn comes from the one loop result

$$\gamma = \frac{3C_2}{2\pi}\alpha = \frac{3(N_c^2-1)}{4N_c\pi}\alpha = \frac{2}{\pi}\alpha \tag{2.80}$$

where α here is the same running coupling from Eq. 2.22. Finally, the effective radial coordinate r is identified with the RG scale μ.

Notice that γ above is exactly what we have defined as r in the first section. Here, let us now re-write Eq. 2.29 assuming r = constant:

$$p^3\Sigma'' + 3p^2\Sigma' + 2r\frac{p^3\Sigma}{p^2+\Sigma^2} = 0. \tag{2.81}$$

We can immediately see that for $p \gg \Sigma(p)$ where Σ can be ignored, this equation is exactly the same as that for L above. They begin to differ significantly as we approach the IR, where the non-linear terms that damp the loop integrals become important.

Finally, the analog of our equation for Δ can be obtained by looking for x dependent excitations around L, $|X| = L_0 + \delta(\rho)e^{-iq\cdot x}$. Eq. 2.78 then leads to an equation of motion for δ [1],

$$\partial_\rho(\rho^3\partial_\rho\delta) - \rho\Delta m^2\delta + \rho L_0\delta\frac{\partial\Delta m^2}{\partial L}\bigg|_{L_0} + M^2R^4\frac{\rho^3}{(\rho^2+L_0^2)^2}\delta = 0. \tag{2.82}$$

As we did for ϕ and π, we must normalize δ such that the kinetic term for the scalar

[4]One can re-write L as $\rho\phi$ to find the canonical form for the $5-d$ action of a scalar in AdS, the mass of which is $(-3+\Delta m^2)$; see Eq. 8 in [1].

meson in Eq. 2.78 be canonical. This takes us to Eq. 11 in [1],

$$\int d\rho \frac{\rho^3}{(\rho^2 + L^2)^2} \delta^2 = 1. \tag{2.83}$$

We can see by comparing this to the Pagels-Stokar (PS) relation discussed in the previous section that, excluding the phase space factors specific to 4 dimensional space-time, this normalization condition agrees with the dominant term of PS as well. Looking at this equation it becomes clear that, as we approach the conformal window and the third term from the left grows smaller, $\delta(\rho)$ will approach the vacuum solution of Eq. 2.79 and the value of M in the fourth term of the RHS above, the mass of the scalar, will tend to 0.

To conclude, from our discussion above we do not find that the soft-wall behaviour in this model can reproduce some of the effects that we have observed in the gauge theory setting studied in the previous sections. While as we have pointed out, some features are in common between the two pictures we do not believe that, in particular, the vanishing dilaton mass $M \to 0$ resulting from Eq. 2.82 can be naturally realized in the gauge theory context.

2.6 Conclusions

In this chapter we have studied the issue of the existence of a dilaton as the lightest scalar particle in gauge theories with chiral symmetry breaking and approximate conformal symmetry. In the framework of a (non-local) auxiliary field effective action, we have derived a differential equation for the dynamically generated fermion mass function in an $SU(N)$ gauge theory with N_f number of fermions, and have shown that working in the renormalization group improved ladder approximation, there are non-trivial solutions for Σ indicating that chiral symmetry is broken. We then studied local scalar and pseudo-scalar fluctuations around these solutions, which describe the scalars and Goldstone bosons in the theory. We have adopted an interesting and not (to our knowledge) commonly used approach from [31] to derive the correct kinetic terms in the scalar and effective actions, and then used them to derive a differential equation, analogous to the gap equation for Σ, for the momentum dependent form factor of the scalars.

The solutions that we have found to these equations, which include effects also from the interaction term in the effective action, are indeed interesting for a few reasons. The first thing to note is that the lightest scalar in the theory is never light relative to the dynamical fermion mass, no matter how close we get to the fixed point of the theory. The mass will always receive contributions from a large range of momentum scales all the way

up to the UV; this has already been pointed out long ago in [13]. From the behaviour of $p\Sigma$ and $p\Delta$ presented in our figures, we believe this to be a robust prediction not specific to any of the approximations we have made. Unlike previous studies that would agree with our last statements however, we additionally find that the momentum dependent form factor of the scalar is in fact very close to Σ itself. This simple fact implies that our scalar will couple to Goldstone bosons, therefore also to the W and Z bosons, very closely resembling a Standard Model Higgs. Of course, as we have just stated, we have not found evidence as to why the lowest lying scalar here should be naturally light as to be anywhere near the 126 GeV observed Higgs boson. But the prediction that a standard gauge theory should generally have this property is we think indeed worthy of attention. With regards to the scalar mass, our results depend on an approximation that is only justified for large N_c. It is thus conceivable that a smaller scalar mass could emerge in a small N_c or strong abelian theory.

We have also studied the pions in this theory, and obtained an integral expression for their decay constant. Comparing to the well known result of Pagels and Stokar [39], we find that while the dominant term agrees with our approach, there are new additional contributions that have a small but noticeable effect on f_π and that are more or less straightforward to include using our approach.

Finally we have commented on the relationship between the equations for the momentum dependent mass functions in our theory and the equations for the radion in the holographic technicolour model of [1]. We do not believe that the type of behaviour they observe, where the radion becomes lighter as the theory approaches the IR fixed point is realizable in the context of a gauge theory.

2.7 Appendix

We begin by giving the numerator for the complete expression for Z before converting four-momenta to Euclidean space. Here, the D represent partial derivatives with respect to the four-momenta squared kk and pp.

$$
\begin{aligned}
&Z_{log}^{\text{num}} := 4\,(\Delta\,(kk))^2\,(\Sigma\,(kk))^4\,(\mathrm{D}\,(\Sigma)\,(kk))^2 \\
&kk{+}12\,\Delta\,(kk)\,\mathrm{D}\,(\Delta)\,(kk)\,kk^3\Sigma\,(kk)\,\mathrm{D}\,(\Sigma)\,(kk){-}8\,\Delta\,(kk)\,\mathrm{D}\,(\Delta)\,(kk)\,kk^2\,(\Sigma\,(kk))^3\,\mathrm{D}\,(\Sigma)\,(kk) \\
&-4\,\Delta\,(kk)\,\mathrm{D}\,(\Delta)\,(kk)\,kk\,\,(\Sigma\,(kk))^5\,\mathrm{D}\,(\Sigma)\,(kk)+6\,\,(\Delta\,(kk))^2\,\Sigma\,(kk)\,\left(D^{(2)}\right)(\Sigma)\,(kk)\,kk^3 \\
&-4\,\,(\Delta\,(kk))^2\,(\Sigma\,(kk))^3\,\left(D^{(2)}\right)(\Sigma)\,(kk)\,kk^2-2\,\,(\Delta\,(kk))^2\,(\Sigma\,(kk))^5\,\left(D^{(2)}\right)(\Sigma)\,(kk)\,kk \\
&-4\,\,(\Delta\,(kk))^2\,\Sigma\,(kk)\,\mathrm{D}\,(\Sigma)\,(kk)\,kk^2-24\,\,(\Delta\,(kk))^2\,(\Sigma\,(kk))^3\,\mathrm{D}\,(\Sigma)\,(kk)\,kk \\
&+24\,\,(\Delta\,(kk))^2\,(\mathrm{D}\,(\Sigma)\,(kk))^2\,kk^2\,(\Sigma\,(kk))^2+2\,\Delta\,(kk)\,\left(D^{(2)}\right)(\Delta)\,(kk)\,kk^4 \\
&+2\,\Delta\,(kk)\,\mathrm{D}\,(\Delta)\,(kk)\,kk^3+4\,\Delta\,(kk)\,\mathrm{D}\,(\Delta)\,(kk)\,(\Sigma\,(kk))^6-2\,\,(\Delta\,(kk))^2\,kk^2 \\
&+4\,\,(\Delta\,(kk))^2\,(\Sigma\,(kk))^4{-}2\,\Delta\,(kk)\,\left(D^{(2)}\right)(\Delta)\,(kk)\,kk^3\,(\Sigma\,(kk))^2{-}2\,\Delta\,(kk)\,\left(D^{(2)}\right)(\Delta)\,(kk)\,kk^2\,(\Sigma\,(kk))^4 \\
&+2\,\Delta\,(kk)\,\left(D^{(2)}\right)(\Delta)\,(kk)\,kk\,\,(\Sigma\,(kk))^6-8\,\Delta\,(kk)\,\mathrm{D}\,(\Delta)\,(kk)\,kk^2\,(\Sigma\,(kk))^2 \\
&+2\,\Delta\,(kk)\,\mathrm{D}\,(\Delta)\,(kk)\,(\Sigma\,(kk))^4\,kk-4\,\,(\Delta\,(kk))^2\,(\Sigma\,(kk))^5\,\mathrm{D}\,(\Sigma)\,(kk) \\
&+6\,\,(\Delta\,(kk))^2\,kk\,\,(\Sigma\,(kk))^2+4\,\,(\Delta\,(kk))^2\,(\mathrm{D}\,(\Sigma)\,(kk))^2\,kk^3
\end{aligned}
$$

The denominator is given by $(kk-\Sigma^2(kk))^4$.

From Fig. 2.4 we write

$$\Gamma^{(2)} := 4\,\frac{\Delta\,(kk)\,\Delta\,(qq)\,(kk-kp+\Sigma\,(kk)\,\Sigma\,(qq))}{\left(kk-(\Sigma\,(kk))^2\right)\left(qq-(\Sigma\,(qq))^2\right)}$$

In order to expand in p given the kp factors in the above expression, we associate the dimensionless quantity ρ to every factor of p. We then write

$$\Gamma^{(2)} := 4\,\frac{\Delta\,(kk)\,\Delta\,(kk+pp\,\rho^2-2\,kp\,\rho)\,\,(kk-kp\,\rho+\Sigma\,(kk)\,\Sigma\,(kk+pp\,\rho^2-2\,kp\,\rho))}{\left(kk-(\Sigma\,(kk))^2\right)\left(kk+pp\,\rho^2-2\,kp\,\rho-(\Sigma\,(kk+pp\,\rho^2-2\,kp\,\rho))^2\right)}$$

It is now straightforward to perform an expansion in ρ; here is the rho^2 term that will give us all p^2 including those coming from kp^2 terms once the angular integrals are performed.

$$\Gamma_{p^2}^{(2)} := 16\,\frac{(\Delta(kk))^2\,kk\,\Sigma(kk)\left(D^{(2)}\right)(\Sigma)(kk)\,kp^2}{\left(kk-(\Sigma(kk))^2\right)\left(-kk+(\Sigma(kk))^2\right)^2}+8\,\frac{(\Delta(kk))^2\,kk\,\Sigma(kk)\mathrm{D}(\Sigma)(kk)\,pp}{\left(kk-(\Sigma(kk))^2\right)\left(-kk+(\Sigma(kk))^2\right)^2}+64\,\frac{(\Delta(kk))^2\,kp^2\,kk\,\Sigma(kk)\mathrm{D}(\Sigma)(kk)}{\left(kk-(\Sigma(kk))^2\right)\left(-kk+(\Sigma(kk))^2\right)^3}$$

$$
\begin{aligned}
&-96\,\frac{(\Delta(kk))^2 kp^2 (\Sigma(kk))^2 \left(\mathrm{D}(\Sigma)(kk)\right)^2 kk}{\left(kk-(\Sigma(kk))^2\right)\,\left(-kk+(\Sigma(kk))^2\right)^3}+32\,\frac{\Delta(kk)kp^2\mathrm{D}(\Delta)(kk)(\Sigma(kk))^5\mathrm{D}(\Sigma)(kk)}{\left(kk-(\Sigma(kk))^2\right)\left(-kk+(\Sigma(kk))^2\right)^3}-32\,\frac{\Delta(kk)kp^2\mathrm{D}(\Delta)(kk)kk^2\Sigma(kk)\mathrm{D}(\Sigma)(kk)}{\left(kk-(\Sigma(kk))^2\right)\left(-kk+(\Sigma(kk))^2\right)^3}+\\
&16\,\frac{(\Delta(kk))^2 kk\left(\mathrm{D}(\Sigma)(kk)\right)^2 kp^2}{\left(kk-(\Sigma(kk))^2\right)\left(-kk+(\Sigma(kk))^2\right)^2}+8\,\frac{(\Delta(kk))^2(\Sigma(kk))^3\mathrm{D}(\Sigma)(kk)pp}{\left(kk-(\Sigma(kk))^2\right)\left(-kk+(\Sigma(kk))^2\right)^2}+16\,\frac{(\Delta(kk))^2(\Sigma(kk))^3\left(D^{(2)}\right)(\Sigma)(kk)kp^2}{\left(kk-(\Sigma(kk))^2\right)\,\left(-kk+(\Sigma(kk))^2\right)^2}+\\
&16\,\frac{(\Delta(kk))^2 kp^2(\Sigma(kk))^2\left(\mathrm{D}(\Sigma)(kk)\right)^2}{\left(kk-(\Sigma(kk))^2\right)\left(-kk+(\Sigma(kk))^2\right)^2}+64\,\frac{(\Delta(kk))^2 kp^2(\Sigma(kk))^3\mathrm{D}(\Sigma)(kk)}{\left(kk-(\Sigma(kk))^2\right)\left(-kk+(\Sigma(kk))^2\right)^3}-32\,\frac{(\Delta(kk))^2 kp^2(\Sigma(kk))^4\left(\mathrm{D}(\Sigma)(kk)\right)^2}{\left(kk-(\Sigma(kk))^2\right)\left(-kk+(\Sigma(kk))^2\right)^3}+\\
&16\,\frac{\Delta(kk)kp^2\mathrm{D}(\Delta)(kk)kk^2}{\left(kk-(\Sigma(kk))^2\right)\left(-kk+(\Sigma(kk))^2\right)^3}\\
&-16\,\frac{\Delta(kk)kp^2\mathrm{D}(\Delta)(kk)(\Sigma(kk))^4}{\left(kk-(\Sigma(kk))^2\right)\left(-kk+(\Sigma(kk))^2\right)^3}+16\,\frac{\Delta(kk)\mathrm{D}(\Delta)(kk)kp^2\Sigma(kk)\mathrm{D}(\Sigma)(kk)}{\left(kk-(\Sigma(kk))^2\right)^2}\\
&+8\,\frac{\Delta(kk)kp^2\mathrm{D}(\Delta)(kk)}{\left(kk-(\Sigma(kk))^2\right)^2}-4\,\frac{(\Delta(kk))^2 kk\,pp}{\left(kk-(\Sigma(kk))^2\right)\left(-kk+(\Sigma(kk))^2\right)^2}\\
&-4\,\frac{(\Delta(kk))^2(\Sigma(kk))^2 pp}{\left(kk-(\Sigma(kk))^2\right)\left(-kk+(\Sigma(kk))^2\right)^2}-8\,\frac{(\Delta(kk))^2 kp^2 kk}{\left(kk-(\Sigma(kk))^2\right)\left(-kk+(\Sigma(kk))^2\right)^3}\\
&-24\,\frac{(\Delta(kk))^2 kp^2(\Sigma(kk))^2}{\left(kk-(\Sigma(kk))^2\right)\left(-kk+(\Sigma(kk))^2\right)^3}+4\,\frac{(\Delta(kk))^2\Sigma(kk)\mathrm{D}(\Sigma)(kk)pp}{\left(kk-(\Sigma(kk))^2\right)^2}\\
&+8\,\frac{(\Delta(kk))^2\Sigma(kk)\left(D^{(2)}\right)(\Sigma)(kk)kp^2}{\left(kk-(\Sigma(kk))^2\right)^2}+4\,\frac{\Delta(kk)\mathrm{D}(\Delta)(kk)pp\,kk}{\left(kk-(\Sigma(kk))^2\right)^2}\\
&+4\,\frac{\Delta(kk)\mathrm{D}(\Delta)(kk)pp\,(\Sigma(kk))^2}{\left(kk-(\Sigma(kk))^2\right)^2}+8\,\frac{\Delta(kk)\left(D^{(2)}\right)(\Delta)(kk)kp^2 kk}{\left(kk-(\Sigma(kk))^2\right)^2}\\
&+8\,\frac{\Delta(kk)\left(D^{(2)}\right)(\Delta)(kk)kp^2(\Sigma(kk))^2}{\left(kk-(\Sigma(kk))^2\right)^2}
\end{aligned}
$$

We can now replace kp^2 by $\frac{(kk)(pp)}{4}$ by symmetry (this is equivalent to going to Euclidean space and performing the angular integrals, then introducing back a factor of $2\pi^2$ and going back to Minkowski space). The coefficient of the pp term is then given by:

$$
\begin{aligned}
\Gamma^{(2)}_{p^2} :=\ &-8\,\frac{\Delta(kk)\mathrm{D}(\Delta)(kk)kk^2(\Sigma(kk))^2}{\left(-kk+(\Sigma(kk))^2\right)^4}+2\,\frac{\Delta(kk)\mathrm{D}(\Delta)(kk)(\Sigma(kk))^4 kk}{\left(-kk+(\Sigma(kk))^2\right)^4}-4\,\frac{(\Delta(kk))^2\Sigma(kk)\mathrm{D}(\Sigma)(kk)kk^2}{\left(-kk+(\Sigma(kk))^2\right)^4}\\
&-24\,\frac{(\Delta(kk))^2(\Sigma(kk))^3\mathrm{D}(\Sigma)(kk)kk}{\left(-kk+(\Sigma(kk))^2\right)^4}+2\,\frac{\Delta(kk)\mathrm{D}(\Delta)(kk)kk^3}{\left(-kk+(\Sigma(kk))^2\right)^4}\\
&+4\,\frac{\Delta(kk)\mathrm{D}(\Delta)(kk)(\Sigma(kk))^6}{\left(-kk+(\Sigma(kk))^2\right)^4}-2\,\frac{(\Delta(kk))^2 kk^2}{\left(-kk+(\Sigma(kk))^2\right)^4}\\
&+4\,\frac{(\Delta(kk))^2(\Sigma(kk))^4}{\left(-kk+(\Sigma(kk))^2\right)^4}-4\,\frac{(\Delta(kk))^2(\Sigma(kk))^5\mathrm{D}(\Sigma)(kk)}{\left(-kk+(\Sigma(kk))^2\right)^4}\\
&-2\,\frac{\Delta(kk)\left(D^{(2)}\right)(\Delta)(kk)kk^3(\Sigma(kk))^2}{\left(-kk+(\Sigma(kk))^2\right)^4}-2\,\frac{\Delta(kk)\left(D^{(2)}\right)(\Delta)(kk)kk^2(\Sigma(kk))^4}{\left(-kk+(\Sigma(kk))^2\right)^4}\\
&+4\,\frac{(\Delta(kk))^2\left(\mathrm{D}(\Sigma)(kk)\right)^2 kk^3}{\left(-kk+(\Sigma(kk))^2\right)^4}+2\,\frac{\Delta(kk)\left(D^{(2)}\right)(\Delta)(kk)kk\,(\Sigma(kk))^6}{\left(-kk+(\Sigma(kk))^2\right)^4}\\
&+6\,\frac{(\Delta(kk))^2 kk\,(\Sigma(kk))^2}{\left(-kk+(\Sigma(kk))^2\right)^4}+2\,\frac{\Delta(kk)\left(D^{(2)}\right)(\Delta)(kk)kk^4}{\left(-kk+(\Sigma(kk))^2\right)^4}\\
&-2\,\frac{(\Delta(kk))^2(\Sigma(kk))^5\left(D^{(2)}\right)(\Sigma)(kk)kk}{\left(-kk+(\Sigma(kk))^2\right)^4}-4\,\frac{\Delta(kk)\mathrm{D}(\Delta)(kk)kk\,(\Sigma(kk))^5\mathrm{D}(\Sigma)(kk)}{\left(-kk+(\Sigma(kk))^2\right)^4}+4\,\frac{(\Delta(kk))^2(\Sigma(kk))^4\left(\mathrm{D}(\Sigma)(kk)\right)^2 kk}{\left(-kk+(\Sigma(kk))^2\right)^4}\\
&+6\,\frac{(\Delta(kk))^2\Sigma(kk)\left(D^{(2)}\right)(\Sigma)(kk)kk^3}{\left(-kk+(\Sigma(kk))^2\right)^4}-4\,\frac{(\Delta(kk))^2(\Sigma(kk))^3\left(D^{(2)}\right)(\Sigma)(kk)kk^2}{\left(-kk+(\Sigma(kk))^2\right)^4}+12\,\frac{\Delta(kk)\mathrm{D}(\Delta)(kk)kk^3\Sigma(kk)\mathrm{D}(\Sigma)(kk)}{\left(-kk+(\Sigma(kk))^2\right)^4}
\end{aligned}
$$

$$-8\,\frac{\Delta(kk)\mathrm{D}_{(\Delta)}(kk)kk^2(\Sigma(kk))^3\mathrm{D}_{(\Sigma)}(kk)}{\left(-kk+(\Sigma(kk))^2\right)^4}+24\,\frac{(\Delta(kk))^2\left(\mathrm{D}_{(\Sigma)}(kk)\right)^2kk^2(\Sigma(kk))^2}{\left(-kk+(\Sigma(kk))^2\right)^4}$$

We can factor out the denominator $\frac{1}{(kk-\Sigma(kk)^2)^4}$, the remaining (numerator) expression is

$$\begin{aligned}
&\Gamma_{p^2}^{(2),\,\mathrm{num}} := 4\,(\Delta(kk))^2(\Sigma(kk))^4(\mathrm{D}(\Sigma)(kk))^2\\
&kk+12\,\Delta(kk)\,\mathrm{D}(\Delta)(kk)\,kk^3\Sigma(kk)\,\mathrm{D}(\Sigma)(kk)-8\,\Delta(kk)\,\mathrm{D}(\Delta)(kk)\,kk^2(\Sigma(kk))^3\,\mathrm{D}(\Sigma)(kk)\\
&-4\,\Delta(kk)\,\mathrm{D}(\Delta)(kk)\,kk\,(\Sigma(kk))^5\,\mathrm{D}(\Sigma)(kk)+6\,(\Delta(kk))^2\,\Sigma(kk)\left(D^{(2)}\right)(\Sigma)(kk)\,kk^3\\
&-4\,(\Delta(kk))^2(\Sigma(kk))^3\left(D^{(2)}\right)(\Sigma)(kk)\,kk^2-2\,(\Delta(kk))^2(\Sigma(kk))^5\left(D^{(2)}\right)(\Sigma)(kk)\,kk\\
&-4\,(\Delta(kk))^2\,\Sigma(kk)\,\mathrm{D}(\Sigma)(kk)\,kk^2-24\,(\Delta(kk))^2(\Sigma(kk))^3\,\mathrm{D}(\Sigma)(kk)\,kk\\
&+24\,(\Delta(kk))^2(\mathrm{D}(\Sigma)(kk))^2\,kk^2(\Sigma(kk))^2+2\,\Delta(kk)\left(D^{(2)}\right)(\Delta)(kk)\,kk^4\\
&+2\,\Delta(kk)\,\mathrm{D}(\Delta)(kk)\,kk^3+4\,\Delta(kk)\,\mathrm{D}(\Delta)(kk)\,(\Sigma(kk))^6-2\,(\Delta(kk))^2\,kk^2\\
&+4\,(\Delta(kk))^2(\Sigma(kk))^4-2\,\Delta(kk)\left(D^{(2)}\right)(\Delta)(kk)\,kk^3(\Sigma(kk))^2-2\,\Delta(kk)\left(D^{(2)}\right)(\Delta)(kk)\,kk^2(\Sigma(kk))^4\\
&+2\,\Delta(kk)\left(D^{(2)}\right)(\Delta)(kk)\,kk\,(\Sigma(kk))^6-8\,\Delta(kk)\,\mathrm{D}(\Delta)(kk)\,kk^2(\Sigma(kk))^2\\
&+2\,\Delta(kk)\,\mathrm{D}(\Delta)(kk)\,(\Sigma(kk))^4\,kk-4\,(\Delta(kk))^2(\Sigma(kk))^5\,\mathrm{D}(\Sigma)(kk)\\
&+6\,(\Delta(kk))^2\,kk\,(\Sigma(kk))^2+4\,(\Delta(kk))^2(\mathrm{D}(\Sigma)(kk))^2\,kk^3
\end{aligned}$$

which exactly agrees with the expression for Z given in the first line above.

The exact same procedure follows through in the case of the pion. We start with the expression obtained by commuting all pion fields to the right to give

$$\begin{aligned}
&Z_{log,\pi} := 4\,\frac{(\Sigma(p2))^4}{\left(-p2+(\Sigma(p2))^2\right)^3}-2\,\frac{(\Sigma(p2))^3\,p2^2\left(D^{(2)}\right)(\Sigma)(p2)}{\left(-p2+(\Sigma(p2))^2\right)^3}\\
&-10\,\frac{(\Sigma(p2))^3\,\mathrm{D}(\Sigma)(p2)\,p2}{\left(-p2+(\Sigma(p2))^2\right)^3}-2\,\frac{(\Sigma(p2))^2\,p2}{\left(-p2+(\Sigma(p2))^2\right)^3}\\
&+8\,\frac{(\Sigma(p2))^2\,p2^2(\mathrm{D}(\Sigma)(p2))^2}{\left(-p2+(\Sigma(p2))^2\right)^3}+2\,\frac{\Sigma(p2)\,p2^3\left(D^{(2)}\right)(\Sigma)(p2)}{\left(-p2+(\Sigma(p2))^2\right)^3}\\
&+2\,\frac{\Sigma(p2)\,\mathrm{D}(\Sigma)(p2)\,p2^2}{\left(-p2+(\Sigma(p2))^2\right)^3}
\end{aligned}$$

From the Fig. 2.4 where the external lines are now pseudo-scalars, we obtain the expression from Section 2.4

$$\Gamma_{\pi}^{(2)} := 4\,\frac{\Sigma(qq)\,\Sigma(kk)\,(-kk+kp+\Sigma(qq)\,\Sigma(kk))}{\left(kk-(\Sigma(kk))^2\right)\left(qq-(\Sigma(qq))^2\right)}$$

Introducing ρ in the same manner as we did for the scalar we have

$$\Gamma_{\pi}^{(2)} := 4\,\frac{\Sigma\left(kk+pp\,\rho^2-2\,kp\,\rho\right)\Sigma\left(kk\right)\,\left(-kk+kp\,\rho+\Sigma\left(kk+pp\,\rho^2-2\,kp\,\rho\right)\Sigma\left(kk\right)\right)}{\left(kk-\left(\Sigma\left(kk\right)\right)^2\right)\left(kk+pp\,\rho^2-2\,kp\,\rho-\left(\Sigma\left(kk+pp\,\rho^2-2\,kp\,\rho\right)\right)^2\right)}$$

The ρ^2 coefficient of the expansion is now given by

$$\begin{aligned}\Gamma_{p^2,\pi}^{(2)} :=\ & 8\,\frac{(\Sigma(kk))^3\mathrm{D}(\Sigma)(kk)pp}{\left(kk-(\Sigma(kk))^2\right)^2}+16\,\frac{(\Sigma(kk))^3\left(D^{(2)}\right)(\Sigma)(kk)kp^2}{\left(kk-(\Sigma(kk))^2\right)^2}-4\,\frac{\Sigma(kk)\mathrm{D}(\Sigma)(kk)pp\,kk}{\left(kk-(\Sigma(kk))^2\right)^2}-8\,\frac{\Sigma(kk)\left(D^{(2)}\right)(\Sigma)(kk)kp^2kk}{\left(kk-(\Sigma(kk))^2\right)^2}\\ & -8\,\frac{\mathrm{D}(\Sigma)(kk)kp^2\Sigma(kk)}{\left(kk-(\Sigma(kk))^2\right)^2}+16\,\frac{(\Sigma(kk))^2kp^2\left(\mathrm{D}(\Sigma)(kk)\right)^2}{\left(kk-(\Sigma(kk))^2\right)^2}\\ & -4\,\frac{(\Sigma(kk))^2pp}{\left(kk-(\Sigma(kk))^2\right)\left(-kk+(\Sigma(kk))^2\right)}+8\,\frac{(\Sigma(kk))^3\mathrm{D}(\Sigma)(kk)pp}{\left(kk-(\Sigma(kk))^2\right)\left(-kk+(\Sigma(kk))^2\right)}\\ & +16\,\frac{(\Sigma(kk))^3\left(D^{(2)}\right)(\Sigma)(kk)kp^2}{\left(kk-(\Sigma(kk))^2\right)\left(-kk+(\Sigma(kk))^2\right)}+16\,\frac{(\Sigma(kk))^2kp^2\left(\mathrm{D}(\Sigma)(kk)\right)^2}{\left(kk-(\Sigma(kk))^2\right)\left(-kk+(\Sigma(kk))^2\right)}-8\,\frac{(\Sigma(kk))^2kp^2}{\left(kk-(\Sigma(kk))^2\right)\left(-kk+(\Sigma(kk))^2\right)^2}\\ & +16\,\frac{(\Sigma(kk))^3kp^2\mathrm{D}(\Sigma)(kk)}{\left(kk-(\Sigma(kk))^2\right)\left(-kk+(\Sigma(kk))^2\right)^2}+16\,\frac{\mathrm{D}(\Sigma)(kk)kp^2\Sigma(kk)kk}{\left(kk-(\Sigma(kk))^2\right)\left(-kk+(\Sigma(kk))^2\right)^2}\\ & -32\,\frac{(\Sigma(kk))^2kp^2\left(\mathrm{D}(\Sigma)(kk)\right)^2kk}{\left(kk-(\Sigma(kk))^2\right)\left(-kk+(\Sigma(kk))^2\right)^2}\end{aligned}$$

Replacing kp^2 as before we find

$$\begin{aligned}\Gamma_{p^2,\pi}^{(2)} :=\ & -10\,\frac{\left(\Sigma\left(kk\right)\right)^3\mathrm{D}\left(\Sigma\right)\left(kk\right)kk}{\left(-kk+\left(\Sigma\left(kk\right)\right)^2\right)^3}-2\,\frac{\left(\Sigma\left(kk\right)\right)^3\left(D^{(2)}\right)\left(\Sigma\right)\left(kk\right)kk^2}{\left(-kk+\left(\Sigma\left(kk\right)\right)^2\right)^3}\\ & +2\,\frac{\Sigma\left(kk\right)\mathrm{D}\left(\Sigma\right)\left(kk\right)kk^2}{\left(-kk+\left(\Sigma\left(kk\right)\right)^2\right)^3}+2\,\frac{\Sigma\left(kk\right)\left(D^{(2)}\right)\left(\Sigma\right)\left(kk\right)kk^3}{\left(-kk+\left(\Sigma\left(kk\right)\right)^2\right)^3}\\ & +8\,\frac{\left(\Sigma\left(kk\right)\right)^2\left(\mathrm{D}\left(\Sigma\right)\left(kk\right)\right)^2kk^2}{\left(-kk+\left(\Sigma\left(kk\right)\right)^2\right)^3}-2\,\frac{\left(\Sigma\left(kk\right)\right)^2kk}{\left(-kk+\left(\Sigma\left(kk\right)\right)^2\right)^3}\\ & +4\,\frac{\left(\Sigma\left(kk\right)\right)^4}{\left(-kk+\left(\Sigma\left(kk\right)\right)^2\right)^3}\end{aligned}$$

which can be seen to agree with the expression obtained for Z above.

Chapter 3

Lepton based Charge Asymmetry Measurements and Diquarks

In this Chapter, we propose a lepton based observable for measuring charge asymmetries of particle pairs produced at the LHC that can be used even when only one particle in the pair decays leptonically. The observable, which we call A_C^l is in some sense analogous to A_{FB}^l used at the Tevatron (see e.g. [40]) to study the $t\bar{t}$ forward-backward asymmetry. Like the latter, our A_C^l does not require reconstruction of the original particle's four-momentum; it could then be of value for studying systems where this step is not readily achievable. As an example of one such case, we present our approach in the context of coloured scalars carrying diquark quantum numbers, and also discuss its application to the $t\bar{t}$ charge asymmetry. In the case of a scalar carrying tt quantum numbers, we find that with several thousand events, a combined measurement of the different channels (which are determined by the number of leptons in the final state) can give an interesting deviation from the Standard Model, if the sample's A_C^l is as small as $\sim 1\%$. We also present our theory calculation of the diquark's charge asymmetry at next-to-leading order in QCD. The work in this chapter was done in collaboration with Bob Holdom and Melissa Ratzlaff, and is currently being prepared for submission.

3.1 Introduction

Asymmetry measurements at particle colliders are interesting to study for many reasons. In the past, they have been of crucial importance to help us test predictions on the fundamental structure of the gauge theories in the Standard Model. Examples are the use of lepton forward-backward asymmetries, pair production asymmetries, and lepton polarization asymmetries, all at the Z pole. More recently, the $t\bar{t}$ forward-backward

asymmetry ($A_{FB}^{t\bar{t}}$) has been the focus of many efforts in the search for experimental evidence of beyond the Standard Model (BSM) physics.

The widespread interest in $A_{FB}^{t\bar{t}}$ from the particle physics community is well motivated: the CDF and D0 experiments at the Tevatron have performed experimental studies of this observable and both collaborations find an effect around 2σ above the expectation for the SM. At the LHC, the charge asymmetry between the central and forward/backward regions of the detector (A_C) originates from the same charge asymmetric contributions to the $t\bar{t}$ cross section at the parton level that give rise to A_{FB} at the Tevatron. These two observables are thus closely related and it is expected that measurements at the LHC of the relevant observables would hint in the direction of a similar anomaly. So far, the ATLAS and CMS collaborations have measured $A_C^{t\bar{t}}$ [41–43], yielding results that all agree well with the SM prediction. In order to extract a value of $A_C^{t\bar{t}}$ from the data, the $t\bar{t}$ system was reconstructed. Lepton based asymmetries have also been used to study the $t\bar{t}$ system, both at the Tevatron and LHC (see [40] for a nice overview). These observables have the advantage that the full reconstruction of the t and $\bar{t}$'s four momentum is not required; leptons (μs and es) are much more simple to identify and reconstruct, and corrections due to detector effects are usually small.

We have noticed that while lepton based asymmetries in both the single lepton channel, A_{FB}^{l}, and dilepton channel, A_{FB}^{l} and A_{FB}^{ll}, have been studied at the Tevatron, only the dilepton channel measurement analogous to A_{FB}^{ll}, A_C^{ll}, has been studied at the LHC. No analog observable for A_{FB}^{l} has been proposed. It is this type of observable that we would like to explore in this chapter, since it could be not only useful to study the $t\bar{t}$ system in conjunction with other asymmetry measurements, but possibly necessary if we wish to study other systems of particle anti-particle pairs where reconstruction of the pair's four momentum is either highly inefficient, or impossible. This could be the case if, for example, such pairs decay to final states with very high jet multiplicity and/or multiple invisible states, or if each particle in the original pair has multiple decay modes. One such example, which we will adopt for illustration purposes in this chapter, is the production of coloured scalar diquark pairs.

These scalars carrying diquark quantum numbers can arise generically in many BSM theories; for example, they can appear as pseudo-Goldstone bosons in certain technicolor or other dynamical models of EWSB [17]. A possibly interesting aspect of diquarks is that their couplings to SM states can have a variety of patterns that are not already ruled out by existing flavour and other precision data [44], something that suggests that their study could teach us something about flavour physics. Diquark pairs produced from $q\bar{q}$ initial states at the LHC would exhibit a charge asymmetry in their differential cross

section, an effect analogous to the charge asymmetry predicted by QCD for $t\bar{t}$ pairs at next-to-leading order (NLO) [45]. Depending on the diquarks' flavour quantum numbers, final states with one, two (same-sign and opposite-sign), three, etc. leptons can arise.

The observable we shall propose provides a simple way of extracting a charge asymmetry measurement in each of these types of events by individually adding each μ or e in the final state to the corresponding $+$ or $-$ lepton's rapidity distribution and then studying the difference between said distributions. Cuts would be imposed to select candidate events requiring a certain number of (isolated, high p_T) leptons in the final state, this number defines the "channel", and results from all channels can be combined later for a more statistically significant result. We have not considered τs as "leptons" in our analysis. τs are also a source of es and μs and in ignoring them we are slightly underestimating the number of events that will pass our cuts in each channel.

This chapter is organized as follows. We define and discuss the general aspects of our method, and how to apply it to scalar diquarks in Section 3.2. In Section 3.3 we discuss this observable in the context of the $t\bar{t}$ charge asymmetry. Since a complete calculation of the charge asymmetry of a charged or coloured scalar does not seem to exist in the literature[1] we also present our theory calculation for a pair of coloured diquark scalars in Section 3.4. Concluding remarks can be found in Section 3.5.

3.2 A new charge asymmetry observable and scalar Diquarks

In hadron-hadron colliders, a charge asymmetric contribution to the production cross section of coloured scalar particle pairs ($\phi\overline{\phi}$) will arise from order α_s^3 corrections to the process $q\bar{q} \to \phi\overline{\phi}$. Similarly to the case of the familiar $t\bar{t}$ (or any $q\bar{q}$ pair) asymmetry, this contribution can be traced back to the interference between initial state and final state gluon emission amplitudes, and between virtual gluon emission (box diagrams) and the Born amplitude (See Fig. 3.1).

At a $p\bar{p}$ collider, this would result in a charge separation of the outgoing scalar pairs between the forward and backward regions of the detectors, with a preference for producing the ϕ (or the $\bar{\phi}$, we will discuss the issue of which below) in the direction of the incoming proton, and the $\bar{\phi}$ (or the ϕ) in the direction of the incoming anti-proton.

[1]The authors of [46] have performed a partial calculation for charged Higgs pair production, where results for only 2 values of $(\sqrt{s}, m_H)$ are presented as a function of the cut on the maximum energy of unresolved radiated photons. The radiation of hard photons must be taken into account in order to eliminate this dependence.

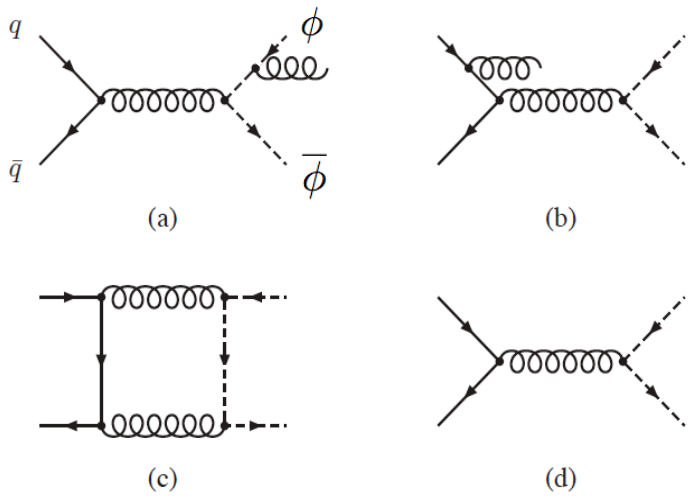

Figure 3.1: Representative diagrams contributing to $\phi\overline{\phi}$ differential charge asymmetry: interference of a) with b) plus c) with d).

There, one could use the single-lepton based observable

$$A_{FB}^{l} = \frac{N_l(Q\eta > 0) - N_l(Q\eta < 0)}{N_l(Q\eta > 0) + N_l(Q\eta < 0)}, \tag{3.1}$$

as used by the Tevatron experiments [47] for $t\bar{t}$, to study the charge asymmetry of the $\phi\bar{\phi}$ system when the final state has only one, or more, leptons. In contrast, at a pp collider like the LHC there is a slight preference for producing the ϕ ($\bar{\phi}$) with momentum direction in the central region (low rapidities) and its antiparticle with more forward/backward momentum (large rapidities). Therefore, the y distribution for charged leptons coming from the scalar being preferentially produced at low $|y|$ is expected to be slightly more centrally peaked than that for leptons coming from the scalar more often produced at large $|y|$.

We shall then define our observable by separating events into two large (pseudo)rapidity bins or "regions", the 1st being at large $|y|$, which combines events at both ends of the detector, and the 2nd being the central one, symmetric about $y = 0$. Since the particle pairs will decay into final states with different numbers of leptons, we would like to perform statistically independent measurements for each different type of final state or channel. The channel will then be defined by the final state lepton multiplicity i, and

observables measured in a given channel will carry the subscript i to indicate so.

For a given sample selected from the data a raw leptonic observable, which we shall call $A^l_{i,\text{raw}}$ where i indicates the channel being studied, can be measured:

$$A^l_{i,\text{raw}} = \frac{\sum_q (qN^q_i(|y| > t) - qN^q_i(|y| < t))}{N_i(|y| > t) + N_i(|y| < t)}. \tag{3.2}$$

The quantities $N^q_i(|y| > t)$ and $N^q_i(|y| < t)$ are the number of leptons of charge q in the 1 and 2 regions respectively, $q = \pm 1$, and $N_i \equiv \sum_q N^q_i$. The value of t, which gives the width of the central region, is crucial to the asymmetry measurement: the central bin must end at the values of $\pm y$ where the positive (negative) lepton count, in the smallest y bins (used in the original binning of events), is expected to become smaller than the negative (positive) lepton count, due to the predicted asymmetry. Therefore a somewhat robust estimate of this number is necessary for this study. We comment more on this point further in this section.

In order to extract the asymmetry of the signal and compare to a given model, we then define the two quantities:

$$A^l_{i,\text{SM}} = \left(\frac{\sum_q (qN^q_{i,\text{bkg}}(|y| > t) - qN^q_{i,\text{bkg}}(|y| < t))}{N_{i,\text{signal}} + N_{i,\text{bkg}}} \right)_{\text{MC}}, \tag{3.3}$$

$$A^l_{i,\text{signal}} = (A^l_{i,\text{raw}} - A^l_{i,\text{SM}}) \left(\frac{N_{i,\text{signal}} + N_{i,\text{bkg}}}{N_{i,\text{signal}}} \right)_{\text{MC}}, \tag{3.4}$$

where the subscript "MC" indicates a necessary input from Monte Carlo simulations. In channels with only one or two opposite-sign leptons in the final state, the SM processes W+jets and $t\bar{t}$ production that pass our selection criteria will contribute to a non-zero background charge asymmetry. Channels with two same-sign leptons, and 3 or more leptons in the final state will have low SM backgrounds, none of which should contribute to an asymmetry. In those channels, A^l_{SM} should be 0 within uncertainties, and $A^l_{i,\text{signal}}$ will be more easily obtained.

Diquarks can transform as a triplet or as a sextet under $SU(3)_C$. We shall call the scalar which has qq content ϕ, and that which has $\bar{q}\bar{q}$ content $\bar{\phi}$. At a symmetric initial state collider like the LHC, the scalar ϕ transforming as $\mathbf{6}$ ($\bar{\mathbf{3}}$) would be produced with preference at larger (smaller) rapidities whereas the $\bar{\phi}$ transforming as $\bar{\mathbf{6}}$ ($\mathbf{3}$) would do the opposite. This difference leads to interesting effects. Triplet scalar pairs, for example, will have a negative integrated charge asymmetry in contrast with the SM prediction for $t\bar{t}$, and with sextet diquarks. Additionally, when the triplets have charge 4/3 or 1/3, the resulting integrated charge asymmetry in the daughter leptons will also be negative.

We shall assume that diquarks have quark components with standard electric charges, and that they decay weakly with a large mixing to heavy quarks. Then, the decay of a scalar diquark will result in 2 down type quarks and a varying number of W bosons. Charge 4/3 diquarks will decay to $bbW^+W^+(W^+W^-)^n$, where the number n (integer or 0) of additional W^+W^- pairs depends on the scalars' mass and intermediate (possibly BSM) states mediating its decay. Similarly, charge 1/3 diquarks will decay to $bbW^+(W^+W^-)^n$, and charge $-2/3$ diquarks to $bb(W^+W^-)^n$. Unless we state otherwise, we will assume by default that no extra W^+W^- pairs arise in the scalars' decay (i.e. $n = 0$, which corresponds to scalars initially decaying to only 2 SM quarks, or particles that decay in the exact same way as them).

We can now see that charge 4/3 diquarks that decay to 2 tops are particularly interesting in the context of lepton based measurements since such $\phi\bar{\phi}$ pairs could produce final states with one, two (same-sign or opposite-sign), three, or four leptons. Probabilities for each of these final states can be found in Table 1 below. Let us focus on this type of diquark for now.

Lepton content in final state	Probability
4 leptons	0.002
3 leptons	0.034
2 opposite sign leptons	0.119
2 same sign leptons	0.060
1 lepton	0.418
0 leptons	0.197
only τ's	0.170

In channels where there are two (or more) opposite sign leptons, we of course have an observable of the type A_C^{ll} [41] at our disposal

$$A_C^{ll} = \frac{N(\Delta|y| > 0) - N(\Delta|y| < 0)}{N(\Delta|y| > 0) + N(\Delta|y| < 0)} \tag{3.5}$$

where $\Delta|y| = |y_{l^+}| - |y_{l^-}|$. Events with exactly two opposite sign leptons give us one data point on the Δy distribution each, those with 3 leptons give us 2 points, and those with 4 leptons give us 4 points. Notice that diquark scalar pairs decay to final states with only one lepton, or two same-sign leptons with a probability close to 50%, and such events cannot be used in this type of approach. On the other hand, a measurement of $A_{C,i}^l$ would be possible in all of the above mentioned channels, and each $\phi\bar{\phi}$ candidate event in channel i contributes i data points to the lepton distributions.

As in the case of $t\bar{t}$, A_C^{ll} from $\phi\bar{\phi}$ is predictably smaller than the original asymmetry in the scalars, $A_C^{\phi\bar{\phi}}$, because the leptons' rapidity distributions are smeared out relative to those of the parent particles[2]. Our observable A_C^l is also predictably smaller than both $A_C^{\phi\bar{\phi}}$ and A_C^{ll} because the asymmetric part of the resulting single-lepton distributions can overlap quite a lot. Hence, in taking the difference as defined in Eq. 3.2 some information of the asymmetry is lost. We have used simulated events to roughly quantify these effects and predict how much smaller our observable is expected to be relative to the other two. Of interest is the comparison to the latter, as we are unable to reconstruct the $\phi\bar{\phi}$ to measure the earlier directly. We estimate A_C^l to be smaller than A_C^{ll} by a factor of ~ 0.8. The procedure used can be found in the next section for the interested reader.

From the above discussion, we can roughly compare the two approaches to measuring charge asymmetries of scalar diquarks. We will assume that detector and selection bias effects affect *the signal* in all channels in a similar way, such that the relative sizes of branching ratios between the signal in the different channels remain true to Table 1 above. For a certain number of $\phi\bar{\phi}$ recorded events, we can estimate the statistical uncertainty of the combined measurement from all channels for A_C^l relative to that associated with A_C^{ll}. Varying the percentage of background events in the single lepton channel (relevant only for A_C^l) between 20 and 60%, and in the 2 opposite-sign lepton channel between 10 and 40%, we find that the statistical uncertainty in the A_C^{ll} approach is larger than that in A_C^l by a factor of ~ 2.

The ATLAS and CMS experiments have recorded about 25 fb^{-1} of data in 2011 and 2012 combined, $\sim 4/5$ of this has been at $\sqrt{s} = 8$ TeV. Based on [48] we estimate that, only in the single lepton channel, each detector has recorded on the order of 3×10^5 $t\bar{t}$ events that pass the selection in [48]. While so far the observed and expected number of events agree within uncertainties, the uncertainty on the expected number of signal ($t\bar{t}$) events is close to 10% in both the e and μ channels. This leaves plenty of room for NP events that pass the same selection cuts, like our $\phi\bar{\phi}$ decays, to be hiding in the $t\bar{t}$ data. However, if we assume we are dealing *only* with the tt type diquarks we have focused on above, then the branching ratios imply that it is the multi-lepton channels that will place the more stringent constrains on the total number of allowed events. For example, recent SUSY searches [49, 50] constrain the anomalous production of multiple-lepton events in signal regions that overlap with ours to be quite small, at most ~ 1 event, in the 4-lepton channel. This would imply that roughly 30 events could be present in the 2 same-sign

[2]The difference between these two distributions can be relevant as it carries information about the polarization of the W's; however we will not be concerned with the issue of polarization in this chapter since we are only considering QCD contributions.

lepton channel. In light of the recently reported hint of an excess at ATLAS in this particular channel [16] it is not impossible to accommodate a dozen or so events coming from tt diquarks to agree with this data. This would also suggest that there could be of the order of 200 leptons from single-lepton events of our diquark's decay hiding in the data. But due to the larger SM backgrounds in this channel, this type of excess would be much harder to discern.

If diquarks are indeed realized in nature, however, there is no reason to expect only one carrying tt quantum numbers would be present. A whole spectrum of them could be expected, as in the model of reference [17] for example, where the different quantum numbers corresponds to the pseudo-Goldstone bosons of the broken, approximate global symmetries of the underlying strongly coupled theory. Diquarks of charge 1/3 with the quantum numbers tb or $t'b$ (where primes denote quarks from a possible fourth family), where the t' is lighter than the b', would decay to final states with only single and two opposite-sign leptons, bringing an enhancement to the signal in these channels without contributing to the more constrained multi-lepton channels.

Let us now illustrate the reach of our observable with some concrete examples. Given two "benchmark" numbers of total $\phi\bar{\phi}$ events, we combine the $A^l_{C,i}$ of all 5 channels and estimate the combined statistical uncertainty by assuming no correlation among the measurements in each channel. We then perform χ^2 tests for various input values of the A^l_C asymmetry versus the null hypothesis (0 asymmetry within uncertainties) in order to obtain expected p-values. We again stress that only statistical uncertainties have been accounted for in this section. For 2000 and 20000 events, we find an expected p-value of ~ 0.04 for an A^l_C of 4% and 1.3% respectively. A p-value of $\sim 5 \times 10^{-7}$ can be expected for A^l_C of 10% and 3% for these same numbers of events. Except for the 1.3% figure, all of these values are quite large compared to the expected asymmetry that diquarks receive from QCD, as we will see in the next section.

Before we move on to discuss $t\bar{t}$ asymmetry measurements, we would like to note that lepto-quarks are also interesting candidates to study through this method. While lepto-quarks with the quantum numbers of electrons or muons are ruled out except at very high masses, there is still room for those carrying tau quantum numbers such as τb, $\tau' b$ etc. [51], which decay to final states containing only one or two opposite sign leptons (this is true for the latter only in the case where it cannot decay directly to ν', otherwise other multi-lepton channels become available).

3.3 A_C^l and the $t\bar{t}$ Charge Asymmetry

We now turn our attention to the $t\bar{t}$ charge asymmetry in the *single*-lepton channel. As in the previous section, the dilepton channel measurement $A_{C,2}^l$ can also be obtained through our method and combined with $A_{C,1}^l$. For the sake of brevity we focus solely on the latter.

A significant percentage of candidate events selected in this channel will be coming from backgrounds.[3] However, with the exception of W+jets, all other backgrounds should give rise to identical y distributions for positive and negative leptons *within uncertainties*. Therefore, in taking the difference of positive and negative (lepton) rapidity distributions, the number of such events in each bin should cancel. This is not true for the $W+$ jets background because the cross section for W^+ production at the LHC is larger than that for W^- production. This is due to the fact that, unlike the case of $p\bar{p}$ collisions, in pp collisions u valence quarks are twice as abundant as d's and so leptons coming from W's will be more abundant with positive charge than with negative charge. The third term in the numerator of $A_{C,1}^l$, which we have called Δa_1, will then be purely a $W+$ jets contribution.

For the case of $t\bar{t}$, we then write our observable as:

$$A_{C,1}^l = \frac{QN_1^l(|y|>1) - QN_1^l(|y|<1) - \Delta a_1}{N_1^l(|y|>1) + N_1^l(|y|<1) - N_{i,\text{ all bkg}}^l}. \tag{3.6}$$

The denominator is just $N_{t\bar{t}}^l$, the number of leptons coming from "true" $t\bar{t}$ decays; $N_{i,\text{ all bkg}}^l$ is the number of events coming from all backgrounds. Δa_i is the contribution to the numerator from backgrounds.

By counting the number of positive and negative leptons (e's and μ's) in our samples, we can estimate the total number of such leptons which are coming from $W+$ jets as

$$N_W^l = \frac{r_+^l + r_-^l}{r_+^l - r_-^l}[N(l^+) - N(l^-)], \tag{3.7}$$

where r_+^l and r_-^l are the fractions of positive and negative Ws respectively ($r_+^l + r_-^l = 1$). $N(l^+)$ and $N(l^-)$ are the total number of positive and negative leptons. The ratio $r_+^l/r_-^l = N(pp \to W^+)/N(pp \to W^-)$ is evaluated from Monte Carlo simulations. In [42], ATLAS finds that for events selected in the electron channel $r_+^e/r_-^e = 1.56 \pm 0.06$, and

[3] In the single lepton channel $t\bar{t}$ analyses of CMS [43] and ATLAS [42] these percentages are about 20% and 30% respectively. The $W+$jets background constitutes about 58% of all background events at ATLAS, and about 50% at CMS.

$r^{\mu}_{+}/r^{\mu}_{-} = 1.65 \pm 0.08$ in the muon channel.

In order to estimate Δa_1 we must also know the shape of the rapidity distributions for e's and μ's coming from the W + jets backgrounds. We write this term as

$$\Delta a_1 = N^l_W \Big[(r^l_+ r^{W^+}_1 - r^l_- r^{W^-}_1) - (r^l_+ r^{W^+}_2 - r^l_- r^{W^-}_2) \Big], \tag{3.8}$$

where $r^{W^+}_i$ and $r^{W^-}_i$ are inputs which contain the information on the shape of the y distributions of W^+ and W^- + jets backgrounds such that $\sum_i r^{W^+}_i = \sum_i r^{W^-}_i = 1$.

From Eq. 3.6 and Eq. 3.8 above, it is straightforward to find the associated statistical uncertainty of $A^l_{C,i}$ in terms of the fluctuations in each individual bin $\delta N^{l^\pm}_i \approx \sqrt{N^{l^\pm}_i}$ by varying $A^l_{C,i}$ with respect to each variable $N^{l^\pm}_i$. Notice that both N^l_W and N^l_{total} are $N^{l^\pm}_i$ dependent. We used an ATLAS study on muons coming from $W^\pm$ decays [52] to get an estimate of the $r^{W^\pm}_i$'s from the y (normalized to 1) distributions therein. We find that the statistical uncertainty associated with a muon sample with ~ 9000 events, as is the case for the data collected by ATLAS and studied in [42], is approximately ± 0.015.

The muon (single lepton) channel uncertainties in A_C as measured by ATLAS are $\pm 0.036(\text{stat}) \pm 0.023(\text{syst})$; this is after correcting the top and anti-top rapidity distributions for detector effects and an event selection bias (unfolding). Since our approach deals almost exclusively with leptons we expect that the unfolding procedure would not only be simpler, but also have less of an effect on the estimate of the uncertainties. In fact, we may even expect the statistical uncertainty to decrease by a few percent after correcting for these effects, as is the case for the A^{ll}_C measurement (see Table 2 in [41]). We also expect the sources of systematic uncertainty that have the largest impact on the A_C(muon) measurement (jet energy scale, jet efficiency and resolution, parton shower/fragmentation, ISR/FSR, top mass, and $t\bar{t}$ modeling all contribute above ± 0.005) to be much less significant in the case of A_l. For reference, in A^{ll}_C these sources (the last two are not considered in that study) are below 0.004 except for ISR/FSR which contributes 0.006, the largest of all systematic contributions, and the total systematic uncertainty is 0.009 [41]. Then, if we believe $\pm \leq 0.015$(stat.) and ± 0.009(syst.) to be good estimates of the uncertainties in A_l, it becomes clear that although this observable has the disadvantage of being numerically smaller than A_C, there is much to be gained in the reduction of uncertainties, even in this case ($t\bar{t}$) where the four-momentum of the original pair can be readily reconstructed.

Relative to A^{ll} we have used simulated events to predict that here A^l_C will be about 0.7 times smaller than A^{ll}_C. However, only about 5% of all $t\bar{t}$ events decay into two leptons, whereas $\sim$ 30% give a single lepton (e, μ) final state. Therefore, relative to di-lepton

channel studies, our approach yields ~ 6 times more statistics.

We can now comment on how we obtained the positive and negative lepton distributions in order to estimate the relative size factors A^l/A^{ll} for $t\bar{t}$ (and $\phi\bar{\phi}$ in the previous section). We generated $t\bar{t}$ events in Madgraph and used CTEQ 6.1l structure functions at $\sqrt{s} = 8$ TeV. Since our asymmetry arises at the α_s^3 level, this first step yields identical distributions for positive and negative leptons. We used the following method to obtain a charge asymmetry such that it is approximately linear in $Y = (y_t + y_{\bar{t}})/2$ in the range $-2 < Y < 2$ as predicted in the SM at NLO [45] (see Figure 12 in this reference, left panel).

First, we demand that the t decay to a lepton. When $Y > 0$ and $y_t > y_{\bar{t}}$, this lepton is considered a candidate to be added to the positive lepton distribution; if instead $y_t < y_{\bar{t}}$, it is considered a candidate for the negative lepton distribution. The candidate event must satisfy the condition $Y/2 > R$, where R is a random number between 0 and 1, to be allowed to populate the corresponding bin in the relevant (positive or negative) distribution. Events not satisfying this condition are discarded. A similar procedure follows for events where $Y < 0$. In this way we obtain the shape of the asymmetric events in the lepton distributions.

From our simulated events, we have also obtained estimates of how much "fainter" we expect A_C^l to be relative to the original parton level asymmetry. We summarize this effect in the ratio that we call κ. In the case of $\bar{t}t$, we find $\kappa = A_C^l/A_C^{q\bar{q}}$ to be ~ 0.29. We have explored how this value of κ varies in different kinematic regimes when the particles that we are interested in have a different mass. We have looked at the resulting positive and negative lepton distributions coming from the decay of a 700 GeV $b' \to Wt$, where the leptons originate from both the W boson's decay as well as that of the daughter top's, and 700 GeV $t' \to bW$ where the leptons originate from the W's. When the lepton originates from a W we find κ values of 0.19 for b' and t' decays. When the lepton originates from a top, the case of b', we obtain $\kappa = 0.23$. We expect the lepton distributions coming from a diquark scalar that decays to $tt/\overline{tt}$ to closely resemble this last case. Notice that these values are not so far off from each other or the result already mentioned for $t\bar{t}$. However, the shapes of the distributions are different in the two cases. The $t\bar{t}$ pair can often be produced at large Y and therefore the positive lepton distribution exhibits 2 clear peaks at high $|y|$ and a dip around $y = 0$, whereas the negative lepton distribution is peaked at $y = 0$. As the decaying quark pair becomes heavier it is less and less produced at high Y, and the two peaks in the positive lepton distribution start getting closer to each other while the negative lepton distribution's central peak becomes sharper (also, distributions are smeared further due to the extra step in the decay chain,

e.g. $b' \to t \to l$). Observation of the distribution shapes can therefore give us additional information about the original particle pair's mass. We also found that in all cases the cross over point between distributions, the value of y which we have called t in Eq. 3.2, happened very close to $y = \pm 1$. This then appears to be a more or less robust estimate for the type of decays we have considered.

3.4 The Diquark Charge Asymmetry

The charge asymmetric cross section from QCD for scalar diquarks can be obtained from the QED result for charged colorless scalar production ($e^+e^- \to H^+H^-$) by replacing $\alpha \to \alpha_s$ and multiplying by the appropriate color factor: $\mathcal{C}_A(R)/\mathcal{C}_0(R)$, where

$$\begin{aligned} \mathcal{C}_0(R) &= \frac{1}{N_c^2}\mathrm{Tr}(\frac{\lambda_a}{2}\frac{\lambda_b}{2})\mathrm{Tr}(T_R^a T_R^b) \\ &= \frac{1}{2N_c^2} d_R C_2(R) \end{aligned} \tag{3.9}$$

and

$$\begin{aligned} \mathcal{C}_A(R) &= \frac{1}{N_c^2}\mathrm{Tr}(\frac{\lambda_a}{2}\frac{\lambda_b}{2}\frac{\lambda_c}{2})\mathrm{Tr}(T_R^a T_R^b T_R^c) \\ &= \frac{1}{4N_c^2} d_R C_3(R). \end{aligned} \tag{3.10}$$

$C_2(3) = 4/3$ and $C_3(3) = 10/9$ for a triplet scalar, $C_2(6) = 10/3$ and $C_3(6) = 35/9$ for a sextet, and d_R is the dimension of R. The factor $\mathcal{C}_0(R)$ comes from the Born cross section whereas $\mathcal{C}_A(R)$ is the color factor for the order α^3 contributions to the charge asymmetric part of the cross section. The factor $\mathcal{C}_A(R)/\mathcal{C}_0(R)$ is 5/12 for the triplet and 7/12 for the sextet.

QED calculation of a colourless scalar's charge asymmetry

Soft infrared singularities are absent from the differential cross section, as they should be, but considered separately, the virtual and real radiation amplitudes contain such divergences which cancel in a non-trivial way. In order to show the cancelation of this divergence we followed [53] to analytically integrate the real photon emission in the soft limit over a thin slice at the border of phase space (using a photon mass regulator) and combined it with virtual radiation. The latter part of this calculation was done by Melissa Ratzlaff. This result no longer contains a soft infrared singularity. It does, however, exhibit a (logarithmic) dependence on E_{cut}, coming from the soft photon integration,

which must cancel once the real, hard photon emission piece is added. In order to obtain a E_{cut} independent result, integration over the rest of the phase-space was performed numerically.

We present analytical expressions for the asymmetric contributions to real photon radiation in the soft limit, and for virtual contributions, all in terms of $\beta = \sqrt{1-4m^2/s}$, the velocity of the diquark. Although we omit the use of hats (e.g. $\hat{s}$) over our variables, the following expressions are valid in the partonic center of mass frame. We will split the differential asymmetric contribution to soft, real photon emission into two parts. Part 1, which is the part that depends on photon energy cutoff E_{cut} is given by

$$\frac{d\sigma_A}{d\theta}^{\text{soft, p1}} = \frac{\beta^3 e^6}{64\pi^3 s}\log\left(4\frac{E_{cut}^2}{s}\right)\sin^2\theta[-\log(1-\beta\cos\theta)+\log(1+\beta\cos\theta)]. \tag{3.11}$$

The photon mass dependence has been cancelled with the loop calculation. The integrated expression is

$$\begin{aligned}\sigma_A^{\text{soft, p1}} = \frac{e^6}{192\pi^3 s}\log\left(4\frac{E_{cut}^2}{s}\right)\Big\{ &- \beta^2 - \log(1-\beta) - \log(1+\beta) + 2\beta^3[-\log(1-\beta)+\log(1+\beta)] \\ &+ 3\beta^2[\log(1-\beta)+\log(1+\beta)]\Big\}.\end{aligned} \tag{3.12}$$

Part 2 of this same contribution, which does not depend on E_{cut}, is given by

$$\begin{aligned}\frac{d\sigma_A}{d\theta}^{\text{soft, p2}} = \frac{\beta e^6}{16\pi^3 s^3}\quad (m^4-ut)\quad &\left\{\text{Li}_2\left(\frac{2m^4-2m^2t+st-\beta st}{2m^4-2m^2t}\right)+\text{Li}_2\left(\frac{2m^4-2m^2t+st+\beta st}{2m^4-2m^2t}\right)\right. \\ &- \text{Li}_2\left(\frac{2m^4-2m^2u+su+\beta su}{2m^4-2m^2u}\right)-\text{Li}_2\left(\frac{2m^4-2m^2u+su-\beta su}{2m^4-2m^2u}\right) \\ &- \left.\text{Li}_2\left(1+\frac{st}{(m^2-t)^2}\right)+\text{Li}_2\left(1+\frac{su}{(m^2-u^2)}\right)\right\}.\end{aligned} \tag{3.13}$$

The asymmetric contribution to virtual photon emission, expressed in terms of the Passarino-Veltmann scalar integrals $C_{01}(x_1,x_2)$ and $C_{02}(x_1,x_2,x_3)$, is given by

$$\begin{aligned}\frac{d\sigma_A}{d\theta}^{\text{virt}} = \frac{\beta e^6}{128\pi^3 s}\quad (m^4-ut)\quad &\left\{\frac{(t-u)(-2m^6-2m^2ut+stu+m^4(s+2t+2u))}{(m^4-2m^2t+st+t^2)(m^4-2m^2u+us+u^2)}\cdot C_{01}(s,m^2)\right. \\ &- \frac{s(t-u)(m^4-ut)}{(m^4-2m^2t+st+t^2)(m^4-2m^2u+us+u^2)}\cdot C_{01}(s,m_e^2) \\ &+ \frac{2t(m^2-t)}{(m^4-2m^2t+st+t^2)}\cdot C_{02}(t,m^2,m_e^2) \\ &- \left.\frac{2u(m^2-u)}{(m^4-2m^2u+us+u^2)}\cdot C_{02}(u,m^2,m_e^2)\right\}.\end{aligned} \tag{3.14}$$

The explicit expressions for the scalar integrals are

$$C_{01}(x_1, x_2) = \int_0^1 \frac{\log(x_1 y) - \log(x_2(1-y)^2)}{x_1 y + x_2(1-y)^2} dy, \tag{3.15}$$

and

$$C_{02}(x_1, x_2, x_3) = -\frac{1}{2}\int_0^1 \frac{\log(y^2 x_1 + y x_2 - y x_3 - y x_1 + x_3)}{(y^2 x_1 + y x_2 - y x_3 - y x_1 + x_3)} dy. \tag{3.16}$$

Finally, the integrated expression for the Born cross section is

$$\sigma_B = \frac{e^4 \beta^3}{48\pi s}. \tag{3.17}$$

We have not included an analytical expression for real hard photon (gluon) radiation; we have not been able to express it in a compact enough form to present here. This last piece is of crucial importance for its role in the cancellation of the unphysical E_{cut} dependence, something which, as mentioned above, we achieved through numerical integration. However, the θ dependence in the fully asymmetric piece of the differential cross section can be seen almost exactly from Eq. 3.11.

In Fig. 3.2 and Fig. 3.3 we present our results for a colorless scalar's charge asymmetry in the partonic center of mass frame, as a function of the angle θ, and as a function of the scalar's pseudorapidity respectively. These predictions have some important dif-

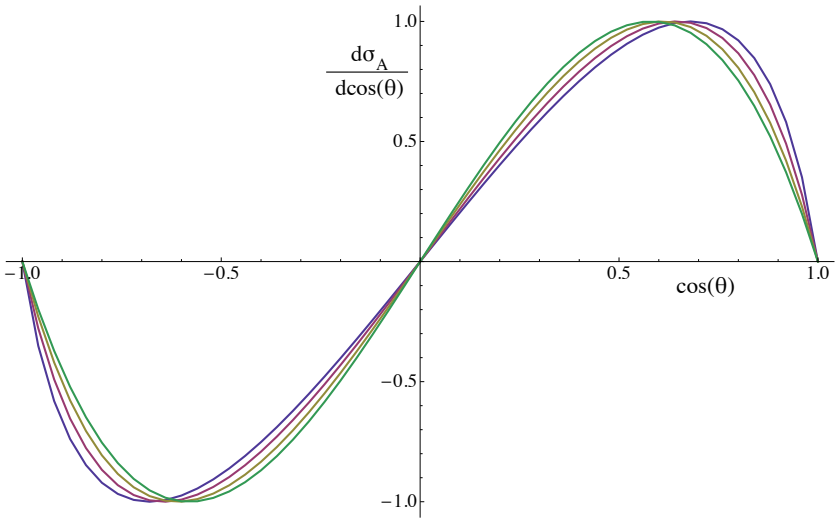

Figure 3.2: Differential charge asymmetry (with amplitude normalized to 1) in the $\phi\bar{\phi}$ partonic center of mass frame as a function of $\cos\theta$ for $m_\phi/\sqrt{s}$ of 0.2, 0.3, 0.4 and 0.49. The green curve (curve with peak at lowest value of θ) corresponds to 0.49, the blue curve (curve with peak at highest value of θ) corresponds to 0.2.

ferences from those for the case of $t\bar{t}$. In particular, unlike the $t\bar{t}$ (or more generally, $q\bar{q}$),

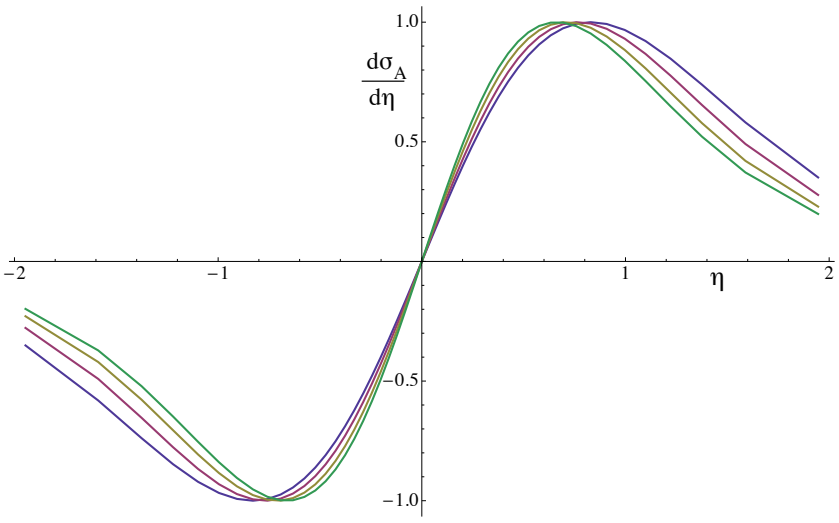

Figure 3.3: Differential charge asymmetry in the $\phi\bar{\phi}$ frame as a function of pseudorapidity for $m_\phi/\sqrt{s}$ of 0.2, 0.3, 0.4 and 0.49. The green curve (curve with peak at lowest value of η) corresponds to 0.49, the blue curve (curve with peak at highest value of η) corresponds to 0.2.

the charge asymmetry for scalars peaks at a value of $\cos(\theta)$ below 1, and vanishes at $\cos(\theta) = 1$. Fig. 3.4 below shows the integrated charge asymmetry in the partonic center of mass frame as a function of $\sqrt{s}/2m_\phi$. In contrast to the same result for $t\bar{t}$, the scalar's charge asymmetry is much flatter (for reference, see Fig. 5 in [45]).

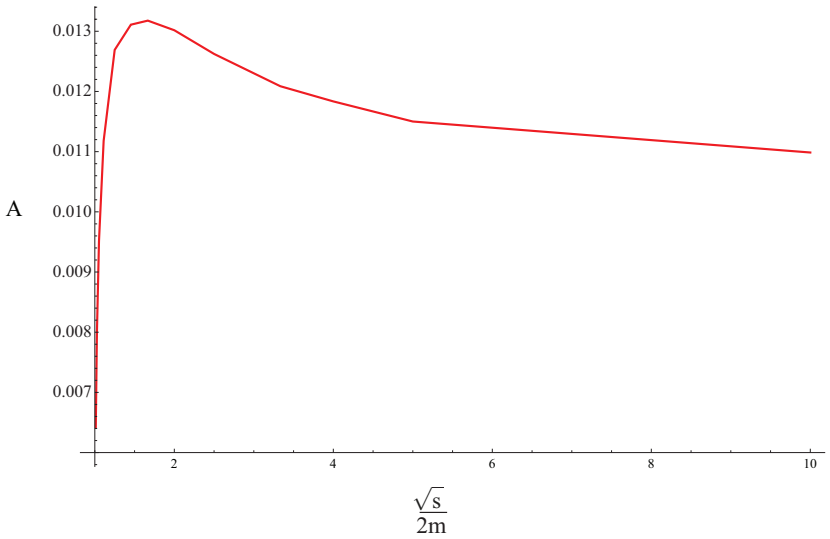

Figure 3.4: Integrated charge asymmetry for $q\bar{q}$ initiated events in the $\phi\bar{\phi}$ frame as a function of $\frac{\sqrt{s}}{2m_\phi}$.

QCD results for a scalar diquark's charge asymmetry

The results for the charge asymmetry in $q\bar{q}$ initiated events of the colored diquarks follow simply by multiplying the above results by $\alpha_s(\mu = m_Z)/\alpha$, and by the previously calculated color factor, 5/12 or 7/12, for the triplet or sextet respectively. These factors amount to quite an enhancement, a factor of ~ 50 and 70 respectively. However, folded in with the proton's structure functions, the resulting inclusive (gg initiated events give a large contribution to the Born cross section) $\phi\bar{\phi}$ charge asymmetry in the lab frame is again very small.

We have produced predictions for the triplet diquark asymmetry at the LHC at 7 TeV, for two values of the diquark mass. For $m_\phi = 400$ GeV we find $A_C = -0.012$, for $m_\phi = 500$ GeV we find $A_C = -0.0073$. As mentioned in the introduction, we would like to focus on ϕ that decay to tt.[4]

A study of the observable A_l on our triplet $\phi\bar{\phi}$ candidate events would require that we be able to measure an A_l of about $-0.012 \times \kappa = -0.003$ for $m_\phi = 400$ GeV and A_l of about $-0.0073 \times \kappa = -0.002$ for $m_\phi = 500$ GeV, where we have assumed $\kappa \approx 0.23$. The challenge then is bringing systematic effects down to these levels. Alternatively, one could also think of taking advantage of the features in the differential charge asymmetry as a function of y to define a related quantity that enhances the observable asymmetry, as for example, restricting the sample to events with large $Y_{out} = (y_\phi + y_{\bar{\phi}})/2$.

We have briefly explored this possibility by selecting (simulated) $pp \to \phi\bar{\phi}$ events where one of the incoming partons is required to have a much larger fraction of the proton's momentum than the other, $x_1/x_2 > 1$. In events where hard gluon jets are absent, this cut on the incoming parton's relative momenta (or the rapidity of the incoming parton's center of mass Y_{in}) is approximately equivalent to a cut on Y_{out}, the relation given by $e^{2Y_{out}} \approx e^{2Y_{in}} = x_1/x_2$. For a 400 GeV triplet scalar, we find $A_C(Y_{cut} = 1.39) = -0.047$ and $A_C(Y_{cut} = 1.04) = -0.027$. For a mass of 500 GeV, we find $A_C(Y_{cut} = 0.69) = -0.053$, where Y_{cut} is the minimum Y_{in} for allowed events. As we do not have access to the scalars' rapidities, a very rough implementation of this cut would consist of adding up the y_i of all reconstructed objets for the candidate event and taking this average to be representative of Y_{out}. The expected A_l would now be an effect of a few percent, and could be observable given several thousand candidate events (in a combined measurement as discussed in Section 3.2) and systematic uncertainties of about 1% each, as the case discussed in Section 3.3.

[4]Note that the masses that we consider here are too light to allow additional W^+W^- pairs in the decay.

3.5 Concluding Remarks

We have proposed a method for measuring charge asymmetries of particle pairs produced at the LHC. Our suggested approach focuses on the rapidity distributions of leptons coming from particle pair decays with one or more leptons in the final state, and does not require reconstruction of the original pair. Some information from the backgrounds is still needed from Monte Carlo simulations in order to obtain a measurement, such as the value of t (which determines the width of the central bin) that goes into the definition of A_C^l. Although the value of this observable is expected to be smaller than A_C of the original pair, systematic uncertainties are expected to be much smaller in this lepton based measurement, and most important, such a measurement may be the best way to access charge asymmetry information in systems where other methods based on partial or full reconstruction fail. Although the dilepton channel observable A^{ll} is still of use in these cases, it can obviously only be applied when two or more opposite sign leptons are present.

We have also presented theory predictions from QCD at NLO for the charge asymmetry of a coloured (triplet/sextet) scalar carrying diquark quantum numbers. A scalar's charge asymmetry (at the parton level) as a function of θ and y has marked differences with that of $q\bar{q}$ pairs. Our numerical results for the integrated charge asymmetry of a triplet diquark pair ($m_\phi = 400,\ 500$ GeV) show that at the LHC, this would be a very small effect, of order 1%. A_l would be about $0.2\% - 0.3\%$. If the sample is restricted to events with high Y, this effect can be enhanced to a few percent. With a large enough number of $\phi\bar{\phi}$ events (several thousand), we could expect to see moderately significant signs of this asymmetry, even if A_l remains at the percent level (and assuming that as in the $t\bar{t}$ A_l analysis the total systematic uncertainty can remain below $\sim 1\%$). Such measurements could turn out to be of great value in discerning the nature of possible new coloured states to be (maybe) discovered at the LHC.

Chapter 4

Monopoles, strings and dark matter

In this chapter, we develop a scenario whereby monopoles in a hidden sector yield a decaying dark matter candidate of interest for the PAMELA and FERMI $e^{\pm}$ excesses. The monopoles are not completely hidden due to a very small kinetic mixing and a hidden photon mass. The latter also causes the monopoles and anti-monopoles to be connected by strings. The resulting long-lived objects eventually decay to hidden photons which tend to escape galactic cores before decaying. The mass scales are those of the hidden photon (≈ 500 MeV), the monopole (≈ 3 TeV) and the mixing scale (close to the Planck scale). A gauge coupling in the hidden sector is the only other parameter. This coupling must be strong and this results in light point-like monopoles and light thin strings. The text in this chapter is reproduced in [54]

4.1 Introduction

We shall describe a decaying dark matter scenario where the dark matter "particle" is a monopole and an anti-monopole connected by one or more strings. We shall refer to these objects as $M\overline{M}$'s. Both the monopoles and the strings are composed of hidden sector fields. A nonabelian gauge symmetry of the hidden sector breaks to a $U(1)_h$ to produce monopoles and then the $U(1)_h$ breaks at a lower scale to produce strings. If the only remaining long range field to which the monopole couples is gravity then the $M\overline{M}$'s can have cosmologically interesting life-times [55]. They can be considered for dark matter since their number densities are not constrained by the Parker bound [56]. The dynamics and evolution of monopoles attached to strings in the early universe has been quite well studied [57–61].

For the natural abundance of monopoles to be appropriate for dark matter they must be much lighter than standard GUT monopoles. This mass can in fact be in a range of

interest for a decaying dark matter interpretation of the PAMELA [22] and FERMI [23] $e^{\pm}$ excesses. A $MS\overline{M}$ survives until the M and $\overline{M}$ finally annihilate into hidden photons. If the hidden photon γ_h experiences kinetic mixing [62] with the photon and is otherwise stable then it decays into pairs of normal charged particles. With the appropriate mass its stable decay products are electrons, positrons and neutrinos [63, 64].

We shall show in the next section that the kinetic mixing in combination with the hidden photon mass implies that a $MS\overline{M}$ will pick up the normal magnetic field of a dipole. These oscillating dipoles lose energy through normal electromagnetic radiation, and when the mixing parameter is extremely small the lifetime of the $MS\overline{M}$'s can be appropriate for decaying dark matter. Thus in our scenario the kinetic mixing is setting the lifetime for both the $MS\overline{M}$'s and the γ_h's, and it is responsible for producing an observable signal.

We first summarize the various parameters and relations between them [65]. When the hidden nonabelian gauge symmetry breaks to $U(1)_h$ some gauge bosons receive mass m_X. If the gauge coupling is e_h then the monopoles have mass

$$m_M \approx \frac{4\pi}{e_h^2} m_X \tag{4.1}$$

and a size of order m_X^{-1}. We assume that the monopoles form at a temperature $T_M \approx m_X/e_h \approx m_M/g_h$ where $g_h = 4\pi/e_h$ is the magnetic coupling. When the surviving $U(1)_h$ gauge symmetry breaks at a lower scale this hidden photon γ_h develops a mass m_h. At this scale the coupling may have run to a new value e_h'. In the results to follow either e_h or e_h' should appear depending on the context, but for simplicity we shall drop the distinction and simply use e_h. Strings have an energy per unit length

$$\mu \approx \frac{\pi}{e_h^2} m_h^2 \tag{4.2}$$

and a thickness of order m_h^{-1}. We assume that the strings form at a temperature $T_S \approx m_h/e_h$.

The two mass scales of the hidden sector, m_M and m_h, are fairly well determined if we are to make contact with the dark matter interpretations of PAMELA and FERMI data. For the stable products of γ_h decays to be electrons, positrons and neutrinos only, m_h could be anywhere from above the e^+e^- threshold up to about a GeV. But a mass above the $\mu^+\mu^-$ and $\pi^+\pi^-$ thresholds is preferred since it gives a broader electron/positron spectrum to fit the FERMI data [26, 66]. Given this and with the mass of the decaying $MS\overline{M}$ close to $2m_M$, the PAMELA data favors a m_M in the 1 to 3 TeV range while the

FERMI data favors a mass at the upper end of this range [26, 66]. We shall adopt the values $m_h = 500$ MeV and $m_M = 3$ TeV for illustration. Adjustments in these masses are still possible.

The remaining parameters are the hidden sector gauge coupling e_h and the kinetic mixing parameter χ. In Section 4.3 we show how the correct initial number density of monopoles constrains e_h. Here and at other points in our discussions we shall find that a strong coupling is required. The lifetime of the $MS\overline{M}$'s as determined by the emission of electromagnetic radiation must be appropriate for decaying dark matter. We study how this is possible in Section 4.4 while in Section 4.5 we consider other energy loss mechanisms. The $MS\overline{M}$'s that decay today are much smaller than average and we can determine enough about the distribution of these sizes so that we are able to fix χ. The lifetime of the γ_h is then also determined. We find that this lifetime tends to be sufficiently long so that γ_h's travel out of galactic cores before decaying, and this may have interesting consequences for the associated gamma ray signal. The lifetime of the mediator particle in secluded models of dark matter often face a constraint from big bang nucleosynthesis [67]. In Section 4.6 we argue that in our case the γ_h's are unstable in the presence of a light string network. In Section 4.7 we briefly consider the late time properties of the dark matter and its self-interactions while in Section 4.8 we look at the possibilities (or lack thereof) for its direct detection.

Here we can comment on the origin of the mixing parameter χ. It is related to the mass scale of the physics responsible for the mixing between the hidden and standard model sectors. If this physics respects the hidden nonabelian gauge symmetry then the lowest dimensional operator that can give rise to the mixing is

$$\frac{1}{M_{mix}} Y_{\mu\nu} G_a^{\mu\nu} \phi_a. \tag{4.3}$$

This couples the gauge bosons of hypercharge and the hidden gauge group to ϕ_a, a hidden adjoint scalar field. If $\langle \phi_a \rangle$ signals the breakdown of the gauge symmetry then $\langle \phi_a \rangle \approx m_X/e_h \approx m_M/g_h$. The induced kinetic mixing χ between the photon and the γ_h, as defined in the next section, is $\chi \approx \langle \phi_a \rangle / M_{mix}$ and so

$$M_{mix} \approx \frac{m_M}{\chi g_h}. \tag{4.4}$$

(The absence of a field ϕ_a would mean that a higher dimensional operator is necessary which would imply a smaller mixing scale.) It would be appealing for M_{mix} to be close to the Planck scale to avoid the introduction of another mass scale. Due to the very small

value of χ required to produce a suitable $MS\overline{M}$ lifetime we shall find that M_{mix} as given by (4.4) must indeed be of this size.

The strong coupling value that we have said is required for e_h could also be viewed as natural, since then the symmetry breakings that are necessary in the hidden sector could be occurring dynamically. In this way are encouraged to find interesting results where the parameters e_h and χ are close to their "natural" values.

4.2 Mixing and monopoles

At low energies the electromagnetic $U(1)$ and the massive $U(1)_h$ gauge fields and their mixing are described by

$$\mathcal{L} = -\frac{1}{4}F'_{\mu\nu}F'^{\mu\nu} - \frac{1}{4}F'_{h\mu\nu}F'^{\mu\nu}_{h} - \frac{1}{2}\chi F'_{\mu\nu}F'^{\mu\nu}_{h} + \frac{1}{2}m_h^2 A'_{h\mu}A'^{\mu}_{h}. \tag{4.5}$$

Diagonal kinetic terms can be regained while retaining the masslessness of the photon by redefining the fields in terms of new fields A and A_h as

$$\begin{aligned} A'_h &\rightarrow A_h \\ A' &\rightarrow A - \chi A_h. \end{aligned} \tag{4.6}$$

This means that all fields coupling to the photon with charge e will pick up a coupling to the hidden photon of strength $-\chi e$ [62].

The $U(1)_h$ has emerged from the breakdown of a larger gauge group such that monopoles arise as regular solutions of the field equations. But the (hidden) magnetic charge of these monopoles must be quantized according to Dirac's quantization condition, and so there is a question of how this is compatible with particles with a hidden charge of $-\chi e$. This is answered in [68] where it is shown that monopoles, including 't Hooft-Polyakov monopoles, can carry a combination of both magnetic charges. The argument for two massless $U(1)$'s is reproduced here, but adapted to our A and A_h basis.

If a charge e is in the presence of a magnetic monopole with magnetic charge g the angular momentum of the fields is

$$\boldsymbol{L} = \int d^3x \boldsymbol{x} \times (\boldsymbol{E} \times \boldsymbol{B}) = \frac{eg}{4\pi}\hat{n}. \tag{4.7}$$

This must be quantized,

$$|\boldsymbol{L}| = \frac{eg}{4\pi} = \frac{n}{2}, \tag{4.8}$$

where n is a non-negative integer. In the case of two $U(1)$'s the magnetic field of a monopole is

$$\begin{pmatrix} \boldsymbol{B} \\ \boldsymbol{B_h} \end{pmatrix} = \frac{\boldsymbol{r}}{4\pi r^3} \begin{pmatrix} g \\ g_h \end{pmatrix}, \tag{4.9}$$

while the electric fields of normal and hidden charges are respectively

$$\begin{pmatrix} \boldsymbol{E} \\ \boldsymbol{E_h} \end{pmatrix} = \frac{e\boldsymbol{r}}{4\pi r^3} \begin{pmatrix} 1 \\ -\chi \end{pmatrix}, \tag{4.10}$$

$$\begin{pmatrix} \boldsymbol{E} \\ \boldsymbol{E_h} \end{pmatrix} = \frac{e_h\boldsymbol{r}}{4\pi r^3} \begin{pmatrix} 0 \\ 1 \end{pmatrix}. \tag{4.11}$$

A system consisting of an ordinary charge and a monopole gives

$$|\boldsymbol{L}| = \frac{-\chi e g_h + eg}{4\pi} = \frac{n}{2}, \tag{4.12}$$

while for a hidden charge and a monopole we have

$$|\boldsymbol{L'}| = \frac{e_h g_h}{4\pi} = \frac{m}{2}. \tag{4.13}$$

These two equations give two types of allowed monopoles:

$$M_{GUT} \to \begin{pmatrix} g \\ g_h \end{pmatrix} = \frac{2\pi n}{e} \begin{pmatrix} 1 \\ 0 \end{pmatrix}, \tag{4.14}$$

and

$$M \to \begin{pmatrix} g \\ g_h \end{pmatrix} = \frac{2\pi m}{e_h} \begin{pmatrix} \chi \\ 1 \end{pmatrix}. \tag{4.15}$$

We shall comment on our choice $g_h = 4\pi/e_h$ ($m = 2$) in Section 4.4.

We see that the combination of magnetic charges carried by the monopole M is orthogonal to the combination of charges carried by a normal charge. As long as γ_h remains massless these monopoles remain hidden to normal charges. However once $U(1)_h$ breaks, this hidden component of the M field becomes confined for length scales larger than m_h^{-1}. Flux tubes, or strings, of the hidden magnetic field can begin on M's and end on $\overline{M}$'s. Thus after $U(1)_h$ breaks the remaining long range field of M is purely electromagnetic (the χ component in (4.15)) and the hidden monopoles become visible to normal charges. The M's now display an apparent violation of the Dirac quantization condition, but this is allowed due to the attached physical string(s). These strings are

also visible to normal charges (due to the χ component in (4.10)) through the Aharonov-Bohm effect as we discuss in Sections 4.5 and 4.8.

Let us return to the point that the $U(1)_Y$ of hypercharge is involved in the origin of the mixing, as in (4.3). In the mass eigenstate basis this can be seen as a mixing of both the photon and the Z boson separately with the hidden photon. The Z mass defines a basis to describe its mixing, and so by the same arguments as before particles charged under $U(1)_h$ acquire a small Z charge while the hidden monopoles do not acquire a Z magnetic charge. In this way we see that the hidden monopoles are not affected by electroweak symmetry breaking.

4.3 Monopole densities

The hidden monopole M number density is n_M and it is equal to the $\overline{M}$ density at all times. For a M mass of 3 TeV we wish to investigate the conditions under which n_M could be appropriate for dark matter. We first consider the case when the magnetic charge is large as in the case of GUT monopoles, so that we can apply the same analysis [69]. (This is the weak gauge coupling case and we turn later to strong coupling.) The density of monopoles when they are first formed at temperature T_M can be reduced through annihilation of M-$\overline{M}$ pairs. This occurs if there are light particles carrying the hidden charge in the plasma. Such fields should be present in our scenario since they are needed at a much lower energy scale to produce an order parameter for the breaking of $U(1)_h$. A M drifting through such a plasma towards an $\overline{M}$ can experience energy loss, capture and thus annihilation. The annihilations end when the mean free path becomes longer than the capture distance and this occurs when the temperature has dropped to T_f [69] where

$$T_f \approx \frac{m_M}{B^2}\frac{1}{\alpha_M^2}, \qquad B = \frac{3\zeta(3)}{4\pi^2}\sum_i \left(\frac{g_h e_h^i}{4\pi}\right)^2. \tag{4.16}$$

Here $\alpha_M \equiv g_h^2/4\pi$ and the sum is over all spin states of relativistic hidden charged particles. The condition $T_f < T_M \approx m_M/g_h$ implies $\alpha_M \gtrsim (4\pi/B^4)^{1/3}$. If this is satisfied then the annihilations reduce the value of n_M/T^3 to

$$\frac{\kappa^3 m_M}{4\pi BC m_{Pl}}\frac{1}{\alpha_M^3} \quad \text{where} \quad C = \left(\frac{45}{4\pi^3 g_*}\right)^{\frac{1}{2}}, \tag{4.17}$$

unless n_M/T^3 is already below this value. The κ factor is introduced since a temperature such as T_f is a hidden sector temperature, and this may be a factor of κ times the temperature T of the observable sector. g_* is the usual total effective number of relativistic

spin degrees of freedom. For the smallest α_M at which this annihilation process is still operative the remaining monopole abundance would be 3 or 4 orders of magnitude below what is required for dark matter (for $C = .05$ and $\kappa = 1$). Thus α_M must be smaller to turn off the annihilations ($T_f > T_M$), and this puts a lower bound on $\alpha_h = 1/\alpha_M \gtrsim 1/2$ for $B \approx 1$.

We thus turn to the initial value of n_M/T^3. If we still believe that α_h could be fairly weak then the density of monopoles produced in a second order phase transition can be related to the correlation length ξ and the relaxation time τ as the system passes through the phase transition at a finite speed. The speed is determined by the Hubble parameter H at that time. This is the Kibble-Zurek mechanism [70,71] (reviewed in [72]). In terms of critical exponents defined from

$$\xi = \xi_0 |\varepsilon|^{-\nu} \tag{4.18}$$

$$\tau = \tau_0 |\varepsilon|^{-\mu} \tag{4.19}$$

where $\varepsilon = (T_M - T)/T_M$, the following result is obtained

$$\xi \approx \left(\frac{\sqrt{\lambda} T_M}{H} \right)^{\frac{\nu}{1+\mu}} \frac{1}{\sqrt{\lambda} T_M}. \tag{4.20}$$

λ is the coupling appearing in a Ginzburg-Landau approximation to the free energy [73]. Since $n_M \approx \xi^{-3}$ this leads to

$$\frac{n_M}{T^3} \approx \kappa^3 \lambda^{3/2} \left(\frac{1}{\kappa^2 \lambda^{1/2} C} \frac{m_M}{g_h m_{Pl}} \right)^{\frac{3\nu}{1+\mu}}. \tag{4.21}$$

The classical values of the exponents are $\nu = \mu = 1/2$ which makes the exponent in (4.21) unity. With $\lambda = \kappa = 1$ and using the upper bound on $\alpha_M = g_h^2/4\pi$ from above, the monopole density would be about two orders of magnitude too small. This could be corrected if μ and ν deviated from their classical values in such a way as to reduce the exponent in (4.21) (the causality constraint is $\nu \leq \mu$). Otherwise we are pushed towards still smaller α_M (larger α_h) and larger λ. In fact the Kibble-Zurek mechanism becomes irrelevant when α_h becomes larger than unity.

When $\alpha_h > 1$ the monopoles become lighter than the massive gauge bosons, $m_M \approx m_X/\alpha_h$. The monopole has a size $\approx 1/m_X$ which is smaller than its Compton wavelength. These relatively light point-like monopoles can be treated like normal particles. With their fairly weak magnetic charge they will experience pair production and annihi-

lation through two to two processes, and in this way they will reach thermal equilibrium with the light degrees of freedom in the dark sector. The monopoles will remain in thermal equilibrium until the temperature falls sufficiently below m_M. The final freeze-out temperature is reached when $n_M\langle\sigma v\rangle \approx H$ where $\langle\sigma v\rangle$ is the annihilation cross section. We assume that this annihilation is analogous to two charged scalars annihilating into 2 photons [64] so that

$$\langle\sigma v\rangle = \frac{\pi\alpha_M^2}{m_M^2}. \tag{4.22}$$

This has to be close to the usual value of 3×10^{-26} cm^{3}s^{-1} to arrive at the correct dark matter abundance [74]. After including the dependence on κ we obtain

$$\alpha_M \approx \frac{1}{4\pi}\sqrt{\kappa}\left(\frac{m_M}{2.8 \text{ TeV}}\right). \tag{4.23}$$

In other words $\alpha_h = 1/\alpha_M \sim 4\pi$ and we note that this agrees with the definition of strong coupling in "naive dimensional analysis" [75]. It suggests that gauge symmetries are breaking dynamically in the hidden sector. Here we note that e_h always represents the charge of the order parameter and so in the case that the latter is a fermion condensate the actual gauge coupling of the fermions is $\overline{e}_h = e_h/2$ and so $\overline{\alpha}_h \sim \pi$.

Thus with a monopole mass close to 3 TeV, as hinted at by PAMELA and FERMI data, the required monopole abundance for dark matter leads us to the strong coupling case. The relations between the various masses and couplings that we mentioned in the introduction are assumed to extrapolate into this regime. In some sense it is not a severe extrapolation, since when $\alpha_M \approx 1/4\pi$ or $g_h \approx 1$ the monopole mass has only come down to the scale of symmetry breaking as given by $m_M/g_h \approx m_X/e_h$.

4.4 Lifetimes

Below some temperature the $U(1)_h$ breaks and the hidden photon develops a mass m_h. M-$\overline{M}$ pairs become connected by strings to form $MS\overline{M}$'s. Here we need to be a little more explicit about how the gauge symmetries are breaking to form monopoles and strings. Let us consider the simplest example, the breakdown of $SU(2)$ to $U(1)_h$ which then itself breaks. If the first step occurs via a scalar triplet $\langle\phi_a\rangle$ then $m = 2$ in (4.15) as we have been assuming. A second scalar triplet with a smaller vacuum expectation value can be used to break $U(1)_h$. In this case the flux carried by a string will be $2\pi/e_h$ and this implies that each monopole will end up with two strings attached. (We assume that two $2\pi/e_h$ strings are energetically favored over a single $4\pi/e_h$ flux string.) If instead

a scalar doublet is used to break the $U(1)_h$ then there are only $4\pi/e_h$ strings and each monopole will have one string attached.

In the first case a "necklace" can also form where equal numbers of monopoles and anti-monopoles are attached to one loop of string. The evolution of necklaces in the early universe was studied in [60] where it was concluded that necklaces tend to cut themselves up into a set of $MS\overline{M}$'s and pure string loops. The evolution of an isolated $MS\overline{M}$ is similar whether it has one or two strings and so the results in the two cases will be similar. On the other hand we have mentioned dynamical symmetry breaking where it is natural to consider a condensate of fermions rather than a vev of a scalar field. Weyl fermions that transform as doublets under $SU(2)$ could develop Majorana condensates that transform as triplets under the $SU(2)$. This suggests that the triplets only case (the two string case) may be more natural, and we shall assume this in the following.

The acceleration of the M caused by the two strings, assuming they are pulling in the same direction, is $a = 2\mu/m_M$. The strings in the $MS\overline{M}$'s should be fairly straight for various reasons. Strings can be fairly straight on formation, especially for the smaller $MS\overline{M}$'s. In the next section we look at mechanisms by which strings very slowly lose energy. But most importantly, a $MS\overline{M}$ with an excess amount of string can emit a loop of string, since when a piece of string intersects itself it may pinch off to form a loop. Thus the $MS\overline{M}$ should end up in a state where the strings remain quite straight as the M and $\overline{M}$ move around their center of mass, with energy moving back and forth between monopole kinetic energy and string rest mass energy. Any angular momentum of the system will keep the M and $\overline{M}$ from colliding. We will consider the peak velocities of the monopoles below, but they can be substantially larger than the typical monopole velocities at the time of string formation.

We will need to determine a distribution of lifetimes of the collection of $MS\overline{M}$'s after they have started to evolve as isolated systems. Some will have already decayed by now, but this is a very small fraction of the original number as is usual with decaying dark matter. We define the probability that a randomly chosen $MS\overline{M}$ will decay between time t and $t + dt$ as $P(t, \overline{\tau})dt$, where $\overline{\tau}$ is the mean lifetime. Then the rate of decay per unit volume at the present time $t_0 = 1/H$ is $n_0 P(t_0, \overline{\tau})$ where n_0 is the present density. We can write $P(t_0, \overline{\tau}) = \tau_{\rm eff}^{-1}$ where $\tau_{\rm eff}$ is an effective lifetime, to be distinguished from the actual mean lifetime $\overline{\tau}$ of the $MS\overline{M}$'s.

For now we focus on the energy loss due to normal electromagnetic radiation; in the next section we shall compare this to other possible energy loss mechanisms. The Larmor formula for a charge with proper acceleration a can be used to find the power radiated

by the M and $\overline{M}$ even in the relativistic case [59],

$$\begin{aligned}\frac{d\mathcal{E}_{em}}{dt} &= -2\frac{\chi^2}{6\pi}(g_h a)^2 = -\frac{\chi^2}{3\pi}\left(\frac{4\pi}{e_h}\frac{2\mu}{m_M}\right)^2 \\ &\approx -\frac{64\pi^2}{3}\frac{m_h^2}{e_h^4 m_M^2}\chi^2\mu. \end{aligned} \tag{4.24}$$

Our choice of χ will make this very small, but it is still larger than the power radiated into the massive γ_h. The latter is exponentially suppressed [59] with a factor $\exp(-2vm_h/3a) \sim \exp(-4v\alpha_h m_M/3m_h)$. For fairly straight strings the total energy to lose is $\approx 2\mu L$ where L is the maximum separation of the M and $\overline{M}$. Then (4.24) gives a lifetime that is simply proportional to L

$$\tau_{em} \approx \frac{3}{2}\alpha_h^2\frac{m_M^2}{m_h^2}\frac{L}{\chi^2}. \tag{4.25}$$

Thus the distribution of lifetimes in the collection of $MS\overline{M}$'s is determined by the distribution of L's.

In this context it is useful to consider the distribution of nearest neighbor distances for a random set of points in 3 dimensions. The nearest neighbor distribution can be derived from the relation

$$P_{nn}(r,n) = 4\pi n r^2\left(1 - \int_0^r P_{nn}(s,n)ds\right), \tag{4.26}$$

where n is the density of points. By solving this relation for $P_{nn}(r,n)$ one finds that the mean r of the nearest neighbor distribution is

$$\overline{r}_{nn} = \frac{\gamma(\frac{1}{3})}{(36\pi n)^{1/3}} \approx 0.554 n^{-1/3}, \tag{4.27}$$

where $\gamma(x)$ is the gamma function. Eliminating n in favor of $\overline{r}_{nn}$ gives

$$P_{nn}(r,\overline{r}_{nn}) = \frac{\gamma(\frac{1}{3})^3 r^2}{9\overline{r}_{nn}^3}\exp\left(-\frac{\gamma(\frac{1}{3})^3 r^3}{27\overline{r}_{nn}^3}\right). \tag{4.28}$$

This satisfies $\int_0^\infty P_{nn}(r,\overline{r}_{nn})dr = 1$ and $\int_0^\infty r P_{nn}(r,\overline{r}_{nn})dr = \overline{r}_{nn}$. The lifetime is proportional to L, and if we associate L with the nearest neighbor distance r then we can obtain a distribution of "nearest neighbor lifetimes",

$$P_{nn}(t,\overline{\tau}_{nn}) = P_{nn}(r,\overline{r}_{nn})|_{(r\to t,\ \overline{r}_{nn}\to\overline{\tau}_{nn})}. \tag{4.29}$$

$P_{nn}(t, \overline{\tau}_{nn})$ is not a physical distribution of lifetimes since it is not even possible for every M to be connected to its nearest $\overline{M}$ and vice versa.

But we wish to argue that $P_{nn}(t, \overline{\tau}_{nn})$ for some $\overline{\tau}_{nn}$ is a good approximation to $P(t, \overline{\tau})$ when $t \ll \overline{\tau}_{nn}$. This corresponds to M-$\overline{M}$ pairs with separations that are much smaller than $\overline{r}_{nn}$, and it is precisely for these pairs that it is very likely that they are connected by strings. Thus for these very close pairs the distribution of L's should be quite similar to the distribution of nearest neighbor separations. These small $MS\overline{M}$'s include those that are decaying today and so we can determine $\overline{\tau}_{nn}$ by setting $P_{nn}(t_0, \overline{\tau}_{nn}) = \tau_{\rm eff}^{-1}$ where $t_0 = 1/H$. A typical value of $\tau_{\rm eff}$ for decaying dark matter is 2×10^{26} sec, and from this we obtain $t_0/\overline{\tau}_{nn} \approx 10^{-3}$. We also have the relation $L_0/\overline{r}_{nn} = t_0/\overline{\tau}_{nn}$. $L_0 \approx 10^{-3}\overline{r}_{nn} = 0.554 \times 10^{-3} n_M^{-1/3}$ is the initial size of those $MS\overline{M}$'s that are decaying today. In the following sections it will become clear that $P_{nn}(t, \overline{\tau}_{nn})$ will be a poor approximation to $P(t, \overline{\tau})$ for times far in the future $t \gg t_0$.

$n_M^{-1/3}$ is obtained by scaling the present value of $n_0^{-1/3}$ for dark matter back to its value at string formation when the temperature is $\approx m_h/\kappa e_h$. The present temperature T_0 is enhanced by 1.4 due to the annihilation of e^+e^- at an intermediate temperature and so

$$L_0 \approx 0.55 \times 10^{-3} \frac{\kappa e_h}{m_h} \frac{T_0}{1.4} \left(\frac{\rho_0}{2m_M} \right)^{-1/3}. \tag{4.30}$$

Note that the explicit κ dependence will cancel the κ dependence of α_h^2 in (4.25) due to (4.23), and henceforth we set $\kappa = 1$. The resulting $L_0 \approx 2 \times 10^{-12}$ cm is small in the sense that it is only about 50 times larger than the thickness of the string $\approx 1/m_h$. For these small $MS\overline{M}$'s the resulting peak velocities of the monopoles are

$$v \approx \left(\frac{2\mu L_0}{m_M} \right)^{1/2} \approx 0.02. \tag{4.31}$$

Much larger $MS\overline{M}$'s can have relativistic internal motions.

We can now determine χ by setting τ_{em} from (4.25) to $t_0 = 1/H$ after replacing L with L_0. We obtain $\chi \approx 1.2 \times 10^{-15}$. From (4.4) we find that the scale of physics responsible for the mixing can be as high as $M_{mix} \approx 3 \times 10^{18}$ GeV $\sim m_{Pl}$ as advertised.

When the $MS\overline{M}$ has lost sufficient energy so that the separation of the M-$\overline{M}$ pair remains less than the string thickness, then the string dynamics no longer plays a role. The M-$\overline{M}$ pair forms a fairly weakly bound "monopolonium" state [76]. It cascades down to the $n = 1$ ground state which has binding energy $R = m_M/4\alpha_h^2$. The classical lifetime for a starting radius of m_h^{-1} is $\tau = \alpha_h^2 m_M^2/8m_h^3\chi^2$. This is much shorter than the original $MS\overline{M}$ lifetime, and it may be even shorter still due to the emission of γ_h's through

quantum $\Delta n > 1$ transitions. $\Delta n = 1$ transitions involving γ_h's are only possible for the lowest levels, $n < (2R/m_{\gamma_h})^{1/3} \sim 3$. Only a few of these low energy γ_h's are produced since $R/m_h \approx 10$. Once in the $n = 1$ state the M-$\overline{M}$ pair finally annihilates to $2\gamma_h$ (usually only two due to the fairly small magnetic coupling).

These final γ_h's are highly relativistic and since their coupling to charged matter is so small they can travel a long distance d_h before decaying,

$$d_h = \gamma \tau_h c \approx \frac{m_M}{m_h} \frac{2}{\alpha \chi^2 m_h} c. \tag{4.32}$$

From the values of parameters as already given this is about 15 kpc. d_h of this order implies that the γ_h's will tend to decay away from the regions where the dark matter densities are the highest, such as galactic cores. Also the γ_h's that give rise to the observed $e^{\pm}$'s will originate from more distant parts of the galactic dark matter halo, but for $d_h \approx 15$ kpc the $e^{\pm}$ flux is only reduced by about 30%. On the other hand d_h cannot be much larger than this. Since $d_h \propto e_h^{-5}$, due to how χ is determined by (4.25) and (4.30), we see this as another constraint that rules out small coupling.

If most γ_h's originating from our galactic core have not decayed by the time they reach earth then this also affects the associated gamma ray signal [77]. In particular this signal should show less enhancement in the direction of the galactic core and thus be more isotropic than expected [78]. The dominant part of the gamma ray signal arises from the $e^{\pm}$'s up-scattering background photons. The inter-stellar radiation field has a harder spectrum in the galactic core, and these photons when up-scattered produce higher energy gamma rays. Thus the typical energy of the gamma rays is also reduced when the γ_h's decay outside the galactic core. The same effect applies to gamma ray signals from decaying dark matter in nearby clusters of galaxies [79]; the typical gamma ray energies are reduced. The gamma ray signal that is not affected comes from the up-scattering of CMB photons and the observational constraint on this signal is the same as in other decaying dark matter models.[1]

[1]This constraint keeps one from arbitrarily decreasing τ_{eff} to compensate for a larger d_h, since decreasing τ_{eff} would increase the CMB gamma ray signal as well as the $e^{\pm}$ signal.

4.5 More energy loss

The moving M and $\overline{M}$ emit gravitational radiation, and the energy loss rate as estimated in [55] (with μ replaced by 2μ) is[2]

$$\frac{d\mathcal{E}_g}{dt} \approx -\frac{256}{5}\frac{G\mu^3 L}{m_M}. \tag{4.33}$$

For the $MS\overline{M}$'s that decay today this is insignificant compared to the electromagnetic radiation studied in the last section. But far enough in the future and for those $MS\overline{M}$'s that still survive this energy loss can become dominant. Then $L(t) = L_i e^{-t/\tau_g}$ where

$$\tau_g \approx \frac{5}{256}\frac{m_M}{G\mu^2}. \tag{4.34}$$

This is about 400 times the age of the universe and up to a logarithmic dependence on L_i, this sets the maximum lifetime of any $MS\overline{M}$. In particular the lifetime is no longer proportional to L on these time scales.

A string loop emits gravitational radiation at a rate [81]

$$\frac{d\mathcal{E}_g^s}{dt} \approx -50G\mu^2, \tag{4.35}$$

and so a loop with length πL has a lifetime

$$\tau_g^s \approx \frac{\pi L}{50G\mu}. \tag{4.36}$$

Thus a string loop will decay within the age of the universe if $L \lesssim 10^{-11}$ cm. The lifetime of a loop of length πL turns out to be similar to the lifetime of a $MS\overline{M}$ with size L, since $\tau_g^s/\tau_{em} \approx 1/5$. The gravitational radiation by the strings in a $MS\overline{M}$ has the effect of causing these strings to lose excess kinetic energy and to straighten.

We now turn to frictional effects [65]. The normal magnetic fields of the M and $\overline{M}$ will induce frictional effects through interactions with charged particles in the plasma,

$$\frac{d\mathcal{E}_f}{dt} \approx -\chi^2 B' T^2 v^2 \tag{4.37}$$

where $B' \approx \pi^{-2}\sum_i (e_i g_h/4\pi)^2$. For friction to remove the energy $2\mu L$ and for the v in

[2]The relativistic case is studied in [80].

(4.31) we obtain

$$\tau_f \approx \frac{2\mu L}{\chi^2 B' T^2 v^2} \approx \frac{m_M}{\chi^2 B' T^2}. \tag{4.38}$$

But due to the tiny χ it is easy to see that $m_M/\chi^2 B' \gg m_{Pl}$ and thus τ_f is much larger than the Hubble time. This friction can be neglected.

Normal charged particles can also scatter off a string via an Aharonov-Bohm (AB) effect, since charged particles carry a hidden charge $\epsilon e_h \equiv -\chi e$ while the strings carry a $2\pi/e_h$ unit of hidden flux. The resulting AB cross section per unit length is [65, 82, 83]

$$\frac{d\sigma_{AB}}{dl} = \frac{2}{p}\sin^2(\pi\epsilon) \tag{4.39}$$

where p is the transverse particle momentum. One can use this to estimate the time on which the transverse velocity of a section of string will be damped out as

$$\tau_{AB} \approx \frac{\mu}{\epsilon^2 B'' T^3}. \tag{4.40}$$

$B'' \approx 2\sum_a b_a$ where b_a is 3/4 for fermions and 1 for bosons. Here again $\mu/\epsilon^2 B'' T \gg m_{Pl}$ and so this effect can be neglected.

Since the hidden magnetic fields of the monopoles have been confined to strings carrying a unit of hidden flux, particles of the hidden sector that carry a unit of hidden charge will not contribute to the two previous frictional mechanisms. On the other hand a particle with hidden charge $e_h/2$ will have AB scattering at full strength, $d\sigma_{AB}/dl = 2/p$. This can be the case for the fermions that develop the $U(1)_h$ breaking condensate. Their masses should be similar to m_h, and in fact they must be greater than $m_h/2$ to prevent γ_h from decaying into them.[3] There can also be a direct interaction of hidden particles with the fields of the string, which for small p/m_h has a cross section [84]

$$\frac{d\sigma_{\rm dir}}{dl} \approx \frac{\pi^2}{p\ln(p/m_h)^2}. \tag{4.41}$$

Thus there could be a damping of transverse motions of the strings if they move in a bath of the massive particles with which they interact with cross sections σ_{AB} and/or $\sigma_{\rm dir}$. In the next section we discuss why there is very little such damping.

The Aharonov-Bohm effect implies that the string interacts with electrons through the vector electron current. This gives rise to a more interesting process where the string

[3]There need not be much lighter or massless particles remaining in the hidden sector. If there are we would need to assume that the γ_h does not decay into them, otherwise the decays of $MS\overline{M}$'s are undetectable. But then it is unlikely that such particles will interact with the string and so they are irrelevant for the string dynamics.

emits e^+e^- pairs. For a fairly smooth string loop of length πL the rate of energy loss estimated on dimensional grounds is [61]

$$\frac{d\mathcal{E}^s_{ee}}{dt} \approx -\frac{\epsilon^2}{L^2} \quad \text{for} \quad L \lesssim \frac{1}{2m_e}, \tag{4.42}$$

which in turn gives a lifetime

$$\tau^s_{ee} \approx \frac{\pi\alpha_h\mu L^3}{3\alpha\chi^2}. \tag{4.43}$$

For $L \approx 1/2m_e \approx 2\times10^{-11}$ cm the lifetime is $\tau^s_{ee} \approx 10^8$ years. For larger L the process is exponentially suppressed, so that loops more than about 3 times as large can last longer than the age of the universe. In any case we see that this process removes the smaller loops at least as effectively as gravitational radiation.

e^+e^- emission can be enhanced if the string loop has kinks and/or cusps. Cusps tend to form on featureless loops with little excitation of higher string harmonics, but such loops are less likely when there is little damping. Kinks also inhibit cusps [85] and since kinks readily form when strings intercommute, they are expected to dominate. Kinky loops of any size could emit e^+e^- pairs to produce an energy loss which is optimistically of order

$$\frac{d\mathcal{E}^s_{ee}}{dt} \approx -\frac{\epsilon^2}{L^2}\sqrt{\mu}\min(L, \frac{1}{2m_e}). \tag{4.44}$$

Here we have included the likely effect that the electron mass has on the results of [86], and the extra factor compared to (4.42) is at most a factor of 70. This is an optimistic estimate for the rate since back-reaction effects will tend to flatten out the kinks (most of the radiation comes from the sharper kinks) and thereby reduce the rate. Thus the presence of kinks probably does not dramatically increase the number of loops that can decay. We also note that the kinematics of kinks on the strings of a $MS\overline{M}$ can be quite different; on a loop the kinks move at the speed of light while on a $MS\overline{M}$ a kink can move slowly or even be stationary (as in a triangular standing wave).

The AB electron-string interaction also implies that a photon-string interaction will be generated through an electron loop [61]. A current involving photons that can be induced by the vector electron current and which doesn't vanish for on-shell photons will involve 3 photons. The lowest dimensional current that can arise after integrating out the electron must then involve three factors of the photon field strength and one extra derivative. It will therefore be suppressed by a $1/m_e^4$ factor. For a string loop of length

πL, now with L larger than $1/2m_e$, the rate will be roughly

$$\frac{d\mathcal{E}^s_{\gamma\gamma\gamma}}{dt} \approx -\frac{\alpha^3}{(2m_e)^8}\frac{\epsilon^2}{L^{10}}. \tag{4.45}$$

So even though this rate is not exponentially suppressed for large L, it has the α^3 suppression and it still drops very quickly for increasing L. It thus has negligible effect. There is also the production of photons through their gravitational coupling [87–89], but this is proportional to $(G\mu)^2$ instead of ϵ^2 and is thus miniscule.

4.6 Strings and γ_h's

The picture of a dilute network of strings interacting with a dense bath of particles is completely altered at strong coupling. The strong coupling has an effect on the string forming transition similar to its effect on the monopole forming transition. In the latter case we saw that the monopoles became point-like and light compared to the massive elementary degrees of freedom (the massive gauge fields and other massive matter). Thus the monopole abundance was not determined by the correlation length (the Kibble-Zurek mechanism) but rather by thermal equilibrium. In the string forming transition it is the string tension $\approx m_h^2/4\alpha_h^2$ that is small relative to particle masses, and so the effective theory is a theory of light, thin strings.[4] These strings also carry fermion zero modes [91]. Thus the strings tend to capture fermions and the γ_h's effectively have a decay channel into these zero modes. For example a γ_h could decay into a zero mode and a normal fermion by interacting with the string. All this indicates that the relevant degrees of freedom after the transition are the strings and their excitations.

Thus the energy that was in a plasma of massless γ_h's and fermions before the transition will be mostly deposited into strings and their kinetic energy after the transition. Due to the energy available in this plasma before the transition, the initial density of strings will be much higher than what the correlation length suggests. The string-string interaction rate will be very high (a section of string of length characteristic of the string spacing will collide many times in the Hubble time) and this should keep most of the total length of string in contact with the rest of the network. Only the loops that are very small may effectively be decoupled soon after the strings form. This should also be the case for the $MS\overline{M}$'s that are small enough to decay today, as we have already discussed.

The dense network of strings persists since it is undamped and since the energy

[4]The strong interaction limit of Nielsen-Olesen strings was considered in the original reference [90].

loss from radiation (gravitational and electromagnetic) is so slow. This is quite unlike the more standard evolution of cosmic strings which involves significant damping after formation. Due to energy considerations the strings are expected to move relativistically $\langle v_s^2 \rangle \approx 1$. A network of strings has an effective pressure [58]

$$p_s = \frac{1}{3}(2\langle v_s^2 \rangle - 1)\rho_s, \tag{4.46}$$

and so relativistically moving strings behave like a normal relativistic gas with $p = \rho/3$. In this limit the energy density in the string network does not increase relative to the total energy density. As long as ρ_s remains a fairly small fraction of the total ρ down to temperatures of about 1 MeV then it avoids constraints from big bang nucleosynthesis. Strings only form at a temperature of order $m_h/e_h \approx 40$ MeV and so this is not a severe constraint.[5]

For weak coupling, which we have already argued is not interesting for other reasons, the γ_h's and massive fermions would remain after the transition. Then in particular the γ_h, with its 500 MeV mass and a lifetime longer than 1 second, would not satisfy the BBN constraints [67].[6]

The violent motions of the strings and their collisions could in principle produce γ_h's. But unlike the case of e^+e^- emission, the mass m_h here is larger than $\sqrt{\mu}$ and so we expect substantial exponential suppression. Any γ_h's that are produced face the prospect of string catalyzed decay back into dark sector degrees of freedom. In the absence of strings the proper lifetime of the γ_h is about 10 years, so at that time γ_h's can decay to ordinary leptons. But we expect that γ_h production and decay only transfers a minor amount of energy from the hidden sector to the observable sector.

4.7 Late times

As the universe expands the interaction rate between $MS\overline{M}$'s gradually decreases, both because their separation increases and because their momenta are being redshifted. Starting from the smallest ones, the size of the $MS\overline{M}$'s that have a collision time larger than the Hubble time gradually increases and eventually most $MS\overline{M}$'s stop colliding. Loops free of monopoles will also be present. Loops of complicated shapes will quickly fragment

[5] We also note that the BBN constraints have recently weakened [92, 93], and may even be in line with indications of new relativistic degrees of freedom from CMB studies [94, 95].

[6] If the γ_h's annihilated fast enough into much lighter or massless particles of the hidden sector then presumably they would also decay into these same particles, which would make them undetectable. Alternatively a γ_h mass closer to a MeV and/or a small κ could be considered in the weak coupling case.

into simpler loops which no longer self-intersect [96,97]. Thus in addition to the $MS\overline{M}$'s there will be a population of loops which also stop interacting and which extend down in size to where they can decay to e^+e^- pairs and gravitons within the age of the universe.

The relativistic string network should also survive to late times. The typical separation between strings in this network is much smaller than the Hubble scale, but its growth is proportional to t. Loops, with or without monopoles, of size anywhere close to this typical separation would be continually interacting and reconnecting with the rest of the network. As this separation increases there is an increasing population of smaller loops and $MS\overline{M}$'s that are more or less decoupled from the network. What is left of the relativistic string network today cannot have an energy density larger than the CMB, and so the typical separation in the string network now can be no less than about 3×10^{10} cm. This of course is much larger than the present separation between $MS\overline{M}$'s.

For the dark matter that accumulates in halos, the increased density and speeds of the $MS\overline{M}$'s and loops leads to a resurgence of their interactions. Let us consider a nontrivial interaction between two $MS\overline{M}$'s with fairly straight strings of length L_1 and L_2 respectively. The cross section is $\sigma = \zeta L_1 L_2$ where ζ accounts for the relative orientations, the fact that each is oscillating, and the probability for intercommuting. We take $\zeta = 0.1$. Then the cross section corresponding to $L_1 = L_2 = 10^{-9}$ cm for example would result in a rate of collisions of $n\sigma v \approx 50H$ for local dark matter densities and speeds. This is a value of interest for self-interacting dark matter models [98] and it suggests that the average L cannot be much larger than 10^{-9} cm. A new feature here is that the cross section depends on the L_i's of the $MS\overline{M}$'s being scattered. The smaller $MS\overline{M}$'s have a lower collision rate and so there can be a nearly collisionless subpopulation of $MS\overline{M}$'s. Also the collisions are not elastic since the sum of the internal energies can change after a collision. The effect that these new features have on the dynamics of dark matter halos remains to be explored.

Also of interest is the probability for two $MS\overline{M}$'s to collide to form a small $MS\overline{M}$ with a size no larger than $L_0 \approx 2\times10^{-12}$ cm, so that it can decay within the Hubble time. For this to happen a M and $\overline{M}$ must be close together not only in position space but also in momentum space, since the kinetic energies of the monopoles in their center of mass frame cannot be larger than the rest mass of a segment of string of length L_0. Also the strings must intercommute at a point which will produce the small segment. Given the large dimensional phase space of possibilities, the production of a small $MS\overline{M}$ is highly suppressed. In fact our previous estimate for the number of small $MS\overline{M}$'s is due to a phase space suppression as well (e.g. the small r behavior of (4.28)). There the suppression is not as strong since only position space was involved; the kinetic energies

of the monopoles at the time of string formation could be neglected. Thus the rate of $MS\overline{M}$'s decaying today should not be substantially changed from our previous estimate.

Collisions among a population of loops and $MS\overline{M}$'s also provide some probability for producing loops a few times $1/2m_e \approx 2 \times 10^{-11}$ cm in size or smaller. As described in the last section these loops decay mostly into e^+e^- pairs. $MS\overline{M}$'s similarly small in size could also emit e^+e^- pairs if their strings are excited. The energies of the e^+e^- pairs are typically not far above threshold and there are up to $\sim 10^3$ such pairs produced from the largest of the small loops which can decay. The production of these small loops need not be very efficient to be of interest for the 511 keV photon flux observed to come from the galactic bulge [99,100]. For example a collision can excite the strings of two $MS\overline{M}$'s, and even when these $MS\overline{M}$'s are not small it is still possible that they can emit a loop that is small enough to decay. From the analysis of [101] we estimate that this probability would have to be smaller than about 10^{-6}, assuming an average L of 10^{-9} cm.

Finally we comment on large $MS\overline{M}$'s. When $L \approx 1$ angstrom (10^{-8} cm $\approx 5000L_0$) the energy in the strings is comparable to the energy in the monopoles $\mu L \approx m_M$. For larger L the $MS\overline{M}$'s have relativistic monopoles and a total energy larger than $2m_M$. But we don't expect the average L to be this large due to the constraints on the self-interactions. We note in passing that for $\mu L \gg m_M$ the ultra-relativistic monopoles can result in the emission of particles with energies $\gamma a \approx (\mu L/m_M)(2\mu/m_M)$ [59]. For γ_h's to be produced this energy must be greater than m_h, and this would require a very large $L > (m_M/\mu)^2 m_h/2 \approx 0.002$ cm.

4.8 Direct detection

For direct detection of $MS\overline{M}$'s the interaction can be between the monopole and a nucleus or the string and a nucleus through Aharonov-Bohm scattering. The differential cross section for the classical scattering of an electric charge off the field of a magnetic monopole for large impact parameter is given by [102]

$$\frac{d\sigma_{MN}}{d\Omega} = \left(\frac{eg}{E}\right)^2 \frac{v^2}{\theta^4}, \tag{4.47}$$

where E and v are the energy and speed of the incoming charge. The differential cross section (per unit length) for AB scattering of an electric charge off a string is given by

$$\frac{d\sigma_{AB}}{d\theta} = \frac{\sin^2(\pi\epsilon)}{2\pi p \sin^2(\theta/2)}, \tag{4.48}$$

where p is the transverse particle momentum.

We can write the above expressions in terms of a nucleon recoil energy E_R, which is the physical quantity measured. The results are

$$\frac{d\sigma_{MN}}{dE_R} = \frac{2\pi Z^2 \alpha \alpha_M \chi^2}{m_N E_R^2} \tag{4.49}$$

and

$$\frac{d\sigma_{AB}}{dE_R} \approx \frac{4L}{3}\frac{\pi\chi^2 v}{E_R^2}\left(\frac{2m_N v^2}{E_R} - 1\right)^{-1/2}. \tag{4.50}$$

For the latter we account for two strings of length L, with each on average 2/3 shorter due to the oscillations.

Among the direct detection experiments, an upper bound on the interaction cross section for heavy dark matter (several hundred GeV to TeV masses) is given by the CDMS experiment [103]. This experiment uses germanium or silicon crystals as the absorber and has a sensitivity threshold $E_R \approx 10$ keV. We use $m_N = 26$ GeV and $Z = 14$ corresponding to silicon, the lighter of the two nuclei. The integrals that determine the total cross sections are dominated by the lower limit, the minimum recoil energies. We find

$$\sigma_{MN} \approx 10^{-54}\ \text{cm}^2, \tag{4.51}$$

$$\sigma_{AB} \approx \left(\frac{L}{10^{-9}\ \text{cm}}\right) 10^{-50}\ \text{cm}^2, \tag{4.52}$$

where we have set $v = 10^{-3}$. Thus the Aharonov-Bohm scattering will be the dominant form of interaction. The current sensitivity is $\sigma_{exp} \approx 10^{-43}(m_{DM}/1\ \text{TeV})\ \text{cm}^2$. The relative sensitivity of the more recent XENON100 experiment [104] is similar after accounting for its heavier nuclei. Thus for a typical L not much above 10^{-9} cm, the AB cross section is still orders of magnitude below the best sensitivities available today.

For monopole-nucleus scattering we should comment on the maximum recoil energy, $E_{R\max} = 2m_N v^2$, since the M and $\overline{M}$ can move at speeds $\sim (\mu L/m_M)^{1/2}$ which could be much greater than $10^{-3}c$. But the $E_{R\max}$ is limited by another effect. Recall that in the massless γ_h limit the mutual coupling between the M's and normal charges vanishes according to the Dirac quantization condition. Thus for distances of approach less than m_h^{-1} the monopoles become invisible to normal charges and therefore scattering events where $q^2 \gtrsim m_h^2$ cannot occur. This implies that $E_{R\max} \approx m_h^2/2m_N$, and at this energy a bump could be expected in the spectrum due to a type of pile-up effect.

4.9 Outlook

We have presented a dark matter candidate, the $MS\overline{M}$, with extremely weak couplings to the observable world (kinetic mixing parameter $\chi \approx 10^{-15}$). When it decays the annihilating monopoles contribute to high energy electron/positron, neutrino and gamma ray signals. Excited strings and string loops may also be a source of low energy e^+e^- pairs. The self-interactions of $MS\overline{M}$'s can have implications for dark halo dynamics. But there is little chance of observing $MS\overline{M}$'s through direct detection or in collider searches. The extremely weak coupling manifests itself as a long lifetime of the particle that mediates the interactions with the dark sector, the γ_h. Only γ_h's that originate farther from us than its typical travel distance will be observable. This travel distance can be somewhat larger than the distance to the galactic core and this could reduce the anisotropy of the gamma ray and neutrino signals.

Meanwhile both the monopole mass and the γ_h mass will be constrained by the characteristics of the observed $e^\pm$ spectra. If m_h is indeed significantly larger than 1 MeV then it will produce an apparent puzzle given the constraints from BBN. This in turn would provide indirect evidence for strong interactions in the hidden sector since, as we have described, in this case energy is dumped into relativistic cosmic strings rather than nonrelativistic γ_h's. A determination of the γ_h travel distance would also fix the mixing parameter χ through (4.32). The parameters of the model are then determined. We may then find that a "miracle" has occurred, since it could turn out that the model gives both the right abundance and the right lifetime for the $MS\overline{M}$'s.

Chapter 5

Conclusions and Future Prospects

The Standard Model of particle physics, as well as the Standard Cosmological model, have provided us with an unprecedented level of understanding and predictive power across a wide range of phenomena. These theories are indeed an outstanding achievement resulting from the efforts of a multitude of talented individuals and groups, across many decades of work. In some sense, we have come to a point where the theories' incredible degree of agreement with experiment has turned into a great difficulty we now face as a scientific community.

The success of the current working theories by no means implies that they are complete. We know that there remain many open questions that are begging to be answered. Furthermore, it is also our hope that in attempting to answer some of these questions, a more unified description of the Universe could arise wherein both the SM and the Standard Cosmological Model could find a home (at least partially). But in recent years there has been little indication from experiment as to where the right path to proceed along this task lies. On the cosmology front, the nature of Dark Matter and Dark Energy remain as mysterious as ever, while observational evidence for extensions to the standard big bang model such as inflation remains elusive [105]. On the particle physics front, no spectacular signs of Supersymmetry, Technicolour, extra dimensions, nor of any other BSM physics model has (yet?) emerged at the LHC, to the surprise and dismay of many. Only the single Standard Model Higgs boson has made an appearance.

In light of this last observation, it appears we are left with the following options:
1. Supersymmetry is indeed the solution to weak scale naturalness; it is realized in some really contrived incarnation such that it has not been observed yet, but is "just around the corner".
2. The observed Higgs boson is not exactly a SM Higgs boson, it just looks quite a lot like it. It is actually only the tip of the iceberg of a whole new (possibly strongly coupled)

sector, signs of which should appear in the near future of LHC searches either in the form of new, heavier resonances, or deviations of the coupling of the Higgs to SM particles.
3. The SM is not "natural", or more precisely, apparently fine-tuned parameters are actually natural in the sense that they happen to occur in nature.
In this thesis we have delved into some of the open questions left by the Standard Model, we could say mostly in the spirit of point number 2 above.

In Chapter 2, we have turned to the issue of whether or not the long theorized dilaton should exist as a light degree of freedom in the context of gauge theories. This is a question that, we believe, remains interesting even as a purely theoretical exercise regardless of whether or not gauge theories with walking-type dynamics are realized in nature at the weak (or any other) scale. However, the prospect that such a particle could be identified with the observed Higgs boson at the LHC brings the problem under a whole new light.

From a CFT perspective, the authors of [35] claim that depending on how the Standard Model is embedded into the conformal sector, a dilaton emerging from a near-conformal theory could reproduce the observed behaviour of the 125 GeV resonance discovered at the LHC (see also [106–108]). In our work we have shown qualitatively how this property, at least as far as the lightest scalar's couplings to the W and Z bosons are concerned, could in fact arise naturally out of a gauge theory. However, we have a much harder time envisioning how the lowest lying scalar in the spectrum could be light.

We find that in a non-local approach to the problem, one is made aware of important effects coming from the UV that give large contributions to the scalar's mass which cannot be accounted for in purely local analyses. Qualitatively, this conclusion also appears to agree with the CFT side of the argument in [35], where the authors conclude that it is not sufficient to begin with a conformal theory and to then introduce a small breaking parameter to keep the would-be dilaton's mass small; they can only achieve this with fine-tuning and special dynamical assumptions that should not generally be present in gauge theories. Going beyond considerations of the value of the "dilaton's" mass, we additionally find that the lowest lying scalar in the theory cannot really be identified as the PNGB of the spontaneous breaking of approximate scale invariance once we consider the shape of the momentum-dependent form factor that determines how the scalar couples to the fermion loops in the theory.

Our conclusions regarding the value of the lightest scalar's mass are only valid in the large N_c limit however. Maybe, some hope yet remains that a light scalar could emerge if the strongly coupled sector consists of a $U(1)$ gauge theory, for example. This type of extension to the SM has been considered in [109].

In Chapter 3, we have considered a lepton based charge asymmetry observable that could become useful at the LHC in the event that anomalies in the lepton counts of the various channels should emerge. If we remain optimistic regarding point 2 above, PNGBs could be the first to show signs of BSM physics in these channels. Some of these PNGBs with complex decay chains may be difficult to reconstruct. If their quantum numbers should be such that a charge asymmetry is expected however, as in the case of scalars carrying diquark quantum numbers that appear in the model of [109], then the observable that we propose, A_C^l, may be one of the few measurements fit to explore it. We have also presented our theory calculation for the charge asymmetry coming from QCD of diquark scalars, to use as benchmark objects for our study. Of course there is no reason why A_C^l should not also be useful to study charge asymmetries in more familiar systems such as $t\bar{t}$ for example.

Finally, in Chapter 4 we have presented a proposal for a dark matter candidate coming from a hidden sector only very weakly coupled to the Standard Model. If we consider the rich gauge and matter structure that exists within our own SM, which only accounts for a small percentage of the matter inventory in the Universe as we have mentioned in Section 1.3, it is reasonable to think that a dark sector could bear some resemblance to this complexity. We have entertained the possibility that some of the astrophysical anomalies that have come to light in the past years could be indirect signals of DM decay (or annihilation) in our own Milky Way's DM halo, hence a portal coupling the dark and visible sectors is necessary. One interesting such portal to consider, is that purveyed by the kinetic mixing of a dark photon with the photon. One then may think of a dark sector with a larger gauge group that could spontaneously break leaving an unbroken $U(1)$. If the original gauge group in which the remaining $U(1)$ is embedded is semi-simple, this type of transition will generically lead to the appearance of topological defects with quantized magnetic charge, i.e. dark magnetic monopoles.

Through the sequential breaking of the dark $U(1)$ we have been able to obtain a very long lived, decaying DM candidate consisting of dark monopoles tied by strings. The parameters in the theory work out in such a way that a strong coupling in the dark sector appears necessary to give the right DM relic density, while at the same time saving our model from BBN constraints. The value of the mixing parameter between the two sectors can be pinned down from the distance a hidden photon can travel before decaying, in order to generate a positron excess in our vicinity. The resulting value $\sim 10^{-15}$ implies little immediate prospect for direct detection and production at colliders, but gives the right DM lifetime to avoid the stringent constraints coming from the isotropic gamma ray signal in the galaxy.

Our model may also be of interest in the context of self-interacting dark matter. Increased density and speeds of the monopoles and strings in the galactic halo can lead to the resurgence of their self-interactions which may occur with large cross sections given that their origin is geometrical. The effects that these interactions may have on the dynamics of dark matter halos remain to be explored.

While our DM model may appear rather exotic, the reader may find that the ideas that have logically led us to consider it as such are all quite reasonable. As direct detection experiments improve their reach towards lower scattering cross sections between atomic nuclei and the DM particles, we expect that they may become sensitive to our model in coming years.

Bibliography

[1] Timo Alho, Nick Evans, and Kimmo Tuominen. Dynamic AdS/QCD and the Spectrum of Walking Gauge Theories. *Phys.Rev.*, D88:105016, 2013.

[2] Serguei Chatrchyan et al. Observation of a new boson at a mass of 125 GeV with the CMS experiment at the LHC. *Phys. Lett.*, B716:30–61, 2012.

[3] Georges Aad et al. Observation of a new particle in the search for the Standard Model Higgs boson with the ATLAS detector at the LHC. *Phys. Lett.*, B716:1–29, 2012.

[4] D Abbaneo et al. A Combination of Preliminary Electroweak Measurements and Constraints on the Standard Model, 2001: addendum. Technical Report hep-ex/0112021. CERN-ALEPH-2001-078. CERN-DELPHI-2001-131. CERN-EP-2001-098. CERN-L3-250. CERN-L3-Note-2723. CERN-LEPEWWG-2001-02. CERN-OPAL-PR-350, CERN, Geneva, Dec 2001.

[5] Christopher T. Hill and Elizabeth H. Simmons. Strong dynamics and electroweak symmetry breaking. *Phys. Rept.*, 381:235–402, 2003. [Erratum: Phys. Rept.390,553(2004)].

[6] Bob Holdom. Raising the Sideways Scale. *Phys. Rev.*, D24:1441, 1981.

[7] Thomas Appelquist, George T. Fleming, and Ethan T. Neil. Lattice study of the conformal window in QCD-like theories. *Phys. Rev. Lett.*, 100:171607, 2008. [Erratum: Phys. Rev. Lett.102,149902(2009)].

[8] Thomas Appelquist, George T. Fleming, and Ethan T. Neil. Lattice Study of Conformal Behavior in SU(3) Yang-Mills Theories. *Phys. Rev.*, D79:076010, 2009.

[9] Curtis G. Callan, Jr., Sidney R. Coleman, and Roman Jackiw. A New improved energy - momentum tensor. *Annals Phys.*, 59:42–73, 1970.

[10] John C. Collins, Anthony Duncan, and Satish D. Joglekar. Trace and Dilatation Anomalies in Gauge Theories. *Phys. Rev.*, D16:438–449, 1977.

[11] Koichi Yamawaki, Masako Bando, and Ken-iti Matumoto. Scale Invariant Technicolor Model and a Technidilaton. *Phys. Rev. Lett.*, 56:1335, 1986.

[12] Chung Ngoc Leung, S. T. Love, and William A. Bardeen. Spontaneous Symmetry Breaking in Scale Invariant Quantum Electrodynamics. *Nucl. Phys.*, B273:649–662, 1986.

[13] Bob Holdom and John Terning. No Light Dilaton in Gauge Theories. *Phys.Lett.*, B200:338–342, 1988.

[14] Thomas Appelquist and Yang Bai. A Light Dilaton in Walking Gauge Theories. *Phys.Rev.*, D82:071701, 2010.

[15] Michio Hashimoto and Koichi Yamawaki. Techni-dilaton at Conformal Edge. *Phys. Rev.*, D83:015008, 2011.

[16] Georges Aad et al. Analysis of events with b-jets and a pair of leptons of the same charge in pp collisions at $\sqrt{s} = 8$ TeV with the ATLAS detector. Technical Report arXiv:1504.04605. CERN-PH-EP-2015-060, CERN, Geneva, Apr 2015.

[17] Bob Holdom. Diquarks from a fourth family. *Phys.Lett.*, B703:576–582, 2011.

[18] K. G. Begeman, A. H. Broeils, and R. H. Sanders. Extended rotation curves of spiral galaxies - Dark haloes and modified dynamics modified dynamics. *Monthly Notices of the Royal Astronomical Society.*, 249:523–537, 1991.

[19] Dennis Zaritsky, Rodney Smith, Carlos Frenk, and Simon D. M. White. More satellites of spiral galaxies. *Astrophys. J.*, 478:39–48, 1997.

[20] Henk Hoekstra, Howard Yee, and Mike Gladders. Current status of weak gravitational lensing. *New Astron. Rev.*, 46:767–781, 2002.

[21] E. Komotasu et al. Seven-Year Wilkinson Microwave Anisotropy Probe (WMAP) Observations: Cosmological Interpretation. *Astrophys.J.Suppl.*, 192:18, 2011.

[22] Oscar Adriani et al. An anomalous positron abundance in cosmic rays with energies 1.5-100 GeV. *Nature*, 458:607–609, 2009.

[23] A.A. Abdo et al. Measurement of the cosmic ray $e^+ + e^-$ spectrum from 20 gev to 1 tev with the fermi large area telescope. *Phys. Rev. Lett.*, 102:181101, May 2009.

[24] Torsten Bringmann, Xiaoyuan Huang, Alejandro Ibarra, Stefan Vogl, and Christoph Weniger. Fermi LAT Search for Internal Bremsstrahlung Signatures from Dark Matter Annihilation. *JCAP*, 1207:054, 2012.

[25] Pasquale D. Serpico. Astrophysical models for the origin of the positron excess. *Astroparticle Physics*, 3940:2 – 11, 2012. Cosmic Rays Topical Issue.

[26] Patrick Meade, Michele Papucci, Alessandro Strumia, and Tomer Volansky. Dark Matter Interpretations of the e+- Excesses after FERMI. *Nucl. Phys.*, B831:178–203, 2010.

[27] Bob Holdom. Raising the Sideways Scale. *Phys.Rev.*, D24:1441, 1981.

[28] R. J. Crewther and Lewis C. Tunstall. $\Delta I = 1/2$ rule for kaon decays derived from QCD infrared fixed point. *Phys. Rev.*, D91(3):034016, 2015.

[29] Hagen Kleinert. Hadronization of Quark Theories and a Bilocal Form of QED. *Phys. Lett.*, B62:429, 1976.

[30] T. Kugo. Dynamical Instability of the Vacuum in the Lagrangian Formalism of the Bethe-Salpeter Bound States. *Phys. Lett.*, B76:625, 1978.

[31] C.M. Fraser. Calculation of Higher Derivative Terms in the One Loop Effective Lagrangian. *Z.Phys.*, C28:101, 1985.

[32] Andrew G. Cohen and Howard Georgi. Walking Beyond the Rainbow. *Nucl. Phys.*, B314:7, 1989.

[33] R.W. Haymaker, T. Matsuki, and F. Cooper. Comparison of Alternative Effective Potentials for Dynamical Symmetry Breaking. *Phys.Rev.*, D35:2567, 1987.

[34] M. K. Transtrum and J.S. Heule. Commutation relations for functions of operators. *Journal of Mathematical Physics*, 46:063510, 2005.

[35] Brando Bellazzini, Csaba Csaki, Jay Hubisz, Javi Serra, and John Terning. A Higgslike Dilaton. *Eur.Phys.J.*, C73:2333, 2013.

[36] Zackaria Chacko, Rashmish K. Mishra, and Daniel Stolarski. Dynamics of a Stabilized Radion and Duality. *JHEP*, 1309:121, 2013.

[37] John B. Kogut, M. Stone, H.W. Wyld, J. Shigemitsu, S.H. Shenker, et al. The Scales of Chiral Symmetry Breaking in Quantum Chromodynamics. *Phys.Rev.Lett.*, 48:1140, 1982.

[38] Bob Holdom. Continuum Limit of Quenched Theories. *Phys. Rev. Lett.*, 62:997, 1989.

[39] Heinz Pagels and Saul Stokar. The Pion Decay Constant, Electromagnetic Form-Factor and Quark Electromagnetic Selfenergy in QCD. *Phys.Rev.*, D20:2947, 1979.

[40] Yvonne Reinhild Peters. Top anti-top Asymmetries at the Tevatron and the LHC. In *Proceedings, 32nd International Symposium on Physics in Collision (PIC 2012)*, pages 27–37, 2012.

[41] Georges Aad et al. Measurement of the charge asymmetry in dileptonic decay of top quark pairs in pp collisions at $\sqrt{s} = 7$ TeV using the ATLAS detector. Technical Report ATLAS-CONF-2012-057, CERN, Geneva, Jun 2012.

[42] Georges Aad et al. Measurement of the charge asymmetry in top quark pair production in pp collisions at $\sqrt{s} = 7$ TeV using the ATLAS detector. *Eur.Phys.J.*, C72:2039, 2012.

[43] Serguei Chatrchyan et al. Inclusive and differential measurements of the $t\bar{t}$ charge asymmetry in proton-proton collisions at 7 TeV. *Phys.Lett.*, B717:129–150, 2012.

[44] Gian Francesco Giudice, Ben Gripaios, and Raman Sundrum. Flavourful Production at Hadron Colliders. *JHEP*, 1108:055, 2011.

[45] J. H. Kühn and G. Rodrigo. Charge asymmetry of heavy quarks at hadron colliders. *Phys. Rev. D*, 59:054017, Feb 1999.

[46] Jaume Guasch, Wolfgang Hollik, and Arnd Kraft. Radiative corrections to pair production of charged Higgs bosons at TESLA. In *5th Workshop of the 2nd ECFA - DESY Study on Physics and Detectors for a Linear Electron - Positron Collider Obernai, France, October 16-19, 1999*, 1999.

[47] Victor Mukhamedovich Abazov et al. Forward-backward asymmetry in top quark-antiquark production. *Phys. Rev.*, D84:112005, 2011.

[48] Georges Aad et al. Measurement of the top quark pair production cross section in the single-lepton channel with ATLAS in proton-proton collisions at 8 TeV using kinematic fits with b-tagging. Technical Report ATLAS-CONF-2012-149, CERN, Geneva, Nov 2012.

[49] Serguei Chatrchyan et al. Search for anomalous production of events with three or more leptons in pp collisions at $\sqrt{(}s) = 8$ TeV. *Phys. Rev.*, D90:032006, 2014.

[50] Georges Aad et al. Search for supersymmetry in events with four or more leptons in $\sqrt{s} = 8$ TeV pp collisions with the ATLAS detector. *Phys. Rev.*, D90(5):052001, 2014.

[51] B. Holdom and M. Ratzlaff. Neglected heavy leptons at the LHC. *Phys. Rev.*, D90(1):013015, 2014.

[52] Georges Aad et al. Measurement of the Muon Charge Asymmetry from W Bosons Produced in pp Collisions at $\sqrt{s} = 7$ TeV with the ATLAS detector. *Phys.Lett.*, B701:31–49, 2011.

[53] Ansgar Denner. Techniques for calculation of electroweak radiative corrections at the one loop level and results for W physics at LEP-200. *Fortsch.Phys.*, 41:307–420, 1993.

[54] Catalina Gomez Sanchez and Bob Holdom. Monopoles, strings and dark matter. *Phys. Rev.*, D83:123524, 2011.

[55] J. J. Blanco-Pillado and Ken D. Olum. Monopole - anti-monopole bound states as a source of ultrahigh-energy cosmic rays. *Phys. Rev.*, D60:083001, 1999.

[56] Eugene N. Parker. The Origin of Magnetic Fields. *Astrophys. J.*, 160:383, 1970.

[57] A. Vilenkin. Cosmological Evolution of Monopoles Connected by Strings. *Nucl. Phys.*, B196:240–258, 1982.

[58] Tanmay Vachaspati and Alexander Vilenkin. Evolution of cosmic networks. *Phys. Rev.*, D35:1131, 1987.

[59] Veniamin Berezinsky, Xavier Martin, and Alexander Vilenkin. High-energy particles from monopoles connected by strings. *Phys. Rev.*, D56:2024–2034, 1997.

[60] Jose J. Blanco-Pillado and Ken D. Olum. Monopole annihilation in cosmic necklaces. *JCAP*, 1005:014, 2010.

[61] Tanmay Vachaspati. Dark Strings. *Phys. Rev.*, D80:063502, 2009.

[62] Bob Holdom. Two U(1)'s and Epsilon Charge Shifts. *Phys. Lett.*, B166:196, 1986.

[63] Nima Arkani-Hamed, Douglas P. Finkbeiner, Tracy R. Slatyer, and Neal Weiner. A Theory of Dark Matter. *Phys. Rev.*, D79:015014, 2009.

[64] Maxim Pospelov and Adam Ritz. Astrophysical Signatures of Secluded Dark Matter. *Phys. Lett.*, B671:391–397, 2009.

[65] A. Vilenkin and E. P. S. Shellard. *Cosmic strings and other topological defects*. Cambridge University Press, 2000.

[66] Michele Papucci and Alessandro Strumia. Robust implications on Dark Matter from the first FERMI sky gamma map. *JCAP*, 1003:014, 2010.

[67] Maxim Pospelov, Adam Ritz, and Mikhail B. Voloshin. Secluded WIMP Dark Matter. *Phys. Lett.*, B662:53–61, 2008.

[68] Felix Brummer and Joerg Jaeckel. Minicharges and Magnetic Monopoles. *Phys. Lett.*, B675:360–364, 2009.

[69] John Preskill. Cosmological Production of Superheavy Magnetic Monopoles. *Phys. Rev. Lett.*, 43:1365, 1979.

[70] T. W. B. Kibble. Topology of Cosmic Domains and Strings. *J. Phys.*, A9:1387–1398, 1976.

[71] W. H. Zurek. Cosmological Experiments in Superfluid Helium? *Nature*, 317:505–508, 1985.

[72] Hitoshi Murayama and Jing Shu. Topological Dark Matter. *Phys. Lett.*, B686:162–165, 2010.

[73] V. L. Ginzburg and L. D. Landau. On the Theory of superconductivity. *Zh. Eksp. Teor. Fiz.*, 20:1064–1082, 1950.

[74] E.W. Kolb and M. S. Turner. *The early universe*. Frontiers in Physics, Reading, MA: Addison-Wesley, 1990.

[75] Andrew G. Cohen, David B. Kaplan, and Ann E. Nelson. Counting 4 pis in strongly coupled supersymmetry. *Phys. Lett.*, B412:301–308, 1997.

[76] Christopher T. Hill. Monopolonium. *Nucl. Phys.*, B224:469, 1983.

[77] Ira Z. Rothstein, Thomas Schwetz, and Jure Zupan. Phenomenology of dark matter annihilation into a long-lived intermediate state. *Journal of Cosmology and Astroparticle Physics*, 2009(07):018, 2009.

[78] Alejandro Ibarra, David Tran, and Christoph Weniger. Detecting Gamma-Ray Anisotropies from Decaying Dark Matter: Prospects for Fermi LAT. *Phys. Rev.*, D81:023529, 2010.

[79] Leanna Dugger, Tesla E. Jeltema, and Stefano Profumo. Constraints on decaying dark matter from fermi observations of nearby galaxies and clusters. *Journal of Cosmology and Astroparticle Physics*, 2010(12):015, 2010.

[80] Xavier Martin and Alexander Vilenkin. Gravitational radiation from monopoles connected by strings. *Phys. Rev.*, D55:6054–6060, 1997.

[81] Paul Casper and Bruce Allen. Gravitational radiation from realistic cosmic string loops. *Phys. Rev.*, D52:4337–4348, 1995.

[82] R. M. Rohm. *Some Current Problems in Particle Physics Beyond the Standard Model*. PhD thesis, Princeton U., 1985.

[83] Mark G. Alford and Frank Wilczek. Aharonov-Bohm Interaction of Cosmic Strings with Matter. *Phys. Rev. Lett.*, 62:1071, 1989.

[84] Allen E. Everett. Cosmic Strings in Unified Gauge Theories. *Phys. Rev.*, D24:858, 1981.

[85] David Garfinkle and Tanmay Vachaspati. Radiation From Kinky, Cuspless Cosmic Loops. *Phys. Rev.*, D36:2229, 1987.

[86] Yi-Zen Chu, Harsh Mathur, and Tanmay Vachaspati. Aharonov-Bohm Radiation of Fermions. *Phys. Rev.*, D82:063515, 2010.

[87] Jaume Garriga, Diego Harari, and Enric Verdaguer. Gravitational Particle Production by Cosmic Strings. *Nucl. Phys.*, B339:560–576, 1990.

[88] Katherine Jones-Smith, Harsh Mathur, and Tanmay Vachaspati. Aharonov-Bohm Radiation. *Phys. Rev.*, D81:043503, 2010.

[89] Daniele A. Steer and Tanmay Vachaspati. Light from Cosmic Strings. *Phys. Rev.*, D83:043528, 2011.

[90] Holger Bech Nielsen and P. Olesen. Vortex Line Models for Dual Strings. *Nucl. Phys.*, B61:45–61, 1973.

[91] R. Jackiw and P. Rossi. Zero Modes of the Vortex - Fermion System. *Nucl. Phys.*, B190:681, 1981.

[92] Yuri I. Izotov and Trinh X. Thuan. The primordial abundance of 4he: Evidence for non-standard big bang nucleosynthesis. *The Astrophysical Journal Letters*, 710(1):L67, 2010.

[93] Erik Aver, Keith A. Olive, and Evan D. Skillman. A new approach to systematic uncertainties and self-consistency in helium abundance determinations. *Journal of Cosmology and Astroparticle Physics*, 2010(05):003, 2010.

[94] E. Komatsu et al. Seven-year wilkinson microwave anisotropy probe (wmap) observations: Cosmological interpretation. *The Astrophysical Journal Supplement Series*, 192(2):18, 2011.

[95] J. Dunkley et al. The atacama cosmology telescope: Cosmological parameters from the 2008 power spectrum. *The Astrophysical Journal*, 739(1):52, 2011.

[96] Craig J Copi and Tanmay Vachaspati. Shape of Cosmic String Loops. *Phys. Rev.*, D83:023529, 2011.

[97] R. J. Scherrer and W. H. Press. Cosmic String Loop Fragmentation. *Phys. Rev.*, D39:371–378, 1989.

[98] David N. Spergel and Paul J. Steinhardt. Observational evidence for selfinteracting cold dark matter. *Phys. Rev. Lett.*, 84:3760–3763, 2000.

[99] Pierre Jean et al. Early SPI / INTEGRAL measurements of 511 keV line emission from the 4th quadrant of the Galaxy. *Astron. Astrophys.*, 407:L55, 2003.

[100] Jurgen Knodlseder et al. Early SPI / INTEGRAL contraints on the morphology of the 511 keV line emission in the 4th galactic quadrant. *Astron. Astrophys.*, 411:L457–L460, 2003.

[101] Charles Picciotto and Maxim Pospelov. Unstable relics as a source of galactic positrons. *Phys. Lett.*, B605:15–25, 2005.

[102] I. Richard Lapidus and Jerry L. Pietenpol. Classical interaction of an electric charge with a magnetic monopole. *American Journal of Physics*, 28(1):17–18, 1960.

[103] Z. Ahmed et al. Dark matter search results from the cdms ii experiment. *Science*, 327(5973):1619–1621, 2010.

[104] E. Aprile et al. Dark matter results from 100 live days of xenon100 data. *Phys. Rev. Lett.*, 107:131302, Sep 2011.

[105] P. A. R. Ade et al. Joint Analysis of BICEP2/$KeckArray$ and $Planck$ Data. *Phys. Rev. Lett.*, 114:101301, 2015.

[106] Shinya Matsuzaki and Koichi Yamawaki. Is 125 GeV techni-dilaton found at LHC? *Phys. Lett.*, B719:378–382, 2013.

[107] Zackaria Chacko, Roberto Franceschini, and Rashmish K. Mishra. Resonance at 125 GeV: Higgs or Dilaton/Radion? *JHEP*, 04:015, 2013.

[108] Ian Low, Joseph Lykken, and Gabe Shaughnessy. Have We Observed the Higgs (Imposter)? *Phys. Rev.*, D86:093012, 2012.

[109] B. Holdom. The accidental Higgs boson. *Phys.Rev.*, D90(1):015004, 2014.